

Transport Behavior of Resin-Coated Ceramic Proppants in Rough Vertical Fractures

by

Gongjue Wei

A thesis submitted in partial fulfillment of the requirements for the degree of

Master of Science

in

Petroleum Engineering

Department of Civil and Environmental Engineering
University of Alberta

© Gongjue Wei, 2019

ABSTRACT

In hydraulic fracturing, resin-coated ceramic proppants can be added to fracturing fluid as an agent for propping the fractures. Resin-coated ceramic proppants have several advantages compared to the traditional silica sands and ceramic proppants. Resin-coated ceramic proppants can withstand much higher pressure than silica sands, while they have a lower density than the ceramic proppants. The transport behavior of resin-coated ceramic proppants in fracturing fluid is seldom investigated in the past. In this study, we aim to investigate the transport behavior of resin-coated ceramic proppants in rough vertical fractures.

First, we conduct experiments to measure drag coefficients of resin-coated ceramic proppants during their settling in static water. Eight resin-coated ceramic particles with diameters between 450 and 924 μm are selected in the tests. Using the high-resolution images obtained from Computer Tomography (CT) scan, we measure the following for the eight resin-coated ceramic particles: bulk volume, mean diameter and volumetric fractions of three constituents making up each particle (i.e., resin coating, ceramic body, and air pockets). CT scan shows that the resin-coated ceramic particles are nearly spherical particles, while the surface of resin-coated ceramic particles is still quite rough with many peaks and valleys. High-precision electronic balance is used to accurately measure the mass of the tested particles. The densities of resin-coated ceramic particles are dependent on the volume of resin-coated ceramic particles. Three methods are applied to estimate the volume of particles. Method #1 calculates the volume of particles by assuming that the particles are ideal spheres which can be characterized with the mean diameter. The densities of particles can be then determined by dividing the mass by the volume estimated by method #1. Method #2 calculates the particle volume based on the three volumetric fractions (i.e., resin coating, ceramic body, and air pockets) and their respective densities. The densities of

particles can be obtained by multiplying the volumetric fractions by their respective densities and then summing them up. Method #3 relies on the volume of particles directly estimated from the CT scan, and then the density of each particle can be calculated by dividing the mass of each particle by the volume estimated by CT scan. Subsequently, the settling velocities of resin-coated ceramic particles in water are measured by recording the settling process of each particle in water using a high-speed camera. After obtaining the diameter, density, and settling velocity of each particle, the drag coefficients of each resin-coated ceramic particle can be determined. Such determined drag coefficient is then compared to those predicted by five empirical correlations in the literature. The comparison shows that the drag coefficients of resin-coated ceramic particles, which are estimated based on the aforementioned three methods for density determination, agree generally well with the drag coefficients estimated by the five empirical correlations. In order to quantify the accuracy of the particle densities estimated by the three methods, we compare the densities estimated by the above three methods against the ideal particle densities estimated by the empirical drag-coefficient correlations. The comparison shows that the method #3 (i.e., CT scan) leads to the minimum discrepancy between the estimated densities and the ideal particle densities, implying that the particle volumes estimated by the method #3 are more accurate than those estimated by the methods #1 and #2. In addition, Roos and Willmarth's correlation is shown to be more appropriate for calculating the drag coefficients of resin-coated ceramic particles than the other four correlations.

Next, we conduct dynamic flow tests to examine the transport behavior of resin-coated ceramic proppants in three rough fracture models which are replicates of a beige limestone, a coarse-grained white marble, and a holocrystalline amphibole granite. In the experiments, a fluid carrying a given concentration of proppants is allowed to flow through the rough fracture model;

the settling behavior of proppants and the relative area covered by the proppants in the fracture model are continuously monitored. Major influential factors on the proppants transport behavior have also been examined, including the location of the injection point (top and bottom), fracturing fluid type (tap water and slickwater), flow rate (10 L/min and 12 L/min), particle size of proppants (20-40 mesh and 30-50 mesh), fracture aperture (2 mm and 4 mm) and fracture model type (Fr.1, Fr.4, and Fr.5). At a given time, the relative coverage of resin-coated ceramic proppants obtained by injecting resin-coated ceramic proppants through the top injection point is larger than that obtained by injecting resin-coated ceramic proppants through the bottom injection point. The area occupied by resin-coated ceramic proppants is much larger than that occupied by silica sands at a given time. The relative coverage of resin-coated ceramic proppants carried by slickwater is lower than that of resin-coated ceramic proppants carried by tap water at a given time. Besides, the slickwater containing a low-concentration polymer can act as a friction reducer, leading to that the injection pressure recorded in the experiments using the slickwater is lower than that recorded in the experiments using the tap water. A higher flow rate can transport the proppants into deeper locations in the fractures, resulting in a lower relative coverage of proppants in the fracture models due to the limited length of the fracture models at a given time. A particle size of 20-40 mesh gives a higher relative proppant coverage in the fracture models at a given time than the 30-50 mesh resin-coated ceramic particles; this can be attributed to the fact that the collisions between the larger particles (i.e., 20-40 mesh particles) and fracture surface are more likely to happen and will retard the movement of resin-coated ceramic particles, leading to a higher relative coverage of 20-40 mesh resin-coated ceramic particles in the fracture models. Besides, when the slurry carries the proppants through the fracture models, there are more collisions between the fractures surface and proppant particles in the 2-mm-aperture fracture than

the 4-mm-aperture fracture. Therefore, at a given time, the relative coverage obtained in experiments using a 2-mm-aperture fracture model is larger than that obtained in experiments using a 4-mm-aperture fracture model. Among the three fracture models, the highest relative coverage of resin-coated ceramic proppants is obtained in Fr.4 (a replication of coarse-grained white marble), while the lowest relative coverage of resin-coated ceramic proppant can be obtained in Fr.1 (a replication of beige limestone with abundant coarse fossil shells). The highest injection pressure can be found in Fr.1 (a replication of beige limestone with abundant coarse fossil shells), while the lowest injection pressure is recorded in Fr.5 (a replication of holocrystalline amphibole granite).

DEDICATION

This dissertation is dedicated to my dearest parents, Mr.
Ping Wei and Mrs. Hongwei Jiang, and my brother, Mr.
Gongjing Wei.

ACKNOWLEDGMENTS

I would like to express my immense gratitude for the support and guidance from my supervisor, Dr. Huazhou Andy Li, for his supervision, advice, dedication, and assistance during my Master program at the University of Alberta.

I, also, would like to express my appreciation to the following individuals for their support during my Master program at the University of Alberta:

- Dr. Hai Huang for providing experimental facilities and technical assistance during my visit at the Xi'an Shiyou University (China);
- Lab staff in Shaanxi Key Laboratory of Advanced Stimulation Technology for Oil & Gas Reservoirs at the Xi'an Shiyou University;
- Dr. Tayfun Babadagli, Dr. Nobuo Maeda and Dr. Lijun Deng for serving as my committee members and their critical comments;
- Dr. Kayhan Develi from the Department of Geological Engineering at the Istanbul Technical University (Istanbul, Turkey) for preparing the rough fracture models; and
- Past and current group members in Dr. Li's research group.

TABLE OF CONTENTS

ABSTRACT	ii
DEDICATION	vi
ACKNOWLEDGMENTS	vii
TABLE OF CONTENTS	viii
LIST OF FIGURES	xi
LIST OF TABLES	xv
CHAPTER 1 INTRODUCTION	1
1.1. Research Background.....	1
1.2. Problem Statement	4
1.3. Objectives and Tasks.....	5
1.4. Thesis Structure.....	6
CHAPTER 2 SETTLING VELOCITY OF RESIN-COATED CERAMIC PROPPANTS IN WATER	12
2.1. Introduction	13
2.2. Experimental Section	17
2.2.1. Materials	17
2.2.2. Experimental Setup.....	17
2.2.3. Experimental Procedure	19
2.3. Results and Discussion.....	20

2.3.1. Volumetric Fractions of Constituents in Each Particle	20
2.3.2. Apparent Particle Density.....	23
2.3.3. Settling Velocity of Resin-Coated Ceramic Particles.....	26
2.3.4. Drag Coefficients of Resin-Coated Ceramic Particles	27
2.4. Conclusions	33
CHAPTER 3 A VISUAL EXPERIMENTAL STUDY: RESIN-COATED CERAMIC PROPPANTS TRANSPORT WITHIN ROUGH VERTICLE MODELS.....	40
3.1. Introduction	41
3.2. Experimental Section	43
3.2.1. Materials	43
3.2.2. Experimental Setup.....	45
3.2.3. Experimental Procedure	46
3.3. Results and Discussion.....	49
3.3.1. Typical Proppant Settling Patterns	49
3.3.2. Effect of Injection Point	50
3.3.3. Effect of Proppant Type	55
3.3.4. Effect of Fracturing Fluid Type.....	60
3.3.5. Effect of Flow Rate.....	63
3.3.6. Effect of Particle Size of Resin-Coated Ceramic Proppant.....	67
3.3.7. Effect of Fracture Aperture.....	69

3.3.8. Effect of Fracture Model	72
3.4. Conclusions	73
CHAPTER 4 CONCLUSIONS AND RECOMMENDATIONS	81
4.1. Conclusions	81
4.2. Recommendations	83

LIST OF FIGURES

Figure 2.1 Schematic of the experimental setup used for measuring settling velocity of a resin-coated particle in water (1. High-speed camera. 2. Nikon lens. 3. Particle settling in fluid medium. 4. Illumination source. 5. Table).....	19
Figure 2.2 A 3D rendering of the particle #1 based on CT scan images	21
Figure 2.3 CT image of the central cross-section of the particle #1	22
Figure 2.4 CT scan images of the central cross-sections of the eight particles	22
Figure 2.5 Parity chart comparing the equivalent spherical diameter against the mean diameter of the eight resin-coated ceramic particles	28
Figure 2.6 Comparison of the drag coefficients of eight resin-coated ceramic particles determined by our experiments using three methods with the drag-coefficients estimated by five empirical correlations [19, 26-29]: (a) experimentally determined drag coefficients using method #1; (b) experimentally determined drag coefficients using method #2; and (c) experimentally determined drag coefficients using method #3	31
Figure 2.7 Average absolute relative discrepancies between the experimentally determined particle density estimated by three methods and “ideal particle density” determined by five empirical correlations.....	33
Figure 3.1 3D images of the rough surfaces of fracture models Fr.1 (a), Fr.4 (b) and Fr.5 (c) [26]	45
Figure 3.2 Schematic of the experimental setup used for conducting the proppants transport experiments	46
Figure 3.3 Four typical distributions of resin-coated ceramic proppant observed in the experiments: (a) Type #1: an image captured at 40 seconds in Experiments #22; (b) Type #2: an	

image captured at 40 seconds in Experiments #10; (c) Type 3: an image captured at 40 seconds in Experiments #2; and (d) Type #4: an image captured at 40 seconds in Experiments #19. 50

Figure 3.4 Changes in relative coverage of resin-coated ceramic proppants and pressure as time elapses: (a) evolution of the relative coverage and pressure recorded for Experiments #1 and #2; (b) evolution of the relative coverage and pressure recorded for Experiments #5 and #6; (c) evolution of the relative coverage and pressure recorded for Experiments #10 and #11; (d) evolution of the relative coverage and pressure recorded for Experiments #14 and #15; (e) evolution of the relative coverage and pressure recorded for Experiments #19 and #20; and (f) evolution of the relative coverage and pressure recorded for Experiments #23 and #24. These experiments are conducted to study the effect of injection point on the proppant settling behavior in rough fracture models. 55

Figure 3.5 Changes in the relative coverage of resin-coated ceramic proppants and pressure as time elapses: (a) evolution of the relative coverage and pressure recorded for Experiments #1 and #3; (b) evolution of the relative coverage and pressure recorded for Experiments #10 and #12; and (c) evolution of the relative coverage and pressure recorded for Experiments #19 and #21. These experiments are conducted to study the effect of proppant type on the proppant settling behavior in rough fracture models. 57

Figure 3.6 Changes in the relative coverage of resin-coated ceramic proppants and pressure as time elapses: (a) evolution of the relative coverage and pressure recorded for Experiments #5 and #7; (b) evolution of the relative coverage and pressure recorded for Experiments #14 and #16; and (c) evolution of the relative coverage and pressure recorded for Experiments #23 and #25. These experiments are conducted to study the effect of fracturing fluid type on the proppant settling behavior in rough fracture models. 63

Figure 3.7 Changes in the relative coverage of resin-coated ceramic proppants and pressure as time elapses: (a) evolution of the relative coverage and pressure recorded for Experiments #1 and #4; (b) evolution of the relative coverage and pressure recorded for Experiments #5 and #8; (c) evolution of the relative coverage and pressure recorded for Experiments #10 and #13; (d) evolution of the relative coverage and pressure recorded for Experiments #14 and #17; (e) evolution of the relative coverage and pressure recorded for Experiments #19 and #22; and (f) evolution of the relative coverage and pressure recorded for Experiments #23 and #26. These experiments are conducted to study the effect of flow rate on the proppant settling behavior in rough fracture models. 67

Figure 3.8 Changes in the relative coverage of resin-coated ceramic proppants and pressure as time elapses: (a) evolution of the relative coverage and pressure recorded for Experiments #1 and #5; (b) evolution of the relative coverage and pressure recorded for Experiments #10 and #14; (c) evolution of the relative coverage and pressure recorded for Experiments #19 and #23. These experiments are conducted to study the effect of particle size of resin-coated ceramic proppant on the proppant settling behavior in rough fracture models. 69

Figure 3.9 Changes in the relative coverage of resin-coated ceramic proppants and pressure as time elapses: (a) evolution of the relative coverage and pressure recorded for Experiments #5 and #9; (b) evolution of the relative coverage and pressure recorded for Experiments #14 and #18; (c) evolution of the relative coverage and pressure recorded for Experiments #23 and #27. These experiments are conducted to study the effect of fracture aperture size on the proppant settling behavior in rough fracture models. 72

Figure 3.10 Changes in the relative coverage of resin-coated ceramic proppants and injection pressure as time elapses in Experiments #1, #10 and #19. These results are shown together to

demonstrate the effect of fracture model on the proppant settling behavior in rough fracture models..... 73

LIST OF TABLES

Table 2.1 Properties of resin-coated ceramic particles	17
Table 2.2 Experimental results from CT scan	20
Table 2.3 Volumetric fractions of air, resin and ceramic body in the eight resin-coated ceramic particles	23
Table 2.4 Measured mass of the eight resin-coated ceramic particles.....	24
Table 2.5 Comparison among the apparent density of each resin-coated ceramic particle estimated by three aforementioned methods.....	25
Table 2.6 Measured settling velocity of the eight resin-coated ceramic particles	26
Table 2.7 Particle Reynolds number of the eight resin-coated ceramic particles.....	27
Table 2.8 Summary of five commonly used empirical drag-coefficient correlations developed for spherical particles.....	29
Table 3.1 Lithological properties of the rock samples and the roughness parameters for the surface of model fractures [26].....	44
Table 3.2 Experimental conditions used in the proppants flow experiments	47
Table 3.3 Digital images captured at different time during Experiments #1 and #3	58

CHAPTER 1 INTRODUCTION

1.1. Research Background

Hydraulic fracturing is a commonly used well stimulation technology in petroleum engineering. It achieves the purpose of stimulating reservoir productivity by injecting pressurized fluid into the formation and creating fractures [1]. After fractures are created by high-pressure fluids, proppants are subsequently injected into fractures to maintain the opening of the fractures [2]. Normally, a good type of proppant is supposed to satisfy the following two properties: the first one is that it should have a high hardness to withstand high closure stress in the formation [3], and the second one is that the proppant should have high chemical and thermal resistance [3]. Up to now, different types of proppants have been developed for accommodating different downhole conditions. Silica sands is one of the most commonly used types of proppants in the field due to its low cost and good availability [4]. However, sand proppants have limited application in deep wells, since its main component, quartz, cannot withstand high closure stress [4].

To overcome the shortcoming of silica sand proppants, many alternative types of proppants have been developed, e.g., resin-coated sand proppants and ceramic proppants [5-8]. Resin coating can provide good encapsulation of each sand particle, helping to maintain a good integrity of the proppant bed surrounding the wellbore [6]. Ceramic proppants are tougher than the silica proppants. However, each type of proppants has drawbacks and limitations when being applied to the field. Resin-coated sands are used in wells in which the pressure is limited to 8000 psi [9]. The cost of making ceramic proppants is relatively high [10]. Besides, the density of the ceramic proppant is higher than that of silica sands, implying that the ceramic particles settle faster and

require a higher injection rate when being injected into the formations compared to silica sand particles.

Exploiting the benefits of resin coated sands and ceramic proppants, the resin-coated ceramic proppants can be thereof developed [10]. Technically, the resin-coated ceramic proppants have several advantages comparing to other types of proppants: 1) The resin-coated ceramic proppants can withstand higher closure stress, helping to maintain good conductivity of the hydraulic fractures in deep formations after the hydraulic fracturing treatments; 2) The resin-coated ceramic proppants tend to have high resistance to chemical and thermal threat in the formations; 3) The resin coating could provide good encapsulation of each ceramic particle and further keep a good integrity of the proppant bed surrounding the wellbore when ceramic particles are broken under closure pressure of the formations, leading to the elimination of the erosion to the tunnels when the proppants flow through tunnels; 4) The bulk density of resin-coated ceramic proppants particles is lower than that of ceramic proppants, implying that the settling velocity of proppant can be slower than that of ceramic proppants particles when being injected into the fractures [6, 11]. Understanding the flowing characteristics of resin-coated ceramic proppants is of great significance for improving the design and field implementation of resin-coated ceramic proppants in hydraulic fracturing operations.

In this research, a comparison between the flow characteristics of silica sand particles and flow characteristics of resin-coated ceramic particles is conducted to find out if resin-coated ceramic proppants could occupy more area in the fractures after the flow tests. In order to better describe the flow characteristics of the resin-coated ceramic particles, accurately measuring and predicting the settling velocity of these particles is of great importance [12, 13]. The terminal velocity of a given particle can be obtained by balancing the gravity, buoyancy force, and drag

force acting on the particle if the particle is released in a static Newtonian fluid [14]. The drag force is calculated based on the drag coefficient. Many researchers have worked on the prediction of the drag coefficient in the past. Stokes first derived the following drag coefficient equation in creeping flow around a spherical particle [15]:

$$C_D = \frac{24}{Re_p} \quad (1.1)$$

where C_D is the drag coefficient, and Re_p is the particle Reynolds number ($Re_p = \frac{\rho v D}{\mu}$, where ρ is fluid density, v is settling velocity, D is particle diameter, and μ is fluid viscosity). However, **Equation 1.1** is only valid for describing the settling behavior of spherical particles in an infinite boundary domain Newtonian fluid at low particle Reynolds number [16]. Afterwards, a number of experimental investigations have been conducted to measure the drag coefficients over a broad range of particle Reynolds number, leading to the development of many empirical and semi-empirical correlations for different ranges of particle Reynolds numbers. However, one common issue of these correlations is that these proposed correlations can only be applied to spherical particles [17]. In nature, many industrial particles are non-spherical particles [18]. To predict the drag coefficient of non-spherical particles, many researchers later conducted experiments in order to explore the drag coefficient for non-spherical particles and accordingly developed correlations to predict the drag coefficient of non-spherical particles in Newtonian fluids [19-25]. As mentioned above, resin-coated proppants have found promising application in hydraulic fracturing. It is of great importance to understand how the resin coating on the proppant particles impacts the migration and settlement of the particles as well as determine the drag coefficient of resin-coated proppants in fracturing fluids. But no experimental studies have been conducted on this subject.

Proppants transport in fractures plays an important role in hydraulic fracturing as the settling of proppants affects the conductivity of the fractures [26]. Many researchers have conducted proppants transport experiments in a laboratory context, but the fracture models used in these experiments are smooth glass models in most cases. The fractures created in subsurface formations have rough surfaces, and the degree of roughness of the fracture surface may vary from a formation to another. The proppants transport in rough fracture models is seldom studied in the past, with the exception that the recent experimental efforts made available at the University of Alberta have used rough fracture models that are replicated models of real rocks [27-29]. As a continuation of these previous studies at the University of Alberta, this thesis further conducts experiments to examine the flow characteristics of resin-coated ceramic proppants in rough vertical fractures.

1.2. Problem Statement

Firstly, reliable estimation of drag coefficient of proppant particles in fracturing fluids is important for achieving accurate numerical simulation of the settling behavior of proppants in a fracture. Most of the drag-coefficient correlations proposed in the literature are not applicable for non-spherical particles. Also, few experimental studies focus on quantifying the drag coefficients of composite materials, such as the resin-coated ceramic particles. Further experiments need to be conducted to elucidate how the non-spherical nature and resin coating of the resin-coated proppants affect the drag coefficient. Secondly, previous proppant-transport experiments are normally conducted in smooth vertical fractures where the surface roughness of the fractures is nonexistent. No visual experiments have been conducted before to examine how resin-coated ceramic proppants transport in rough vertical fractures as well as how their transport behavior differs from that of silica sand proppants. To fill this gap, more realistic experiments need to be

conducted by using rough fracture models. These experiments are expected to provide important insights into how to achieve the optimal placement of resin-coated ceramic proppants in hydraulic fractures in the field.

1.3. Objectives and Tasks

The primary objectives of this research are first to accurately determine the drag coefficient of the resin-coated ceramic proppants in water and secondly to visually study the flow characteristics of the resin-coated ceramic proppants in rough vertical fractures. The detailed tasks to be conducted to achieve such objectives include the following:

- 1) To use computed tomography (CT) scan to accurately measure the volume of the resin-coated ceramic particles and find out the fractions of each constituent (e.g., air pockets inside the ceramic body, and resin coating) inside a resin-coated ceramic particle;
- 2) To accurately obtain the density of resin-coated ceramic particles based on the volume measured by CT scan and the weight measured by a high precision electronic balance;
- 3) To accurately measure the settling velocities of resin-coated ceramic particles in water using a high-speed camera;
- 4) To compare the drag coefficient determined by the settling velocity experiments with the results obtained from the commonly used drag-coefficient correlations;
- 4) To conduct visual experiments to study how the resin-coated ceramic proppants are being transported in three rough vertical fractures by considering the essential process parameters (including location of the injection point, proppant type, proppant size, slurry type, flow rate, and fracture aperture); and

5) To analyze the influences of these parameters on the relative coverage of resin-coated ceramic proppants in the fracture and try to determine the operating conditions that can yield the highest coverage of resin-coated ceramic proppants in the fracture.

1.4. Thesis Structure

Chapter 1 covers research background, problem statement, research objectives, and thesis structure.

In Chapter 2, eight resin-coated ceramic particles are firstly tested by CT scan technique to accurately measure the volume, mean diameters, and the fractions of three constituents in particles, i.e., resin, ceramic body, and air pockets, while the high-precision electronic balance is used to obtain an accurate mass of the tested particles. The settling velocity of a given resin-coated ceramic particle is calculated by dividing the travel distance of the tested particle in static water by the travel duration obtained by a high-speed camera. Three methods are used to estimate the particle density in this research. After obtaining the diameter, density, and settling velocity of each particle, the drag coefficient of each resin-coated ceramic particle can be determined. The comparison shows that the drag coefficients of resin-coated ceramic particles, which are estimated based on the aforementioned three methods for density determination, agree generally well with the drag coefficients estimated by five empirical correlations. A comparison is conducted between the density of resin-coated ceramic particles calculated by all three methods and the “ideal particle density”. Roos and Willmarth’s correlation [30] is more appropriate for calculating the drag coefficients of resin-coated ceramic particles than the other four correlations.

Chapter 3 presents the experimental results of the transport behavior of resin-coated ceramic proppants in three rough vertical fractures under the influence of the essential process parameters (including location of the injection port, proppant type, proppant size, slurry type, flow rate, and fracture aperture). We analyze the effects of these process parameters on the relative coverage of resin-coated ceramic proppants in the fracture, and, based on the conducted experiments, we find the optimal operating conditions yielding the highest coverage of resin-coated ceramic proppants in the fracture.

Chapter 4 summarizes the conclusions of this study as well as the recommendations for future work.

References

- [1] S.M. Patel, C.H. Sondergeld, C.S. Rai, Laboratory studies of cyclic injection hydraulic fracturing. *Int. J. Rock Mech. Min. Sci.* 95 (2017) 8-15.
- [2] Y. Tang, P.G. Ranjith, M.S.A. Perera, Major factors influencing proppant behavior and proppant-associated damage mechanisms during hydraulic fracturing. *Acta Geotechnica*. 13 (4) (2018) 757-780.
- [3] F. Liang, M. Sayed, G.A. Al-Muntasheri, F.F. Chang, L. Li, A comprehensive review on proppant technologies. *Petroleum*. 2 (2016) 26-39.
- [4] D.R. Underdown, K. Das, New proppant for deep hydraulic fracturing, *SPE J.* 37(1) (1985) 98-104.
- [5] M. Zoveidavianpoor, A. Gharibi, Application of polymers for coating of proppant in hydraulic fracturing of subterranean formations: A comprehensive review. *J. Nat. Gas. Sci. Eng.* 24 (2015) 197-209.
- [6] L. Fu, G. Zhang, J. Ge, K. Liao, P. Jiang, H. Pei, X. Li, Surface modified proppants used for proppant flow back control in hydraulic fracturing. *Colloids. Surf. A Physicochem. Eng. Asp.* 507 (2016) 18-25.
- [7] P.D. Nguyen, B.T. Dewprashad, J.D. Weaver, A new approach for enhancing fracture conductivity. Paper SPE 50002 presented at the SPE Asian Pacific Oil & Gas Conference and Exhibition, Perth, Australia, 12-14, October 1998.
- [8] K. Hu, A. Schmidt, J. Barhaug, J. Wong, J. Tian, B.E. Hall, Sand, resin-coated sand or ceramic proppant? The effect of different proppants on the long-term production of Bakken shale

wells. Paper SPE 174816 presented at the SPE Annual Technical Conference and Exhibition, Houston, Texas, USA, 28-30, September 2015.

[9] N. Bestaoui-Spurr, Materials science improves silica sand strength. Paper SPE 168158 presented at the SPE Symposium and Exhibition on Formation Damage Control, Lafayette, Louisiana, USA, 26-28, February 2014.

[10] A.R. Rickards, H.D. Brannon, W.D. Wood, High strength, ultralightweight proppant lends new dimensions to hydraulic fracturing applications. *SPE Prod. Oper.* 21 (02) (2006), pp.212-221.

[11] F. Liang, M. Sayed, G.A.A. Muntasheri, F.F. Chang, L. Li, A comprehensive review on proppant technologies. *Petroleum.* 2 (2016) 26-39.

[12] S.F. Chien, Settling velocity of irregularly shaped particles. *SPE Drill & Compl.* 9 (04) (1994) 281-289.

[13] M. Hartman, O. Trnka, K. Svoboda, Free settling of nonspherical particles. *Ind. Eng. Chem. Res.* 33 (1994) 1979-1983.

[14] F. Dioguardi, D. Mele, A new shape dependent drag correlation formula for non-spherical rough particles. Experiments and results. *Powder Technol.* 277 (2015) 222-230.

[15] G.G. Stokes, On the effect of the internal friction of fluids on the motion of pendulums. *Trans. Camb. Phil. Soc.* 9 (8) (1851).

[16] X. Song, Z. Xu, G. Li, Z. Pang, Z. Zhu, A new model for predicting drag coefficient and settling velocity of spherical and non-spherical particle in Newtonian fluid. *Powder Technol.* 321 (2017) 242-250.

- [17] S.K. Arnipally, E. Kuru, Settling velocity of particle in viscoelastic fluids: a comparison of the shear-viscosity and elasticity effects. *SPE J.* 23 (05) (2018) 1689-1705.
- [18] M. Mandø, C. Yin, H. Sørensen, L. Rosendahl, On the modelling of motion of non-spherical particles in two-phase flow. Paper presented at the 6th International Conference on Multiphase Flow, Leipzig, Germany, 9-13, July 2007.
- [19] A. Haider, O. Levenspiel, Drag coefficient and terminal velocity of spherical and nonspherical particles. *Powder Technol.* 58 (1989) 63-70.
- [20] M. Sarifzadeh, M. Javadi, K. Shahriar. Effect of surface roughness on velocity field through rock fractures. Paper ISRM-EUROCK-2009-054 presented at the ISRM Regional Symposium, Cavtat, Croatia, 29-31, October 2009.
- [21] M. Dejam, H. Hassanzadeh, Z. Chen, Shear dispersion in a rough-walled fracture. *SPE J.* 23 (05) (2018) 1669-1688.
- [22] S. Brown, A. Cprihan, R. Hardy, Experimental observation of fluid flow channels in a single fracture. *J. Geophys. Res.* 103 (1998) 5125-5132.
- [23] R. Smith, Longitudinal dispersion coefficients for varying channels. *J. Fluid. Mech.* 130 (1983) 299-314.
- [24] L.W. Gelhar, Stochastic subsurface hydrology from theory to application. *Water Resour. Res.* 22 (1986) 135S-145S.
- [25] D.G. Dronfield. S.E. Silliman, Velocity dependence of dispersion for transport through a single fracture of variable roughness. *Water Resour. Res.* 29 (1993) 3477-3483.

- [26] I. Ippolite, G. Daccord, E.J. Hinch, J.P. Hulin, Echo tracer dispersion in model fractures with a rectangular geometry. *J. Contam. Hydrol.* 16 (1994) 87-108.
- [27] G. Drazer, J. Koplik, Tracer dispersion in two-dimensional rough fractures. *Phys. Rev. E.* 63 (2001) 056104.
- [28] H. Huang, T. Babadagli, H. Li, K. Develi, Visual analysis on the effects of fracture-surface characteristics and fracture model on proppant transport in vertical fractures. Paper SPE 189892 presented at the SPE Hydraulic Fracturing Technology Conference & Exhibition, Woodlands, Texas, USA, 23-25, January 2018.
- [29] H. Huang, T. Babadagli, H. Li, A quantitative and visual experimental study: effect of fracture roughness on proppant transport in a vertical fracture. Paper SPE 187520 presented at the SPE Eastern Regional Meeting, Lexington, Kentucky, USA, 4-6, October 2017.
- [30] F.W. Roos, W.W. Willmarth, Some experimental results on sphere and disk drag. *AIAA J.* 9 (2) (1971) 285-291.

**CHAPTER 2 SETTLING VELOCITY OF RESIN-COATED CERAMIC PROPPANTS IN
WATER**

2.1. Introduction

In hydraulic fracturing operations, proppants displacement in fractures can determine the conductivity of fractures and productivity of wells [1]. To accurately estimate the proppants displacement in fractures, it is of great significance to predict the terminal velocity of proppant particles in fractures with wall effect. Terminal velocity of a particle is the maximum velocity a particle can reach as it falls in a fluid [2]. Liu and Sharma showed that the terminal velocity of proppant particles in bounded water is related to the settling velocity of particles in unbounded water [1]:

$$\frac{V_w}{W_t} = 1 - f(\mu) * \frac{a}{B} \left(\frac{a}{B} < 0.9\right) \quad (2.1)$$

$$\frac{V_w}{W_t} = g(\mu) * \left(1 - \frac{a}{B}\right) \left(\frac{a}{B} \geq 0.9\right) \quad (2.2)$$

$$f(\mu) = 0.16\mu^{0.28} \quad (2.3)$$

$$g(\mu) = 8.26e^{-0.0061\mu} \quad (2.4)$$

where V_w is terminal velocity for the present of walls, W_t is terminal velocity, μ is fluid viscosity, a is particle radius, and B is cell half-width. As shown by **Equations 2.1-2.4**, predicting the terminal velocity of proppant particles in unbounded water plays an important role in estimating the terminal velocity of proppant particles in real fractures.

Many researchers have worked on studying the terminal velocity of particles in unbounded liquid [2]. The terminal velocity of a particle is reached when gravitation equals drag force and buoyant force [3]:

$$F_G = F_d + F_b \quad (2.5)$$

where F_G is gravitational force ($F_G = \frac{1}{6}\pi D^3 g \rho_p$, where D is diameter of the particle, g is gravitational constant, and ρ_p is density of the particle), F_d is drag force, and F_b is buoyant force ($F_b = \frac{1}{6}\pi D^3 g \rho$, where ρ is the density of fluid). By substituting the equations of F_G and F_b into **Equation 2.5**, the drag force could be obtained as:

$$F_d = \frac{D^3}{6} g \pi (\rho_p - \rho) \quad (2.6)$$

Stokes pioneered the work in measuring the drag force of a particle settling in an incompressible Newtonian fluid, leading to the following Stokes' law [4]:

$$F_d = 3\pi\mu v D \quad (2.7)$$

where v is particle's settling velocity. Note that **Equation 2.7** is applicable to spherical particles in an infinite-domain fluid system at a low Reynolds number. Combining **Equations 2.6** and **2.7** yields the terminal velocity of a particle settling in a Newtonian fluid:

$$W_t = \frac{g D^2 (\rho_p - \rho)}{18\mu} \quad (2.8)$$

A dimensionless parameter, the so-called drag coefficient C_D , can be defined as [5]:

$$C_D = \frac{F_d}{\frac{1}{8}\rho W_t^2 \pi D^2} \quad (2.9)$$

Then, the terminal velocity can be re-expressed in terms of the drag coefficient as follows [6]:

$$W_t = \sqrt{\frac{4gD(\rho_p - \rho)}{3C_D\rho}} \quad (2.10)$$

As we can see from **Equations 2.10**, terminal velocity is dependent of the drag coefficient; therefore, to accurately describe the settling process of the particles, we require an accurate value

of the drag coefficient, calculated by a robust predictive drag-coefficient correlation. There are several factors affecting the value of the drag coefficient of a particle: shape, bulk-density, size of the particles, and fluid viscosity [3]. Shape plays a vital role in determining the drag force acting on the particles [7-10], and the effects of bulk-density and size of the particle and fluid viscosity on terminal velocity can be considered by the particle Reynolds number [11]:

$$R_{ep} = \frac{\rho v D}{\mu} \quad (2.11)$$

Since the application scope of Stokes' law is limited to the creeping regime at a low Reynolds number, some researchers conduct additional experiments in order to precisely measure the drag coefficient at a higher particle Reynolds number [12-29]. However, correlations proposed in the literature have two drawbacks; first, most correlations are designed for regular shaped particles, (circular and cylindrical particles), and second, the effect of surface roughness of the particle on the drag coefficient has not been investigated [30]. To investigate the drag coefficient for non-spherical particles, in the past few decades, many researchers conducted experiments and came up with new correlations to determine the drag coefficient for non-spherical particles, but **maintained** one unresolved issue in determining the drag coefficient and accurately measuring the density of tiny particles, as it requires advanced measuring tools to accurately find both volume and mass of the particles.

Resin-coated ceramic proppant is one promising proppant, as said proppants have several advantages over silica sand, including high chemical and thermal resistance and high crush resistance [31]. Reliable estimation of the drag coefficient of resin-coated ceramic particles in fracturing fluids is important for carrying out accurate numerical simulations of the settling behavior of proppants in a fracture. Up to now, to our knowledge, no study has been conducted

to investigate the settling characteristics of the resin-coated ceramic particle with the goal of discovering the effects of resin coating and its roughness on the drag coefficient in a Newtonian fluid.

In this study, we investigate the settling characteristics of resin-coated ceramic particles in water. To accurately determine drag coefficient for these resin-coated ceramic particles, we apply the computed tomography (CT) scan technique to accurately measure the volume of the particles and find out the volumetric fractions of each constituent inside, use a high precision electronic balance to measure the weight of each particle, and use a high-speed camera to record the settling process of a single particle. Density of each particles is estimated by three methods: (1) Dividing the mass measured by high-precision electronic balance and volume calculated by assuming the particle is a sphere with the mean diameter measured by CT scan, (2) considering different densities and volumetric fractions of three constituents (air pocket, ceramic body, and resin coating) in the resin-coated ceramic particle, and (3) Dividing the mass measured by high-precision electronic balance and volume determined by a CT scan. A comparison is then conducted between the densities of resin-coated ceramic particles, calculated by all three aforementioned methods, and those calculated by five commonly used empirical drag coefficient correlations. The results show that an accurate density of resin-coated ceramic particles can be estimated using a CT scan, based on the precise particle volume measured by CT scan. Roos and Willmarth's correlation [29] can give a more accurate prediction of the drag coefficient of resin-coated ceramic particles compared with those estimated by the other four empirical correlations.

2.2. Experimental Section

2.2.1. Materials

Eight resin-coated particles are randomly selected and used in the experiments (Henan Tianxiang New Material Co., LTD, China), and **Table 2.1** lists the properties of the selected resin-coated ceramic particles. Bulk Density is the ratio of the mass of dry solids to the bulk volume of the soil; the bulk volume includes the volume of the solids and the pore space [32]. Apparent density is the ratio of the mass to apparent solid volume. Roundness is defined as the ratio of the average radius of curvature of the circle inscribed in the maximum cross-section of the particle, whereby a particle is given some value from 0.1 (very sharp edges) to 1.0 (perfectly rounded edges) [33]. The crush resistance at 10,000 psi determines the amount of proppants crushed at 10,000 psi. Distilled water is used as the Newtonian fluid and placed into a transparent container when measuring the settling velocity of particles.

Table 2.1 Properties of resin-coated ceramic particles

Property	Value
^a Bulk density, g/cm ³	1.46
^b Apparent density, g/cm ³	2.63
^c Average roundness	0.9
^d Crush resistance at 10,000 psi, %	1

Note: a: The bulk density is defined as the mass of a number of particles divided by their bulk volume (the particles are tightly packed together); b: The apparent density is the mass of a given particle divided by its bulk volume; c: Roundness is defined as the ratio between the radii of the minimum inscribed circle and the maximum circumscribed circle that fit the particle (ISO 1101); d: The crush resistance at 10,000 psi measures how much percentage of the tested proppants are crushed at 10,000 psi.

2.2.2. Experimental Setup

A CT scanner (ZEISS Xradia 510 Versa 3D X-ray Microscopes, ZEISS Company, Germany) is used to scan the eight resin-coated ceramic particles in order to accurately obtain the exact volume of each particle. The scanning resolution of the CT apparatus is 1 micrometer. A high-

precision electronic balance (BM-252, A&D, USA) is used to accurately measure the mass of each particle; its measurement accuracy is ± 0.00001 g.

The schematic shown in **Figure 2.1** shows the experimental setup used to conduct the particle-settling experiments. A similar setup has been used in the study by Bagheri and Bonadonna [34]. The water container shown in **Figure 2.1** is a transparent cubical column made of Plexiglas. The length, width, and height of the tank are 30 cm, 10 cm, and 60 cm, respectively. A DC lamp is used to provide a shadowless illumination source, ensuring that no shadow appears in the photo taken during the settling of a given particle in water. When a given resin-coated ceramic particle is settling in water, a high-speed camera (Pco. Dimax S4, PCO, Germany) in conjunction with a Nikon 105 mm 1:2.8G ED lens is used to take 200 photos per second to monitor the settling process of a given particle. The high-speed camera can capture a minimum pixel size of $11 \mu m \times 11 \mu m$ and cover a sight of $2016 \text{ pixels} \times 2016 \text{ pixels}$.

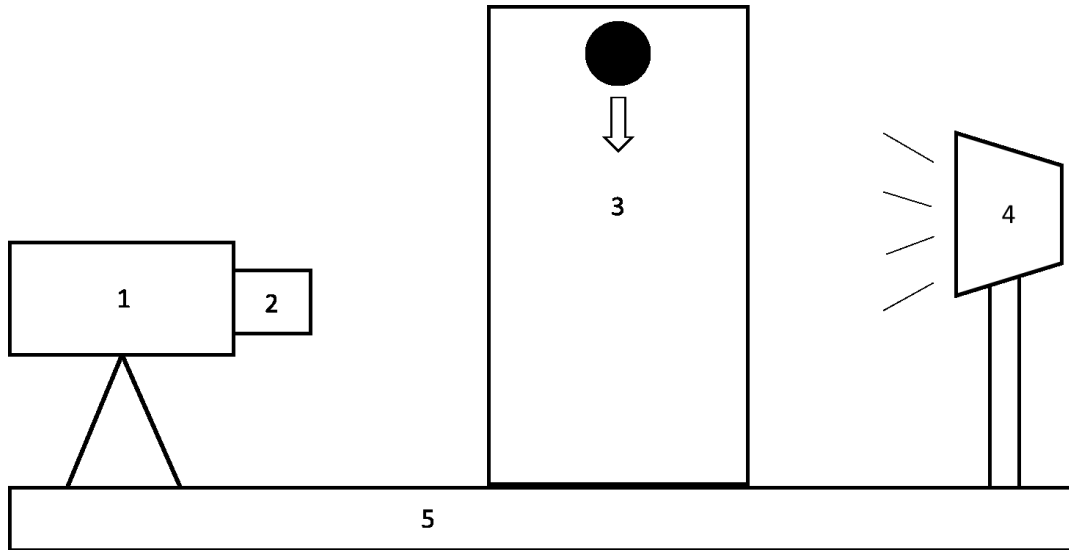


Figure 2.1 Schematic of the experimental setup used for measuring settling velocity of a resin-coated particle in water (1. High-speed camera. 2. Nikon lens. 3. Particle settling in fluid medium. 4. Illumination source. 5. Table)

2.2.3. Experimental Procedure

Eight resin-coated ceramic particles differing in density, shape, size, and resin thickness are studied in these experiments. The experimental procedure is briefly introduced as follows:

1. Measure the volume of each resin-coated ceramic particle by using the CT setup. Prior to activating the X-ray source, all eight particles are attached to a sample holder which is placed on the platform of the CT scan machine. After setting up proper working parameters of the CT scan machine (including voltage, power, and number of images to be acquired), we start the CT scanning process. Because it is a high-resolution scan, scanning of each particle takes approximately 10 hours.
2. After the CT scan, measure the mass of each particle using the high-precision electronic balance.
3. Conduct the particle settling experiments. Fourteen liters of distilled water is added into the transparent cuboidal column. The water tank is left alone for 24 hours to eliminate

the air bubbles in the water. Each settling test gets started by releasing a given particle into water; the settling process is being continuously recorded by the high-speed camera. To make sure the experiments are robust and repeatable, the settling test for each particle is repeated three times.

2.3. Results and Discussion

2.3.1. Volumetric Fractions of Constituents in Each Particle

Table 2.2 summarizes the CT scanning results. As can be seen from **Table 2.2**, the diameters of the eight particles fall in the range of 0.450 mm to 0.924 mm. Besides, the volumes of all the particles are also measured by the CT scan machine and they are listed in **Table 2.2**. **Figure 2.2** shows a 3D rendering of the particle #1 based on CT scan images. We can observe from **Figure 2.2** that the resin-coated ceramic particle is actually quite rough with many peaks and valleys appearing on the surface.

Table 2.2 Experimental results from CT scan

Particle No.	^a Mean particle diameter captured by CT, μm	Maximum resolution in length measurements, μm	Volume, $\times 10^8 \mu\text{m}^3$	Maximum resolution in volume measurements, μm^3
1	923.512	1.042	4.025	1.13
2	697.521	1.072	1.324	1.23
3	654.995	1.094	1.446	1.31
4	603.133	1.065	0.969	1.21
5	450.155	1.081	0.458	1.01
6	525.961	1.004	0.745	1.26
7	925.596	1.060	2.954	1.19
8	934.019	1.064	2.938	1.20

Note: a: Mean particle diameter captured by CT is the average of the maximum diameter determined as the maximum circumscribed circle diameter and the minimum diameter determined as the minimum circumscribed circle diameter.

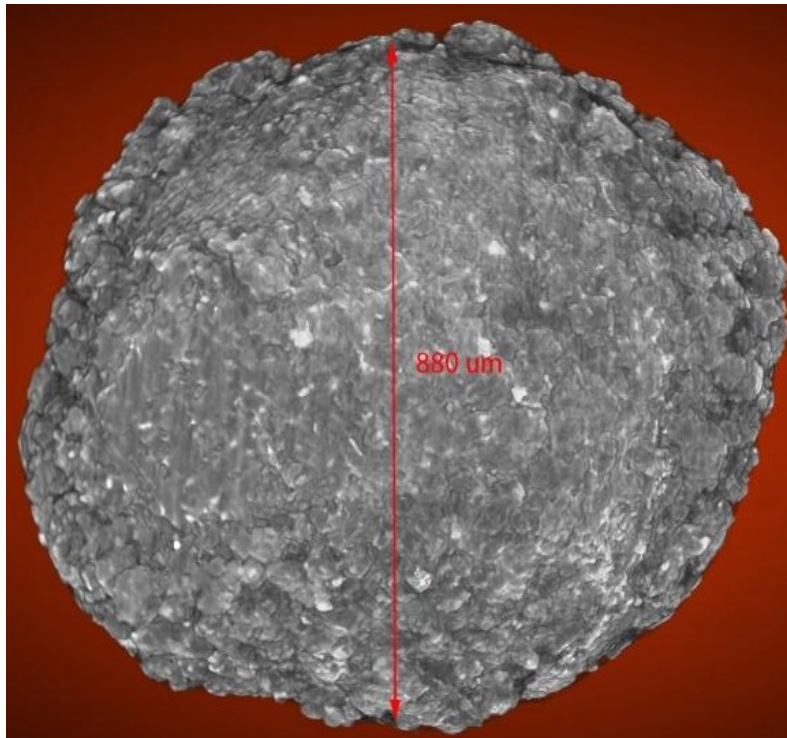


Figure 2.2 A 3D rendering of the particle #1 based on CT scan images

Figure 2.3 shows the CT image of the central cross-section of the particle #1. We can see from **Figure 2.3** that a thin layer is coated on the ceramic body, which corresponds to the resin coating, and some air pockets are encapsulated in the particle. As such, there are three constituents in the particle, namely, ceramic body, air pockets, and resin coating. In addition, **Figure 2.3** shows that the resin-coating thickness varies much from a location to another, partially leading to the rough nature of the resin-coated ceramic particle. **Figure 2.4** shows CT scan images of the central cross-sections of the eight particles. As seen from these images, the internal structures of these eight particles are slightly different from each other.

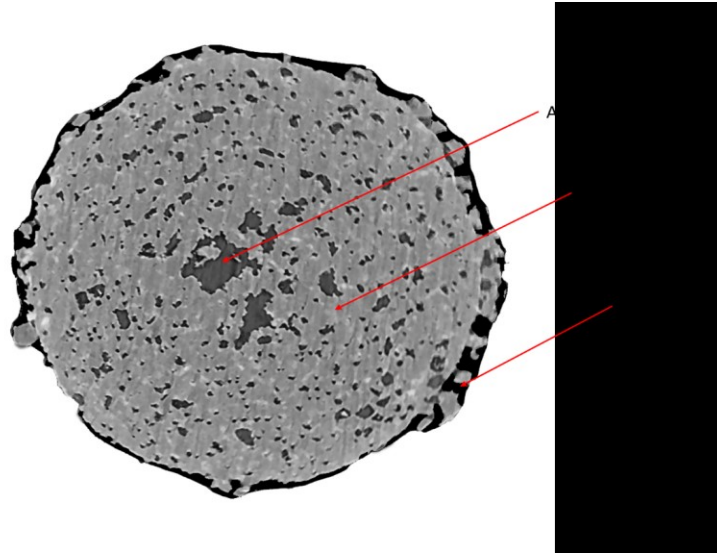


Figure 2.3 CT image of the central cross-section of the particle #1

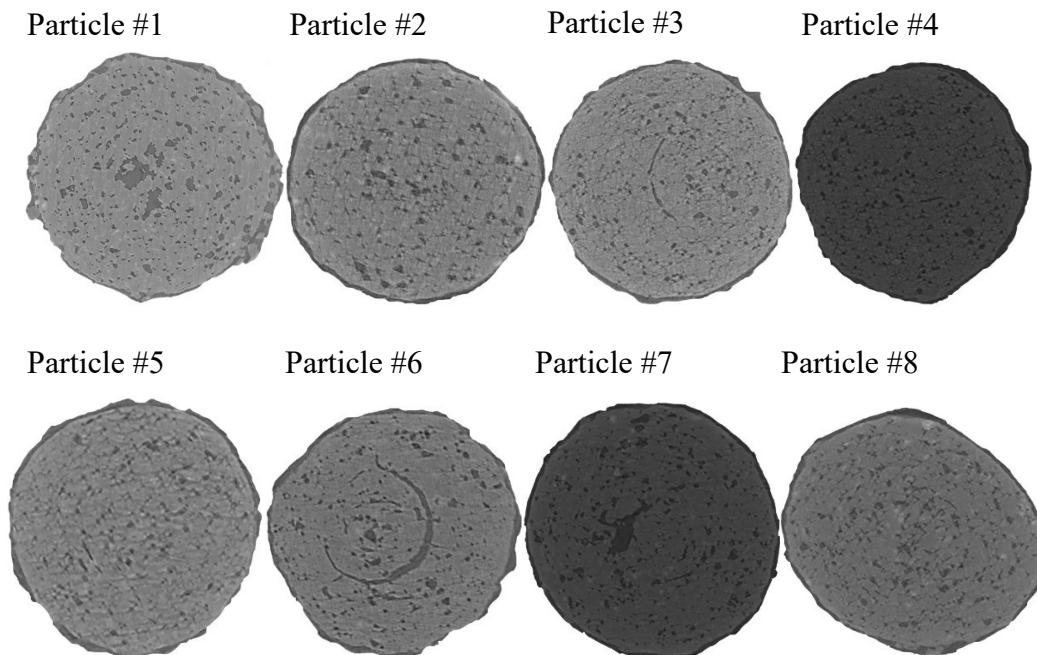


Figure 2.4 CT scan images of the central cross-sections of the eight particles

Based on the cross-section images in **Figure 2.4**, the fractions that different constituents occupy in each particle (i.e., air pocket, ceramic body, and resin coating) can be calculated based on the areas covered by these constituents. These fractions, together with the densities of the

constituents, can be thereby used to determine the apparent density of the resin-coated ceramic particles. Herein, we use image analysis software to figure out the fractions that different constituents occupy in each particle. First, we distinguish different constituents on the basis of the grayness contrast and establish the boundaries among the three constituents. Second, we count the number of pixels present in each constituent. Third, we determine the areal fraction of each constituent based on the ratio of the number of pixels present in each constituent versus the total number of pixels. Fourth, we estimate the volumetric fraction of each constituent based on the areal fraction of each constituent by using the proper relationship between the circular area and spherical volume. **Table 2.3** summaries the volumetric fractions of the three constituents in the eight particles that are determined based on the CT scan images. It can be seen from **Table 2.3** that the major constituent of all the particles is ceramic material, while the total volumetric fraction of air pockets and resin coating is generally falling below 20%.

Table 2.3 Volumetric fractions of air, resin and ceramic body in the eight resin-coated ceramic particles

Particle No.	Volume fraction of air (α)	Volume fraction of resin (β)	Volume fraction of ceramic body ($1-\alpha-\beta$)
1	0.117	0.044	0.839
2	0.153	0.017	0.830
3	0.134	0.019	0.847
4	0.130	0.067	0.803
5	0.129	0.063	0.808
6	0.161	0.032	0.807
7	0.119	0.055	0.826
8	0.142	0.042	0.816

2.3.2. Apparent Particle Density

The mass of each particle is measured by employing the high-precision electronic balance. **Table 2.4** shows the measured mass of the eight particles. Again, it is noted that the measurement accuracy is ± 0.00001 g.

Table 2.4 Measured mass of the eight resin-coated ceramic particles

Particle No.	Mass, g
1	0.00116
2	0.00035
3	0.00037
4	0.00022
5	0.00011
6	0.00025
7	0.00082
8	0.00082

In this study, three methods are used to predict the density of resin-coated ceramic particles. In previous studies, particles are assumed to be perfect spheres [34]. With this assumption, particle volume can be calculated based on its mean diameter. In method #1, we assume that the resin-coated ceramic particles are perfect spheres. The particle volumes are calculated by the formula of spherical volume, the mean diameters obtained by the CT scan are assumed to be the spherical diameters, and the density is estimated by dividing the measured mass by the spherical volume.

In method #2, based on the measured total mass (shown in **Table 2.4**) as well as the measured volumetric fraction of each constituent (shown in **Table 2.3**), we can then determine the apparent density of each particle as per **Equation 2.12**.

$$\rho_P = \rho_A\alpha + \rho_R\beta + \rho_C(1 - \alpha - \beta) \quad (2.12)$$

where ρ_P is density of particle, ρ_A is density of air, ρ_R is density of resin, and ρ_C is density of ceramic. In this study, the densities of air, resin, ceramic material are 1.1225 kg/m^3 , $1.1 \times 10^3 \text{ kg/m}^3$, and $3.3 \times 10^3 \text{ kg/m}^3$, respectively.

In method #3, as shown in **Table 2.2**, the CT scan can provide a precise particle volume. An alternative method to estimate the particle density is dividing the particle mass by this measured volume.

Table 2.5 shows a comparison among the apparent density of each resin-coated ceramic particle estimated by three aforementioned methods. As shown in **Table 2.5**, the average density estimated by method #1 is the smallest with a value of 2337 kg/m³ among average densities estimated by three methods. This value is much smaller than the value provided by the supplier (2630 kg/m³). This may be caused by overestimating the particle volume. The average densities estimated by methods #2 and #3 are 2759 kg/m³ and 2710 kg/m³, respectively, of which is similar to the average density provided by the supplier. The density of each particle estimated by methods #1 and #3 has a large discrepancy between one another, whereas particle densities estimated by method #2 are similar among all eight samples.

Table 2.5 Comparison among the apparent density of each resin-coated ceramic particle estimated by three aforementioned methods

Particle No.	Mass, g	Volume, ×10 ⁸ μm ³	Density (estimated by method #1), kg/m ³	Density (estimated by method #2), kg/m ³	Density (estimated by method #3), kg/m ³	Average density provided by supplier, kg/m ³
1	0.00116	4.025	2813	2817	2882	2630
2	0.00035	1.324	1970	2758	2643	
3	0.00037	1.446	2515	2816	2559	
4	0.00022	0.969	1915	2724	2270	
5	0.00011	0.458	2303	2736	2402	
6	0.00025	0.745	3282	2698	3356	
7	0.00082	2.953	1975	2786	2776	
8	0.00082	2.938	1922	2739	2791	
Average density, kg/m³			2337	2759	2710	

2.3.3. Settling Velocity of Resin-Coated Ceramic Particles

As mentioned above, we use a high-speed camera to record the settling process during the settling-velocity measurement for each particle. After the particle reaches terminal velocity, we determine it by first counting the number of pictures captured by the high-speed camera when a given particle falls down 1 cm in water; then, based on the shooting speed of the high-speed camera, we can know the duration needed for the particle to travel 1 cm; lastly, the terminal velocity can be readily calculated by dividing the travel distance (1 cm in this case) by the travel duration. **Table 2.6** shows the measured results regarding the terminal velocity of eight resin-coated ceramic particles, and it can be seen that the measured settling velocity can vary from one particle to another, of which can be partially attributed to the difference in the volumes and apparent densities of these particles. According to the measured settling velocity, we can also determine the particle Reynolds number as per **Equation 2.11**. **Table 2.7** lists the measured particle Reynolds number of the eight resin-coated ceramic particles, with the particle Reynolds number ranging from 30 to 140.

Table 2.6 Measured settling velocity of the eight resin-coated ceramic particles

Particle	Settling velocity, cm/s
1	13.33
2	11.76
3	8.70
4	8.00
5	5.88
6	8.00
7	13.33
8	13.33

Table 2.7 Particle Reynolds number of the eight resin-coated ceramic particles

Particle	<i>Re</i>
1	138
2	92
3	64
4	54
5	30
6	47
7	139
8	140

2.3.4. Drag Coefficients of Resin-Coated Ceramic Particles

Before we finally determine the drag coefficient of resin-coated ceramic particles, we need to find out if the particles are spherical, so that we can possibly apply the drag-coefficient correlations developed for spherical particles to the resin-coated ceramic particles used in this study. The supplier has provided an average roundness of 0.9 for these particles, and to verify this high roundness value, we first calculate the equivalent diameter of an imaginary sphere that gives the same volume as a given resin-coated ceramic particle, then we use a parity chart to compare the calculated equivalent diameters and the mean diameters measured by the CT scan (as shown in **Table 2**). **Figure 2.5** shows a parity chart comparing the equivalent diameters against the mean diameters of the eight resin-coated ceramic particles. As shown in **Figure 2.5**, the mean diameters of the eight resin-coated ceramic particles are approximately equal to their equivalent diameters, meaning that the resin-coated ceramic particles are nearly spherical particles.

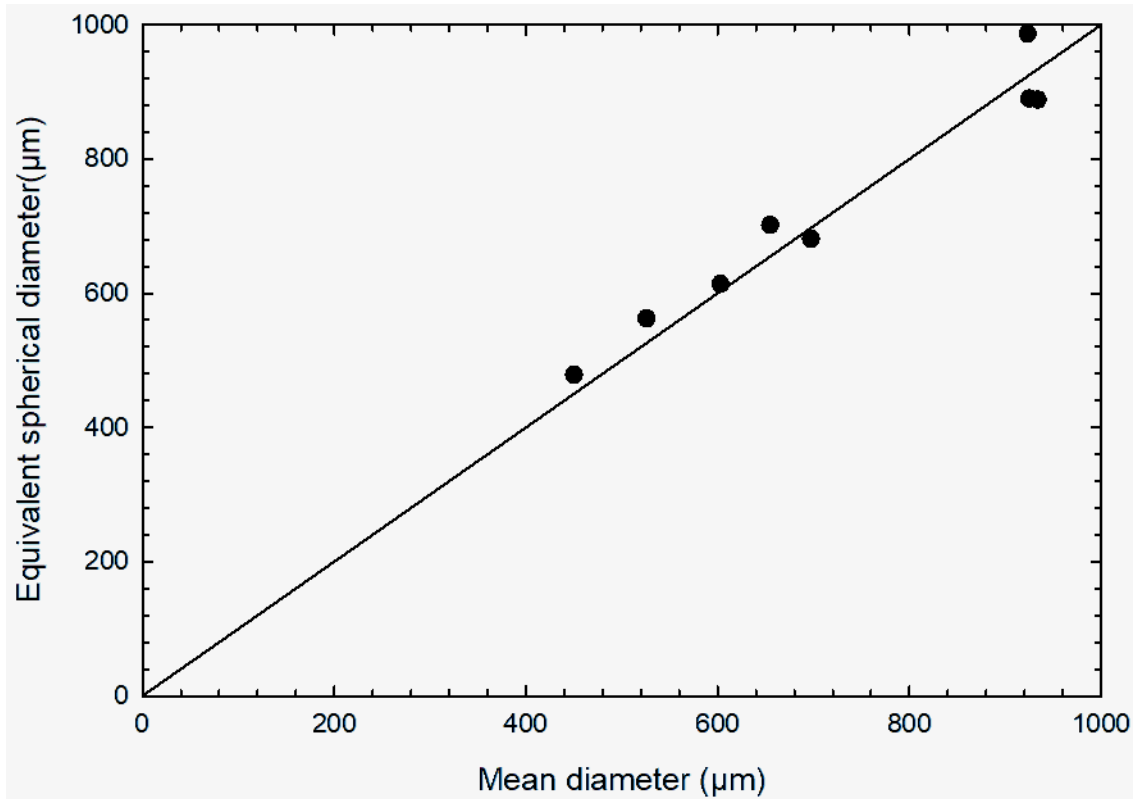


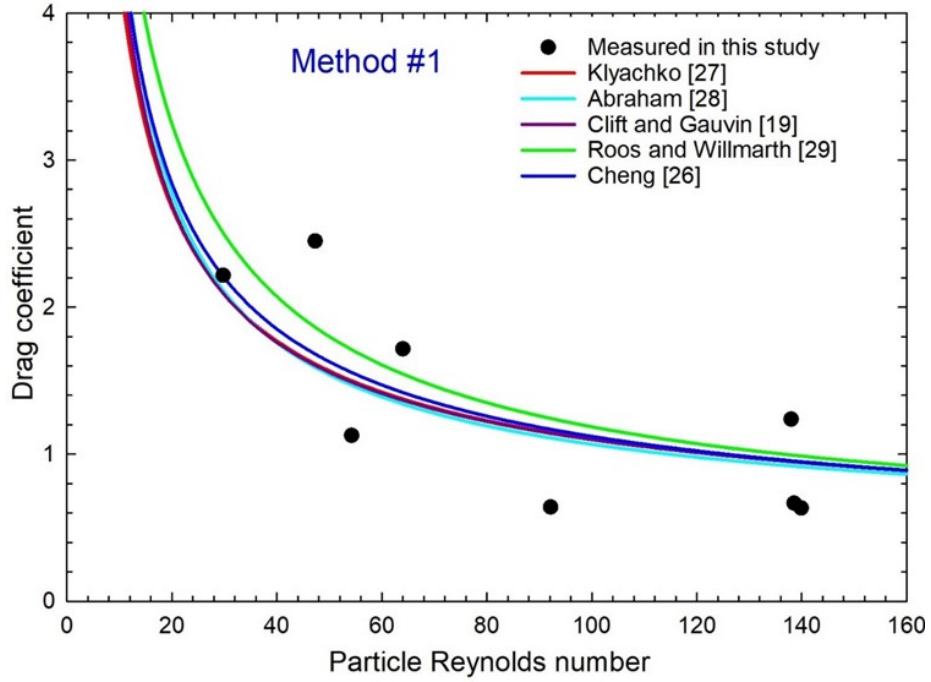
Figure 2.5 Parity chart comparing the equivalent spherical diameter against the mean diameter of the eight resin-coated ceramic particles

Table 2.8 lists five commonly used empirical drag-coefficient correlations developed for spherical particles. R_{ep} in these correlations can be calculated using **Equation 2.11**. These correlations are developed based on the assumption that particles are spheres with a smooth surface; however, our resin-coated ceramic particles are not exactly spherical particles and have rough surface. Therefore, the drag-coefficient calculated by these empirical drag-coefficient correlations cannot accurately describe the drag coefficient of our resin-coated ceramic particles.

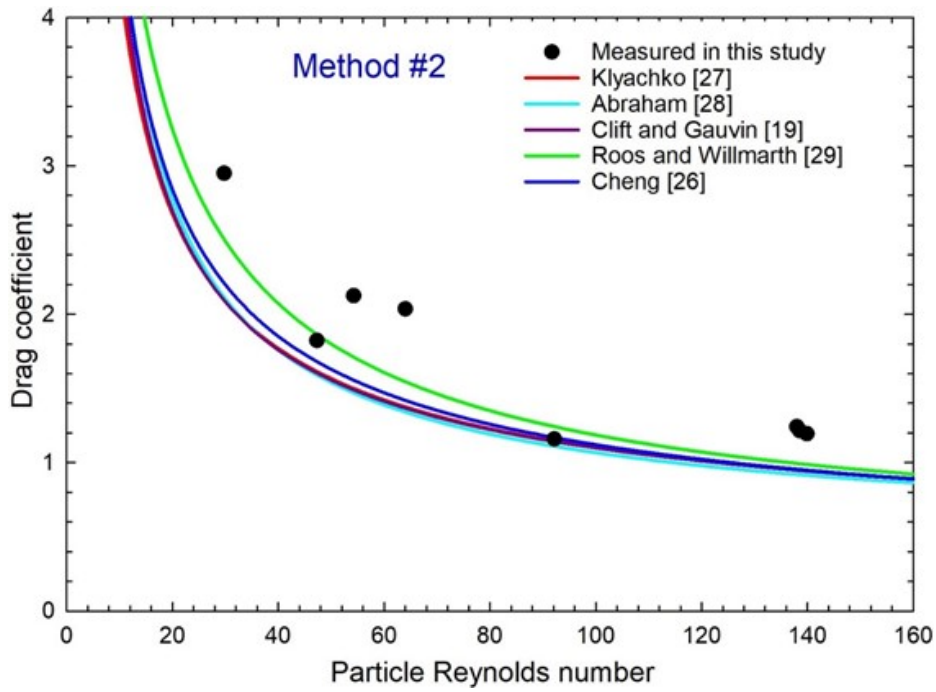
Table 2.8 Summary of five commonly used empirical drag-coefficient correlations developed for spherical particles

Reference	Formula
Clift and Gauvin [19]	$C_D = \frac{24}{Re_p} (1 + 0.15Re_p^{0.687}) + \frac{0.42}{1 + \frac{42500}{Re_p^{1.16}}}$
Klyachko [27]	$C_D = \frac{24}{Re_p} \left(1 + \frac{1}{6} Re_p^{\frac{2}{3}}\right)$
Abraham [28]	$C_D = \left(\sqrt{\frac{24}{Re_p}} + 0.5407\right)^2$
Cheng [26]	$C_D = \frac{24}{Re_p} (1 + 0.27Re_p^{0.687})^{0.43} + 0.47[1 - e^{(-0.04Re_p^{0.38})}]$
Roos and Willmarth [29]	$C_D = \frac{777\left(\frac{669806}{875} + \frac{114976}{1155} Re_p + \frac{707}{1380} Re_p^2\right)}{646Re_p\left(\frac{32869}{952} + \frac{924}{643} Re_p + \frac{1}{385718} Re_p^2\right)}$

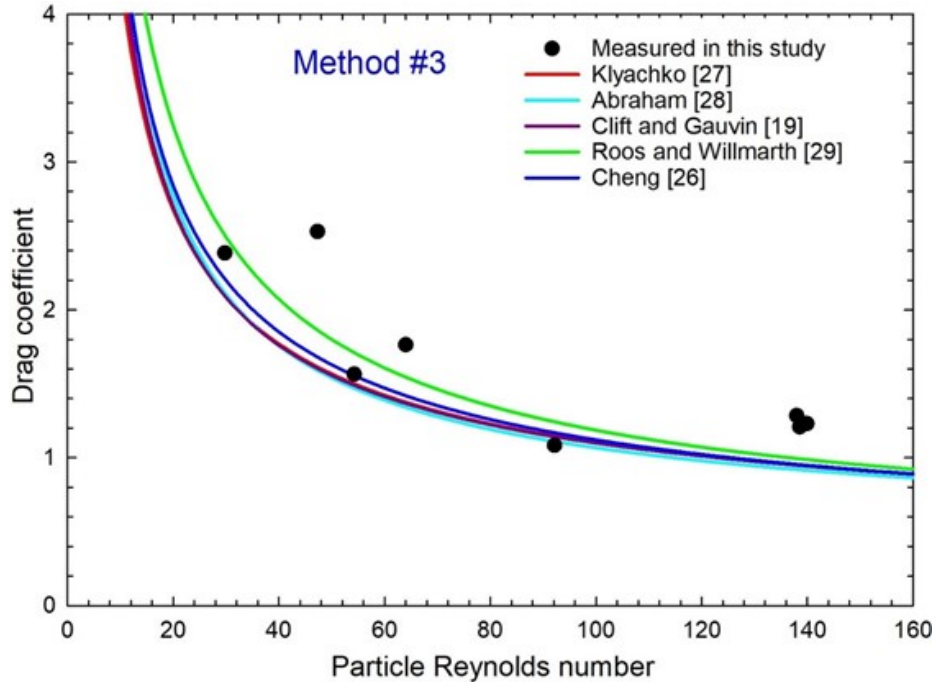
As previously mentioned, the density, mean diameter, and settling velocity of particles have been measured in our experiments. Based on these experimental data, the drag coefficients of resin-coated ceramic particles can be calculated using **Equation 2.10**. **Figure 2.6** illustrates the comparison of the drag coefficients of eight resin-coated ceramic particles determined by our experiments using three methods with the drag coefficient estimated by five empirical correlations (**Table 2.8**). As shown in **Figure 2.6**, similar drag coefficient can be estimated by the five empirical correlations. Moreover, the comparison shows that the drag coefficient of resin-coated ceramic particles, which are estimated based on the aforementioned three methods for density determination, agree generally well with the drag coefficient estimated by the five empirical correlations.



(a)



(b)



(c)

Figure 2.6 Comparison of the drag coefficients of eight resin-coated ceramic particles determined by our experiments using three methods with the drag-coefficients estimated by five empirical correlations [19, 26-29]: (a) experimentally determined drag coefficients using method #1; (b) experimentally determined drag coefficients using method #2; and (c) experimentally determined drag coefficients using method #3

Based on our experiments, it is easy to obtain an accurate settling velocity, mass, and diameter of each particle. The accurate settling velocity and the diameter of a particle can give an accurate particle Reynolds number, based on **Equation 2.11**. However, it is hard to precisely measure the particle volume, leading to an inaccurately estimated particle density. As previously mentioned, we apply three methods to calculate the density of resin-coated ceramic particles, looking to find which method can provide the most accurate density. Since empirical drag-coefficient correlations are proposed based on a large number of experimental data, they are considered to be reliable. Therefore, we can evaluate the accuracy of density estimated by the three methods using the following equation:

$$err = \frac{|\rho_{p_exp} - \rho_{pi}|}{\rho_{pi}} \quad (2.13)$$

where err is absolute relative discrepancy, ρ_{p_exp} is the experimentally determined density, and ρ_{pi} is the so-called “ideal particle density” in this work. The “ideal particle density” of a given particle can be calculated based on a modification of **Equation 2.10** as shown below:

$$\rho_{pi} = \frac{3W_{t_exp}^2 C_{D_emp} \rho}{4gD_{exp}} + \rho \quad (2.14)$$

where W_{t_exp} is the experimentally determined settling velocity of this particle, C_{D_emp} is the drag coefficient calculated by the empirical correlations at the experimentally determined particle Reynolds number of this particle, and D_{exp} is the experimentally measured mean diameter of this particle.

Figure 2.7 shows the average absolute relative discrepancies between the experimentally determined particle density estimated by three methods and “ideal particle density” determined by five empirical correlations. As can be seen from **Figure 2.7**, the average absolute relative discrepancy between the density estimated by method #3 and the “ideal particle density” is the smallest compared with that between the density estimated by methods #1 and #2 and the “ideal particle density”. This result is general for the “ideal particle density” calculated by all five empirical correlations, leading to the conclusion that method #3 can give the most accurate density of the resin-coated ceramic particle. Moreover, the average absolute relative discrepancy between the experimental determined density using method #3 and the “ideal particle density” calculated by Roos and Willmarth’s correlation [29] is the smallest comparing with that between the experimental determined density using method #3 and the “ideal particle density” calculated

by the other four empirical correlations. Therefore, we recommend employing Roos and Willmarth's correlation [29] to calculate the drag coefficients of resin-coated ceramic particles.

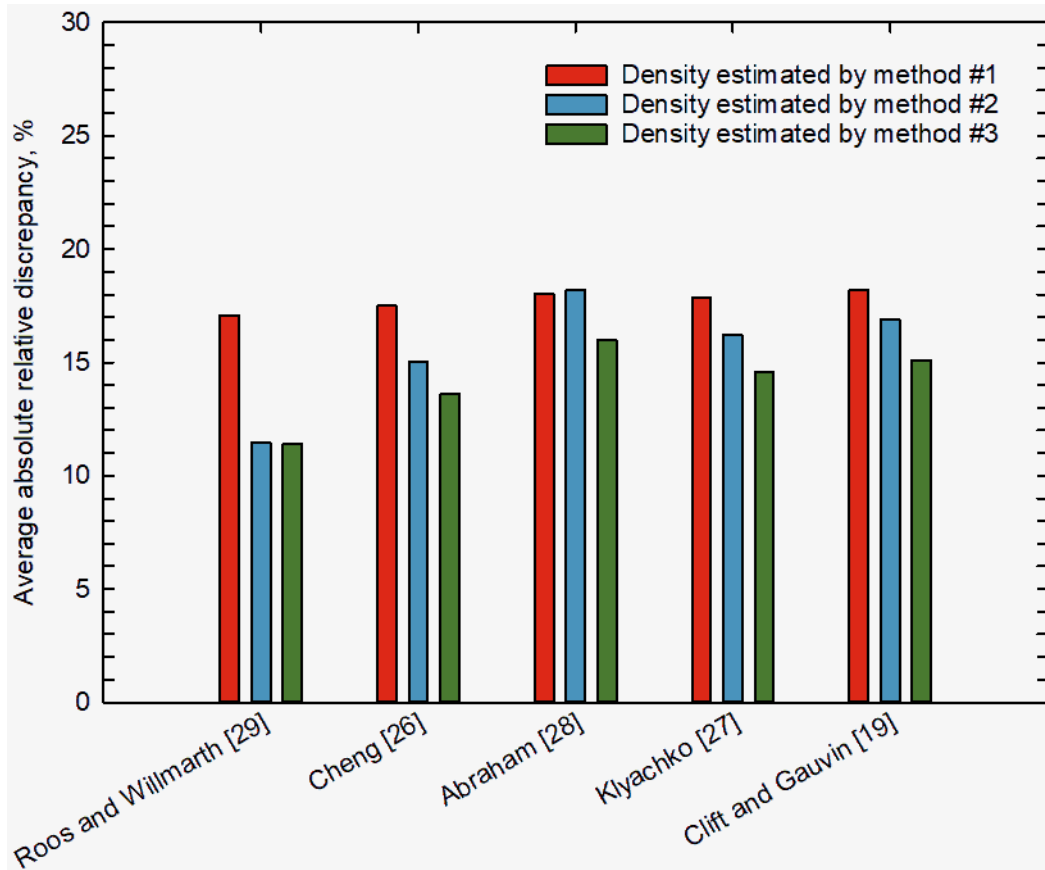


Figure 2.7 Average absolute relative discrepancies between the experimentally determined particle density estimated by three methods and “ideal particle density” determined by five empirical correlations

2.4. Conclusions

This study measures the drag coefficients of resin-coated ceramic particles in a Newtonian fluid. To do this, eight resin-coated ceramic particles are first tested by CT scan technology to accurately measure the volumes, mean diameters, and the fractions of three constituents in particles (i.e., resin, ceramic body, and air pockets), while the high-precision electronic balance is used to obtain an accurate mass of the tested particle. The settling velocities of resin-coated

ceramic particles are calculated by dividing the travel distance of the tested particle in static water by travel durations obtained by a high-speed camera. The most challenging part is the determination of the particle density, due to the difficulties of the measurement of particle volume; three methods are used to estimate the particle density in this research. After obtaining the density, diameter, and settling velocity of the particle, the drag coefficients of resin-coated ceramic particles can be calculated based on these experimental data. Moreover, a comparison is conducted between the density of resin-coated ceramic particles calculated by all three methods and the “ideal particle density”. The major experimental findings can be summarized as follows:

- 1) The resin-coated ceramic particle is not homogenous. There are three constituents of resin-coated ceramic particles: resin, ceramic body, and air pockets. The majority of resin-coated ceramic particles are ceramic body. Based on the eight tested particles, the contents of resin in the resin-coated ceramic particles range from 1.7% to 6.7%, while the contents of air pockets range from 11.7% to 16.1%.
- 2) The surface of the resin-coated ceramic particles is rough with many peaks and valleys.
- 3) The resin-coated ceramic particles are nearly spherical particles.
- 4) The smallest average density was estimated by method #1, with the value being 2337 kg/m³, which is much smaller than the value provided by the supplier (i.e., 2630 kg/m³). The average densities estimated by methods #2 and #3 both have a similar value as that provided by the supplier with the values being 2759 kg/m³ and 2710 kg/m³, respectively.
- 5) Method #3 (CT scan) gives the most accurate densities of resin-coated ceramic particles compared with the densities estimated by methods #1 and #2.
- 6) The average absolute relative discrepancy between the experimentally determined density using method #3 and the “ideal particle density” calculated by Roos and Willmarth’s

correlation [29] is smallest comparing with that between the experimentally determined density using method #3 and the “ideal particle density” calculated by the other four empirical correlations. Therefore, we recommend applying Roos and Willmarth’s correlation [29] to calculate the drag coefficient of resin-coated ceramic particles.

- 7) The discrepancy between the experimentally determined drag coefficients and the drag coefficients calculated by the empirical correlations may be caused by the roughness of the particles or the uneven distribution of resin coating within the particles.

References

- [1] Y. Liu, M.M. Sharma, Effect of fracture width and fluid rheology on proppant settling and retardation: An experimental study. Paper SPE 96208 presented at the SPE Annual Technical Conference and Exhibition, Dallas, Texas, USA, 9-12, October 2005.
- [2] R.A.E.E. Eltilib, H.H. AlKaiem, A. Jaafar, Investigation on the particle settling velocity in non-Newtonian fluids. *J. Appl. Sci.* 11 (9) (2011) 1528-1535.
- [3] W.E. Dietrich, Settling velocity of natural particles. *Water Resour. Res.* 18 (6) (1982) 1615-1626.
- [4] G.G. Stokes, On the effect of the internal friction of fluids on the motion of pendulums. *Trans. Camb. Phil. Soc.* 9 (8) (1851).
- [5] P.A. Reynolds, T.E.R. Jones, An experimental study of the settling velocities of single particles in non-Newtonian fluids. *Int. J. Miner. Process.* 25 (1-2) (1989) 47-77.
- [6] T. Vítěz, P. Trávníček, Study of settling velocity of sand particles located in wastewater treatment plant. *Acta Univ. Agric. Silvic. Mendelianae Brun.* 59 (1) (2014) 249-254.
- [7] J.S. McNown, H.M. Lee, M.B. McPherson, S.M. Engez, Influence of the boundary proximity on the drag of spheres. *Proc. Int. Cong. Appl. Mech.* 31 (1) (1950) 74-82.
- [8] F. Concha, A. Christiansen, Settling velocities of particulate systems, 5. Settling velocities of suspensions of particles of arbitrary shape. *Int. J. Miner. Process.* 18 (3-4) (1986) 309-322.
- [9] M. Hartman, O. Trnka, K. Svoboda, Free settling of nonspherical particles. *Ind. Eng. Chem. Res.* 33 (8) (1994) 1979-1983.

- [10] B.E. Davaadorj, Y. Kim, J. Lee, Settling velocity of irregularly shaped particles in Newtonian fluids. *Geosyst. Eng.* 16 (3) (2013) 225-230.
- [11] F. Dioguardi, D. Mele, A new shape dependent drag correlation formula for non-spherical rough particles. Experiments and results. *Powder Technol.* 277 (2015) 222-230.
- [12] N.S. Cheng, Simplified settling velocity formula for sediment particle. *J. Hydraulic. Eng.* 123 (2) (1997) 149-152.
- [13] A. Haider, O. Levenspiel, Drag coefficient and terminal velocity of spherical and nonspherical particles. *Powder Technol.* 58 (1) (1989) 63-70.
- [14] A. Hölzer, M. Sommerfeld, New simple correlation formula for the drag coefficient of non-spherical particles. *Powder Technol.* 184 (3) (2008) 361-365.
- [15] J. Almedeij, Drag coefficient of flow around a sphere: Matching asymptotically the wide trend. *Powder Technol.* 186 (3) (2008) 218-223.
- [16] P.P. Brown, D. F. Lawler, Sphere drag and settling velocity revisited. *J. Environ. Eng.* 129 (3) (2003) 222–231.
- [17] R.J. Gibbs, M.D. Matthews, D.A Link, The relationship between sphere size and settling velocity. *J. Sediment. Res.* 41 (1) (1971) 7-18.
- [18] R. Ouchene, M. Khalij, B. Acren, A. Taniere, A new set of correlations of drag, lift and torque coefficients for non-spherical particles and large Reynolds numbers. *Powder Technol.* 303 (2016) 33-43.

- [19] R. Clift, W.H. Gauvin, Motion of entrained particles in gas streams. *Can. J. Chem. Eng.* 49 (4) (1971) 439-448.
- [20] R. Turton, O. Levenspiel, A short note on the drag correlation for spheres. *Powder Technol.* 47 (1) (1986) 83-86.
- [21] R.L.C. Flemmer, C.L. Banks, On the drag coefficient of a sphere. *Powder Technol.* 48 (3) (1986) 217-221.
- [22] A.R. Khan, J.F. Richardson, The resistance to motion of a solid sphere in a fluid. *Chem. Eng. Commun.* 62 (1-6) (1987) 135-150.
- [23] R. Elgaddafi, R. Ahmed, M. George, F. Growcock, Settling behavior of spherical particles in fiber-containing drilling fluids. *J. Petrol. Sci. Eng.* 84-85 (2012) 20-28.
- [24] Z.D. Hensley, D.V Papavassiliou, Drag coefficient correction for spherical and nonspherical particles suspended in square microducts. *Ind. Eng. Chem. Res.* 53 (25) (2014) 10465-10474.
- [25] G.H. Ganser, A rational approach to drag prediction of spherical and nonspherical particles. *Powder Technol.* 77 (2) (1993) 143-152.
- [26] N.S. Cheng, Comparison of formulas for drag coefficient and settling velocity of spherical particles. *Powder Technol.* 189 (3) (2009) 395-398.
- [27] L.S. Klyachko, Equations of motion of dust particles in dust collectors. *Otoplenie Ventilyatsiya*, 4 (1934).
- [28] F.F Abraham, Functional dependence of drag coefficient of a sphere on Reynolds number. *Phys. Fluids.* 13 (8) (1970) 2194-2195.

- [29] F.W. Roos, W.W. Willmarth, Some experimental results on sphere and disk drag. *AIAA J.* 9 (2) (1971) 285-291.
- [30] M.D. Mikhailov, A.P.S. Freire, The drag coefficient of a sphere: An approximation using Shanks transform. *Powder Technol.* 237 (2013) 432-435.
- [31] D. Droppert, P. Fiore, Y. Dessureault, F. Cardarelli, High strength, heat- and corrosion-resistant ceramic granules for proppants. Canadian Patent CA 2329834 (2002).
- [32] M. Makhuvha, R.M. Arellano, D.M.W. Harney, Determination of bulk density, methods and impacts, with a case study from Los Bronces Mine, Chile. *Appl. Earth. Sci.* 123 (3) (2014) 196-205.
- [33] E.P. Cox, A method of assigning numerical and percentage value to the degree of roundness of sand grains. *J. Paleontol.* 1 (3) (1927) 179-183.
- [34] G. Bagheri, C. Bonadonna, On the drag of freely falling non-spherical particles. *Powder Technol.* 301 (2016) 526-544.

**CHAPTER 3 A VISUAL EXPERIMENTAL STUDY: RESIN-COATED CERAMIC
PROPPANTS TRANSPORT WITHIN ROUGH VERTICLE MODELS**

3.1. Introduction

Hydraulic fracturing is one commonly used well stimulation technique in petroleum engineering, which is mainly used for creating fractures in tight formations [1-3]. In hydraulic fracturing, the formations are cracked by injecting fluid at a high flow rate [4]. After the fractures are created by pressurized fluid, a fracturing fluid mixed with proppants is usually pumped into the induced hydraulic fractures [5]. Proppants transport and settle inside the newly formed fractures [6]. When the fluid injection stage is over, the fractures tend to close due to the formation stresses [7]. But the proppants injected into the fractures can maintain the opening of the fractures, leading to the enhancement of conductivity of fractures [8-11]. In general, the final distribution of proppants in the induced fractures plays a pivotal role in determining the fracture conductivity.

However, one severe issue that needs to be prevented if we are injecting the proppants into the formations is proppants flow back [12]. Proppants flow back occurs when the proppants injected into fractures flow back to the surface [13]. Several concerns are associated with the proppant flow back. First, flow back of the proppants could damage the downhole equipments [14]. Second, the width of the fractures decreases when proppants flow back occurs, which will reduce the effective length of the fractures and efficiency of the fracturing treatment [15]. Therefore, to ensure the success of hydraulic fracturing, it is highly necessary to implement measures to prevent the flow back of proppants and improve the placement of proppants in fractures.

Resin-coated ceramic proppant is one promising proppant that can mitigate the proppants flow back issue [16-18]. The thin layer of resin coated on the surface of ceramic particles contributes to the bonding of the proppant particles and the formation of relatively stable sediment [13]. Besides, resin coating can provide good encapsulation of each particle, helping to maintain a good integrity of the proppant bed [16]. In addition, resin-coated ceramic proppants combine the

technical characteristics of resin-coated sands and ceramic proppants. Compared to traditional proppants, the resin-coated ceramic proppants exhibit the following advantages: 1) Higher crushing strength and compressive strength than silica sands and resin-coated silica sands; 2) Good chemical and thermal stability; 3) Lower specific gravity than ceramic proppants [16]. These advantages enable resin-coated ceramic proppants to be suitable for deep well applications, but the high cost makes them primarily suitable to be placed in the near-wellbore region.

Previous experimental studies have examined the effects of some major influential factors on proppant transport in fractures in order to improve proppants placement and maximize the volume occupied by proppants within the fractures, including injection rate, wall effect and rough surface of the fractures [19]. For example, by increasing the injection rate, the equivalent height of proppant bed will become smaller, which allows more proppants to be transported to deeper locations and hence increases the effective length of fractures [19-22]. In addition, it is found that proppants collide with the fracture surface during the settling process of proppants in a small fracture aperture, which is called as wall effect [23, 24]. Liu and Sharma showed that the wall effect does not dramatically influence the distribution of settling particles unless the aperture is 10%-20% larger than the particle diameter [24]. Moreover, the rough fracture surface will retard the settling of proppants, leading to accumulation of proppants in fractures [25-29]. Besides the aforementioned three factors, the injection location at the fracture-wellbore interface, proppants type, and slurry type have a remarkable impact on the distribution of proppants in fractures. However, there is a lack of understanding of the transport and distribution behavior of the resin-coated ceramic proppants in rough fractures since there is no available experimental studies on this subject. It is necessary to conduct further experiments to investigate the settling

characteristics and transport behavior of resin-coated ceramic proppants in rough vertical fractures.

Our research group completes a series of experiments to investigate the proppants transport in rough vertical fractures prior to this study, but no experiments has been conducted to study the transport behavior of the resin-coated ceramic proppants in rough vertical fractures [30, 31]. Hence, in this work, we study the transport behavior of the resin-coated ceramic proppants based on visual experimental methods, i.e., monitoring the injection pressure across the vertical fracture model and recording the distribution of the proppants in the fracture models. The effects of major influential factors on the proppants transport and distribution behavior have been experimentally studied, including the location of the injection point, proppants type, fracturing fluid type, flow rate, particle size of proppants, fracture aperture and fracture model type. These experimental results presented in this study may shed some light on the optimal design of hydraulic fracturing treatment involving the use of resin-coated ceramic proppants.

3.2. Experimental Section

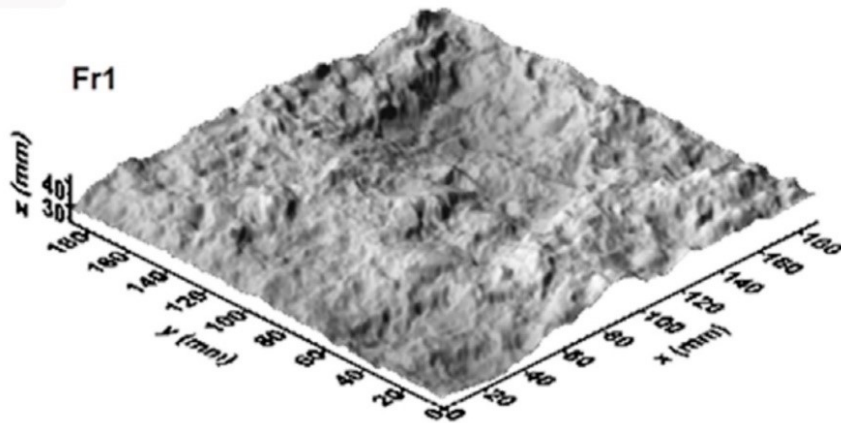
3.2.1. Materials

Three rough surface fracture models used by Raimbay *et al.* have been used in the study [32-34]. A transparent plastic is mounted on one side of the fracture models for the convenience of observation, while a non-transparent silicone rubber is mounted on the other side. Fracture models are made with a size of $20 \times 20 \times 5$ cm. The fracture models are made of epoxy resin and silicone rubber and can maintain the structure stability during the proppant-laden slurry injection. We can quantify the roughness of fracture surface using four fractal factors [35]. **Figure 3.1** shows 3D images of the rough surfaces of fracture models Fr.1, Fr.4, and Fr.5 models [36].

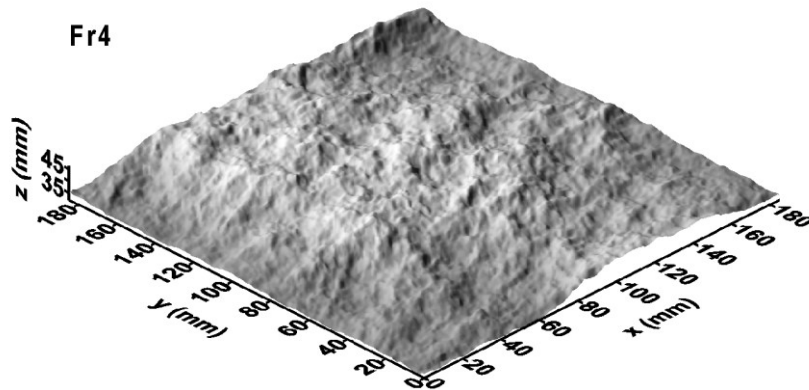
Table 3.1 Lithological properties of the rock samples and the roughness parameters for the surface of model fractures [26]

Fracture model	Material	^a D_{va}	^b D_{psd}	^c D_{tp}	^d A_t/A_p	Average grain size (mm)
Fr.1	Beige limestone with abundant coarse fossil shells	1.373	2.277	2.012	1.145	Not measured
Fr.4	Coarse-grained white marble	1.390	2.418	2.009	1.098	3
Fr.5	Holocrystalline amphibole granite	1.299	2.335	2.008	1.083	2

Note: a: D is the fractal dimension, va is the variogram analysis; b: D is the fractal dimension, psd is the power spectral density; c: D is the fractal dimension, tp is the triangular prism; d: A_t/A_p is the ratio of the total area to the planar fracture surface.



(a)



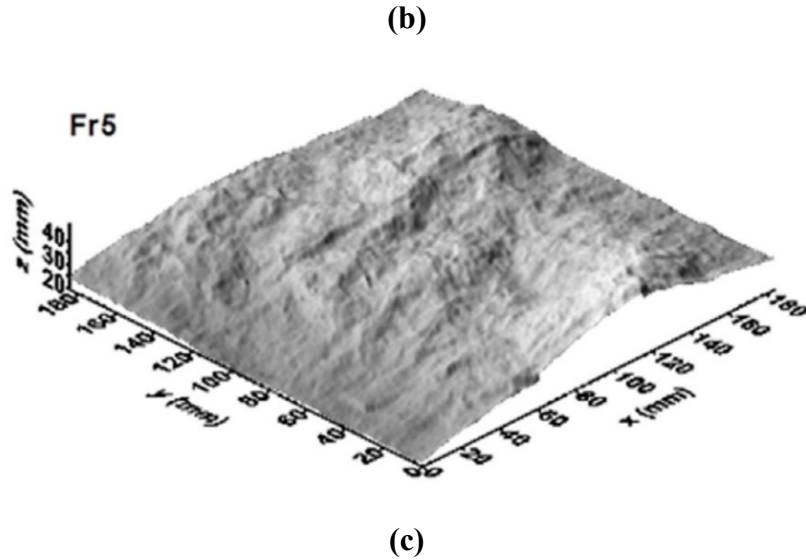


Figure 3.1 3D images of the rough surfaces of fracture models Fr.1 (a), Fr.4 (b) and Fr.5 (c) [26]

In this study, the tap water and slickwater are used to carry the resin-coated ceramic proppants into the fracture models. The viscosities of the tap water and slickwater are 8.9×10^{-4} cp and 5.32 cp, respectively. The slickwater contains 0.08 wt% guar. The resin-coated ceramic proppants (Henan Tianxiang New Material Co., LTD, China) with sizes of 20-40 mesh and 30-50 mesh and a bulk density of 1.46 g/cm^3 are used as the propping agents in the experiments.

3.2.2. Experimental Setup

The setup used for conducting the proppants transport experiments is shown in **Figure 3.2**. One propeller is used to rigorously stir the slurry prepared in a 100-gallon tank in order to ensure a good suspension of proppants in the slurry before being pumped into the fracture models. A progressive cavity pump (NM031BY02S12B, NEMO PUMP, Germany) is used to inject the proppant-laden slurry into the vertical fracture. The maximum flow rate of this pump is 30 L/min. The flow rate may be altered through the variable frequency drive (SK 90L/4 TF F, NORD, Germany). A pressure transducer (DMF-1-4, Beijing Sincerity Automatic Equipment Co., LTD, China) equipped with a data acquisition system is utilized to monitor the pressure across the

vertical fracture. The measuring range of the pressure transducer is 0-30 MPa. The distribution of proppants in the fracture model at different times is recorded by a camera (Nikon D7100, Nikon, Japan). In the flow experiments, the flow inlet is a point source injection, while the flow outlet is along the whole right edge of the fracture model.

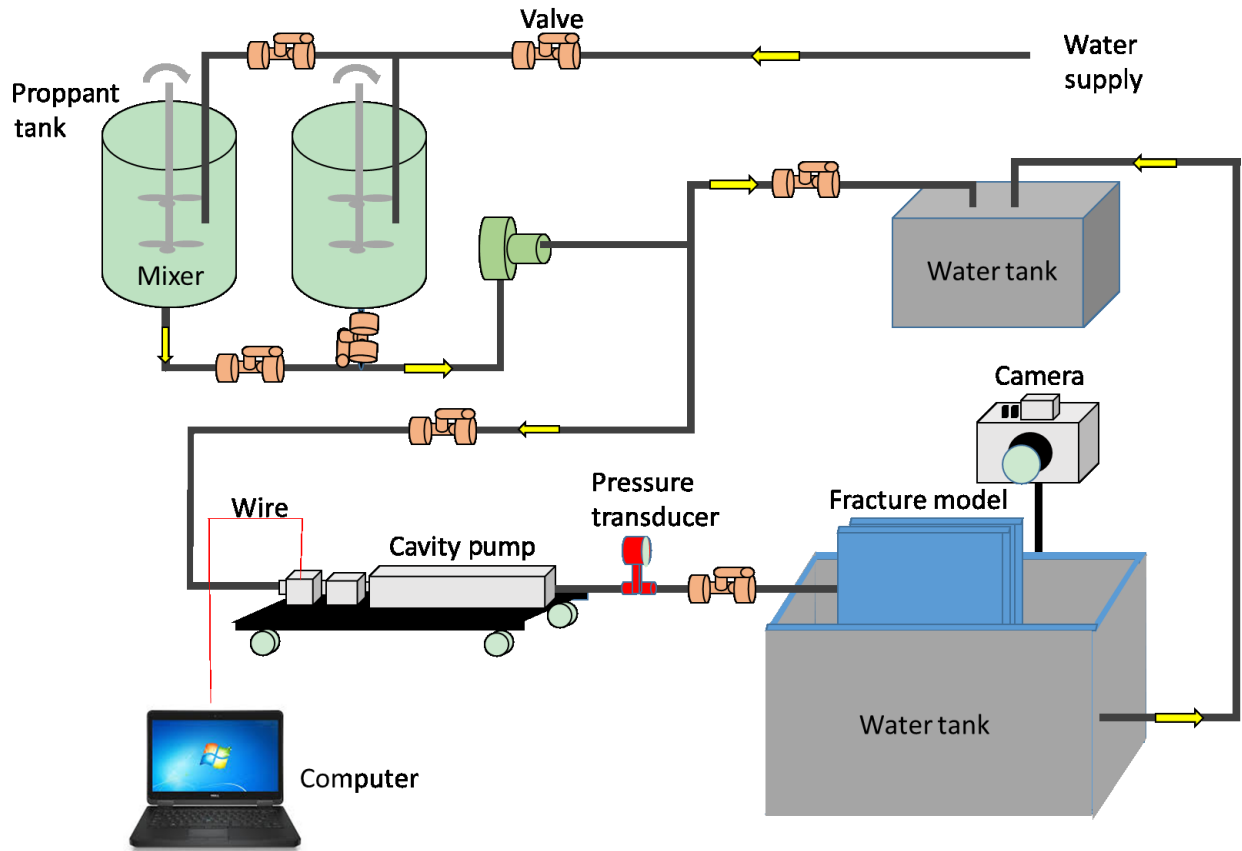


Figure 3.2 Schematic of the experimental setup used for conducting the proppants transport experiments

3.2.3. Experimental Procedure

The slurry and proppants are first blended using the propeller in a 100-gallon container. Then, the progressive cavity pump is used to pump the slurry into the rough vertical fracture model. As the slurry is being pumped into the fracture models, we use the camera to real-time record the slurry flow in the rough vertical fractures. Meanwhile, the injection pressure is recorded by a

pressure transducer; such measured pressure reflects the differential pressure across the fracture model as the flow outlet of the fracture model is open to the air.

We study the effect of major influential factors on the distribution and transport behavior of proppants in rough surface fracture models, including the location of the injection point (top and bottom), proppants type (silica sands and resin-coated ceramic proppants), slurry type (tap water and slickwater), flow rate (10 L/min and 12 L/min), proppants size (20-40 mesh and 30-50 mesh), fracture aperture (2 mm and 4 mm) and type of fracture models (Fr.1, Fr.4, and Fr.5). **Table 3.2** lists the detailed conditions used in the proppants flow experiments. In total, we have conducted 27 experiments to study the transport behavior and distribution of resin-coated ceramic proppants in vertical rough surface models.

Table 3.2 Experimental conditions used in the proppants flow experiments

Run No.	Fracture model	Mesh	Fracture aperture, mm	Injection rate, L/min	Type of proppant	Injection point	Duration, s	Slurry type
1	Fr.1	20-40	2	10	Resin-coated ceramic proppant	Top	80	Tap water
2	Fr.1	20-40	2	10	Resin-coated ceramic proppant	Bottom	80	Tap water
3	Fr.1	20-40	2	10	Silica sand proppant	Top	80	Tap water
4	Fr.1	20-40	2	12	Resin-coated ceramic proppant	Top	80	Tap water
5	Fr.1	30-50	2	10	Resin-coated ceramic proppant	Top	80	Tap water
6	Fr.1	30-50	2	10	Resin-coated ceramic proppant	Bottom	80	Tap water
7	Fr.1	30-50	2	10	Resin-coated ceramic proppant	Top	80	Slickwater

8	Fr.1	30-50	2	12	Resin-coated ceramic proppant	Top	80	Tap water
9	Fr.1	30-50	4	10	Resin-coated ceramic proppant	Top	80	Tap water
10	Fr.4	20-40	2	10	Resin-coated ceramic proppant	Top	80	Tap water
11	Fr.4	20-40	2	10	Resin-coated ceramic proppant	Bottom	80	Tap water
12	Fr.4	20-40	2	10	Silica sand proppant	Top	80	Tap water
13	Fr.4	20-40	2	12	Resin-coated ceramic proppant	Top	80	Tap water
14	Fr.4	30-50	2	10	Resin-coated ceramic proppant	Top	80	Tap water
15	Fr.4	30-50	2	10	Resin-coated ceramic proppant	Bottom	80	Tap water
16	Fr.4	30-50	2	10	Resin-coated ceramic proppant	Top	80	Slickwater
17	Fr.4	30-50	2	12	Resin-coated ceramic proppant	Top	80	Tap water
18	Fr.4	30-50	4	10	Resin-coated ceramic proppant	Top	80	Tap water
19	Fr.5	20-40	2	10	Resin-coated ceramic proppant	Top	80	Tap water
20	Fr.5	20-40	2	10	Resin-coated ceramic proppant	Bottom	80	Tap water
21	Fr.5	20-40	2	10	Silica sand proppant	Top	80	Tap water
22	Fr.5	20-40	2	12	Resin-coated ceramic proppant	Top	80	Tap water
23	Fr.5	30-50	2	10	Resin-coated ceramic proppant	Top	80	Tap water

24	Fr.5	30-50	2	10	Resin-coated ceramic proppant	Bottom	80	Tap water
25	Fr.5	30-50	2	10	Resin-coated ceramic proppant	Top	80	Slickwater
26	Fr.5	30-50	2	12	Resin-coated ceramic proppant	Top	80	Tap water
27	Fr.5	30-50	4	10	Resin-coated ceramic proppant	Top	80	Tap water

3.3. Results and Discussion

3.3.1. Typical Proppant Settling Patterns

In the 27 flow experiments, we can observe four representative types of proppant settling patterns in the fracture model. **Figure 3.3** shows the four typical proppant settling patterns of resin-coated ceramic proppants observed in the experiments. As for Type #1 (**Figure 3.3a**), the resin-coated ceramic proppants cannot fully fill the proppant bed and some parts inside the proppant bed are hollow. This incomplete-filling phenomenon is different from the observation made in the flow experiments which were conducted using flat glass models [30]; in the flow experiments using flat glass models, the proppant bed does not have hollow spots. The incomplete filling of the proppant bed is mainly caused by the rough nature of the fracture model [17]. As for Type #2 (**Figure 3.3b**), the resin-coated ceramic particles gradually settle down, forming a complete proppant bed. As for Type #3 (**Figure 3.3c**), the proppant bed consists of two parts: a lower stable layer formed by the resin-coated ceramic particles and an upper fluidized layer being mobilized by the slurry. As for Type #4 (**Figure 3.3d**), a stable proppant

bed cannot be formed due to the large flow rate used in the experiments. In the 27 experiments, the most commonly observed proppant settling pattern is Type #2.

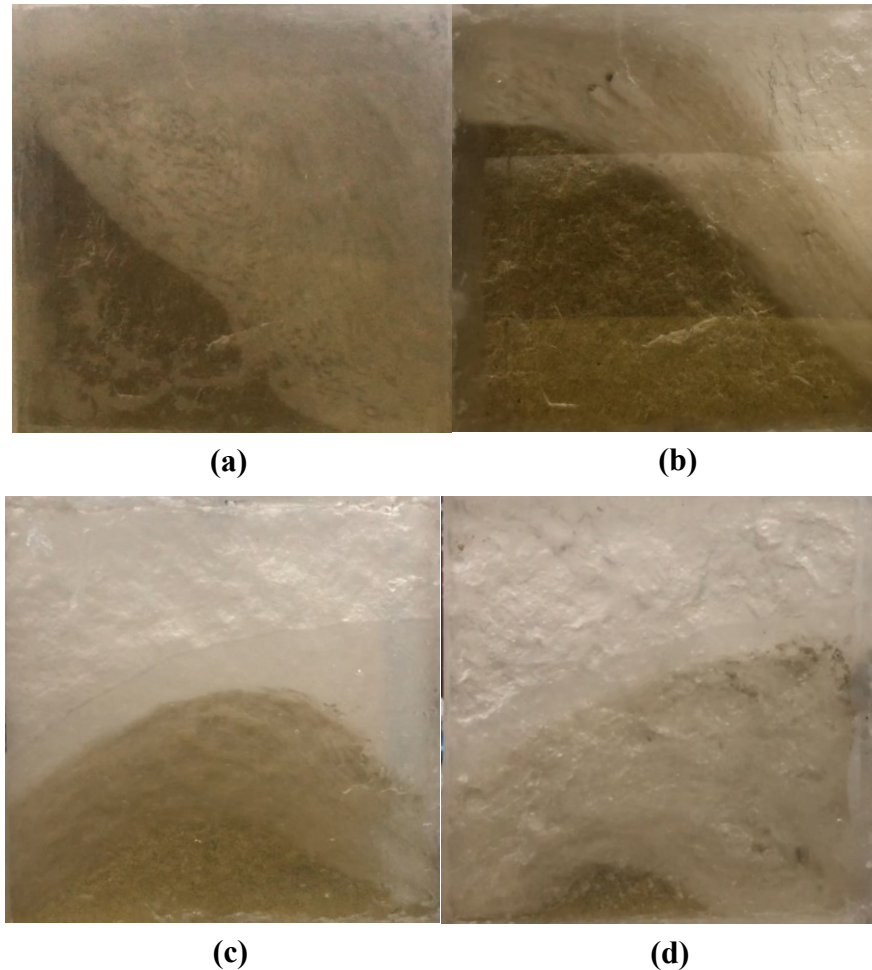
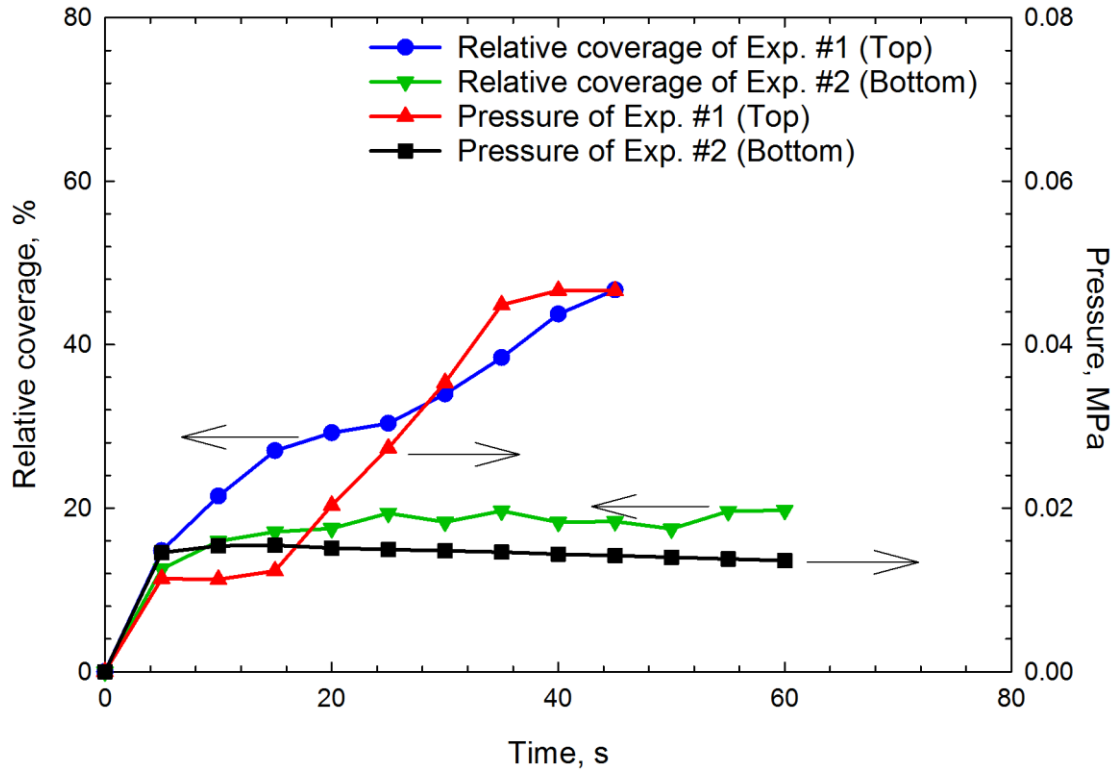


Figure 3.3 Four typical distributions of resin-coated ceramic proppant observed in the experiments: (a) Type #1: an image captured at 40 seconds in Experiments #22; (b) Type #2: an image captured at 40 seconds in Experiments #10; (c) Type 3: an image captured at 40 seconds in Experiments #2; and (d) Type #4: an image captured at 40 seconds in Experiments #19.

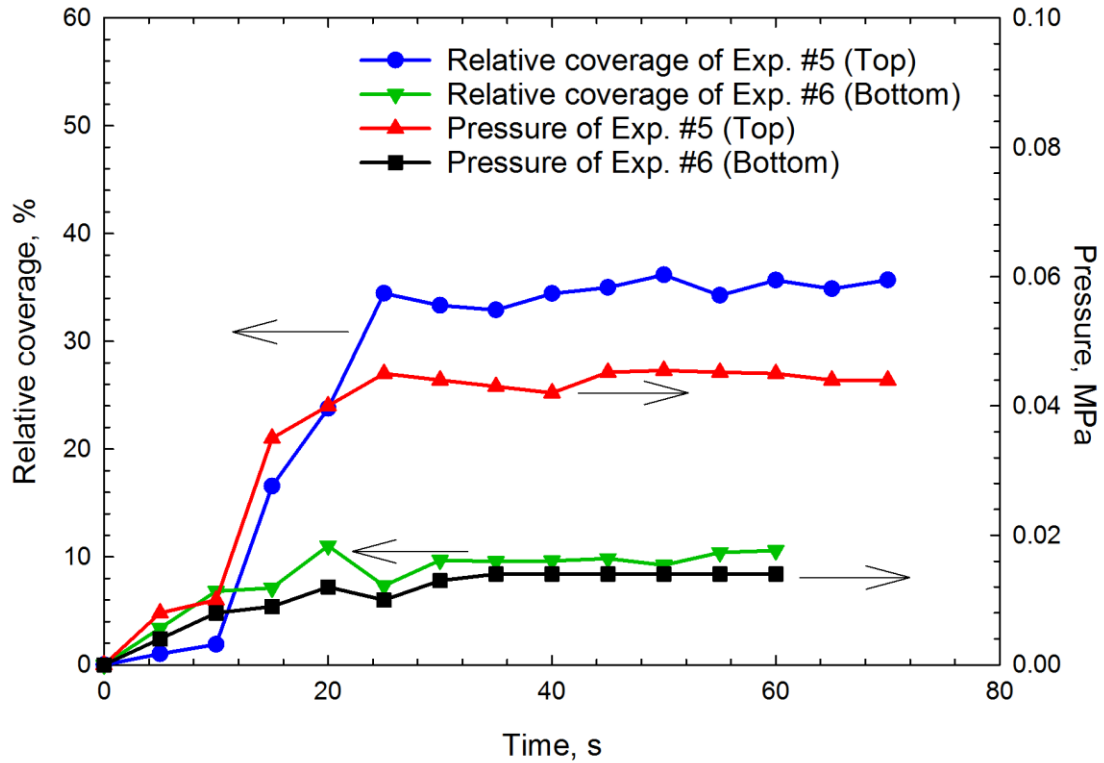
3.3.2. Effect of Injection Point

We define a quantitative index, namely the relative coverage of proppants in the fracture, to quantify the filling area of the proppants in the fracture [30]. The relative coverage of proppants in the fracture is defined as the ratio of the area occupied by the proppants to the whole area of the fracture model. The more area occupied by the proppants, the higher relative coverage of

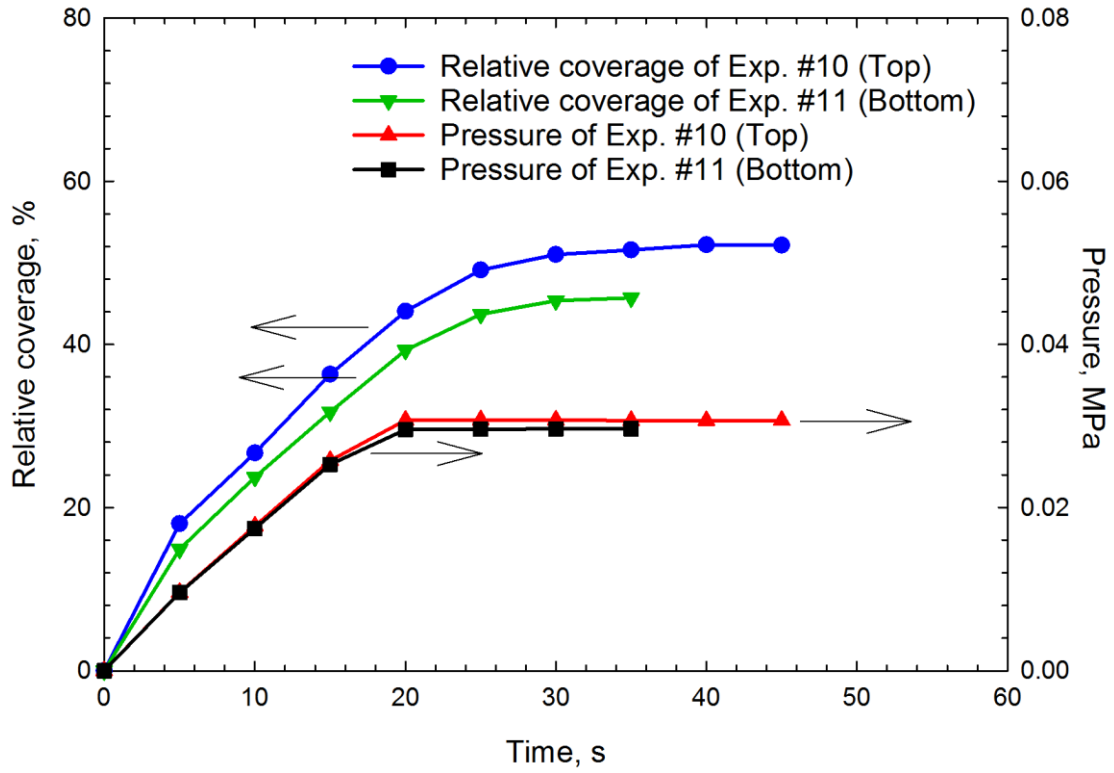
proppants in the fracture. **Figure 3.4** shows the changes of relative coverage and pressure as time elapses in Experiments #1, #2, #5, #6, #10, #11, #14, #15, #19, #20, #23 and #24; these experiments are conducted to study the effect of injection point on the proppant settling behavior in rough fracture models. Experiments #1 #5, #10, #14, #19, and #23 are conducted by injecting the proppant-laden fluid into fracture models through the top injection point, while Experiments #2, #6, #11 #15, #20 and #24 are conducted by injecting proppant-laden fluid through bottom injection point. As shown in **Figure 3.4**, the relative coverage increases as time elapses, while the injection pressure increases with an increase in the relative coverage. When more proppants are filling up the fracture, a larger flow friction ensues, which leads to a higher injection pressure. With other experimental conditions kept the same, the relative coverage obtained at a given time by injecting resin-coated ceramic proppants through the top injection point is larger than that obtained by injecting resin-coated ceramic proppants through the bottom injection point. Such result is physically understandable. When the proppants are injected into the fracture models through the top injection point of the fracture models, the particles can settle down gradually and form a proppant bed. However, when the proppant is injected into the fracture models through the bottom injection point, the high velocity of the slurry at the bottom of fracture models can dramatically decrease the height of proppant bed, resulting in low relative coverage of the proppants in the fracture models. These results imply that, when multistage hydraulic fracturing is applied to a horizontal well, proppants have a tendency to first fill up the lower side of the transverse fractures, ultimately leading to the creation of preferentially propped fractures.



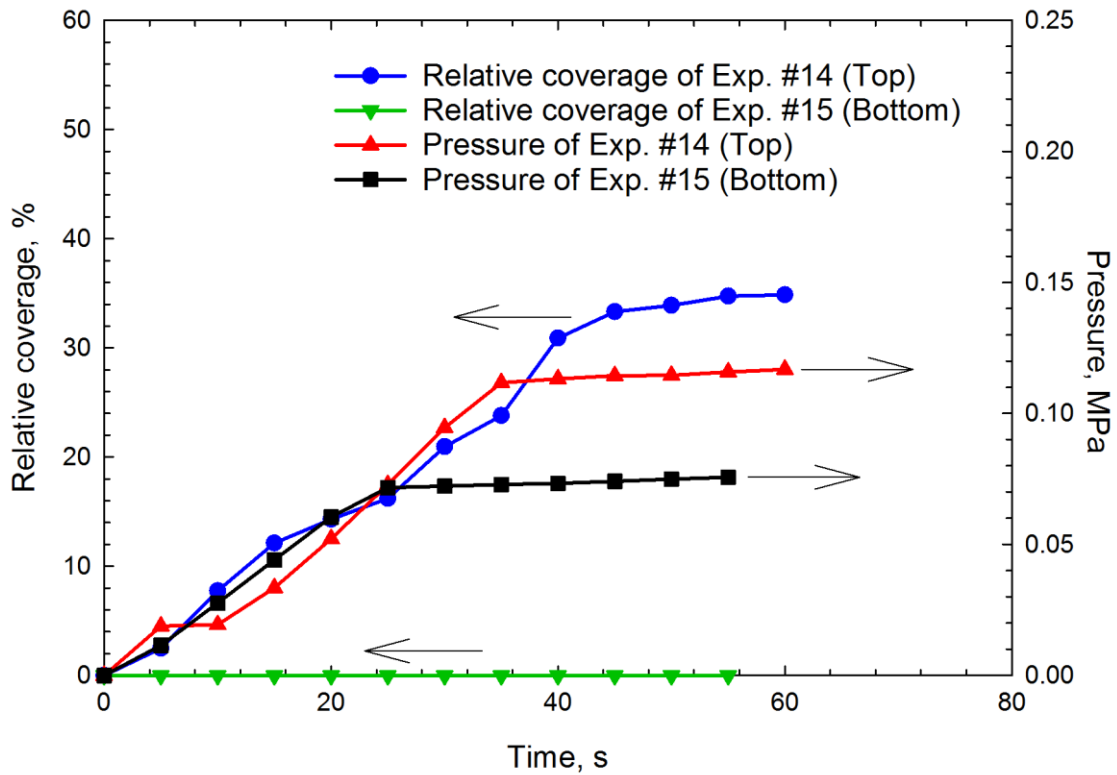
(a)



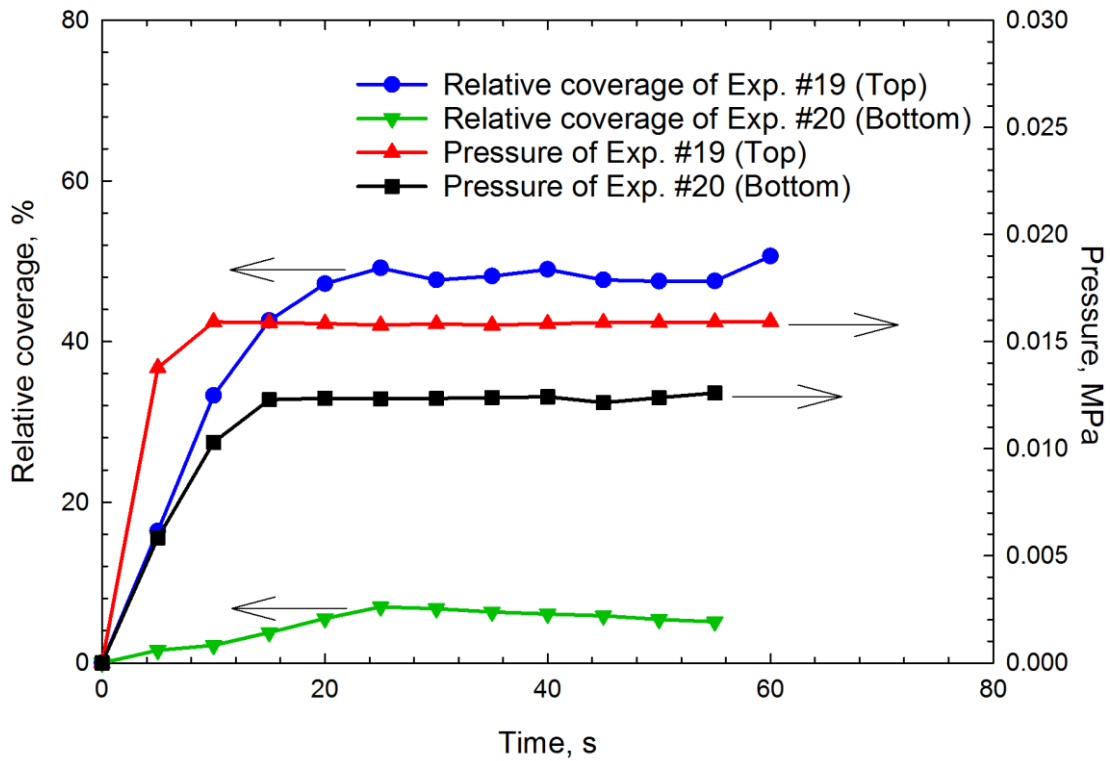
(b)



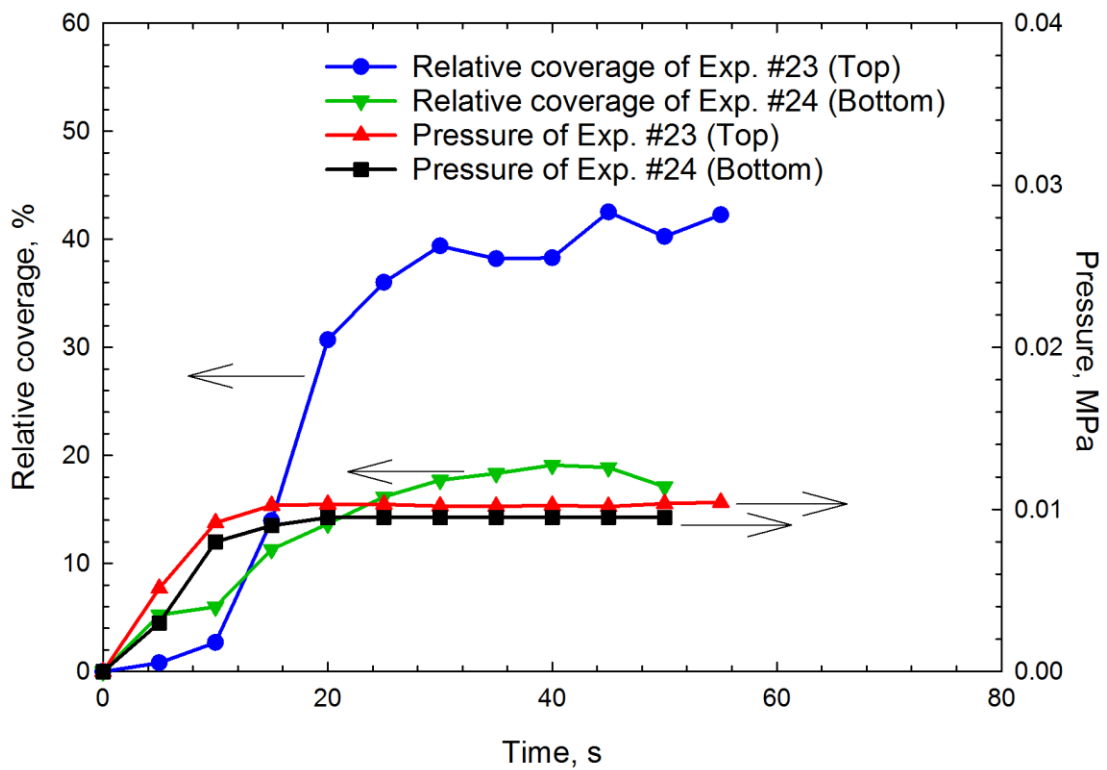
(c)



(d)



(e)

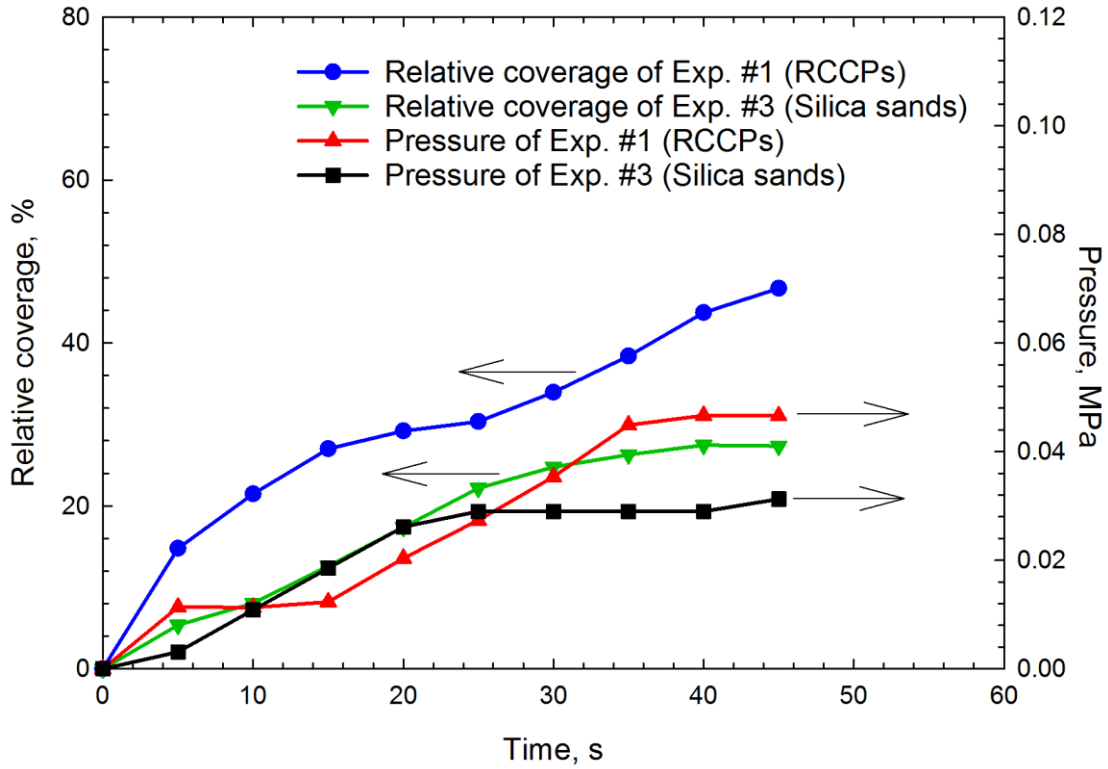


(f)

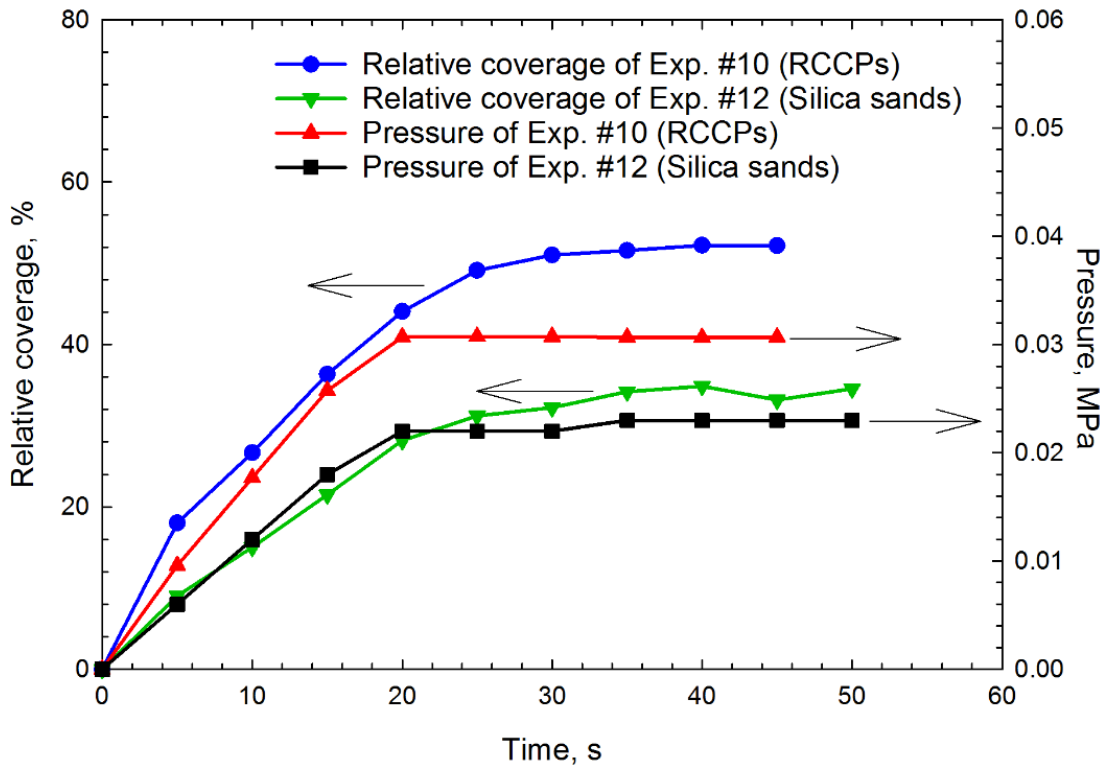
Figure 3.4 Changes in relative coverage of resin-coated ceramic proppants and pressure as time elapses: (a) evolution of the relative coverage and pressure recorded for Experiments #1 and #2; (b) evolution of the relative coverage and pressure recorded for Experiments #5 and #6; (c) evolution of the relative coverage and pressure recorded for Experiments #10 and #11; (d) evolution of the relative coverage and pressure recorded for Experiments #14 and #15; (e) evolution of the relative coverage and pressure recorded for Experiments #19 and #20; and (f) evolution of the relative coverage and pressure recorded for Experiments #23 and #24. These experiments are conducted to study the effect of injection point on the proppant settling behavior in rough fracture models.

3.3.3. Effect of Proppant Type

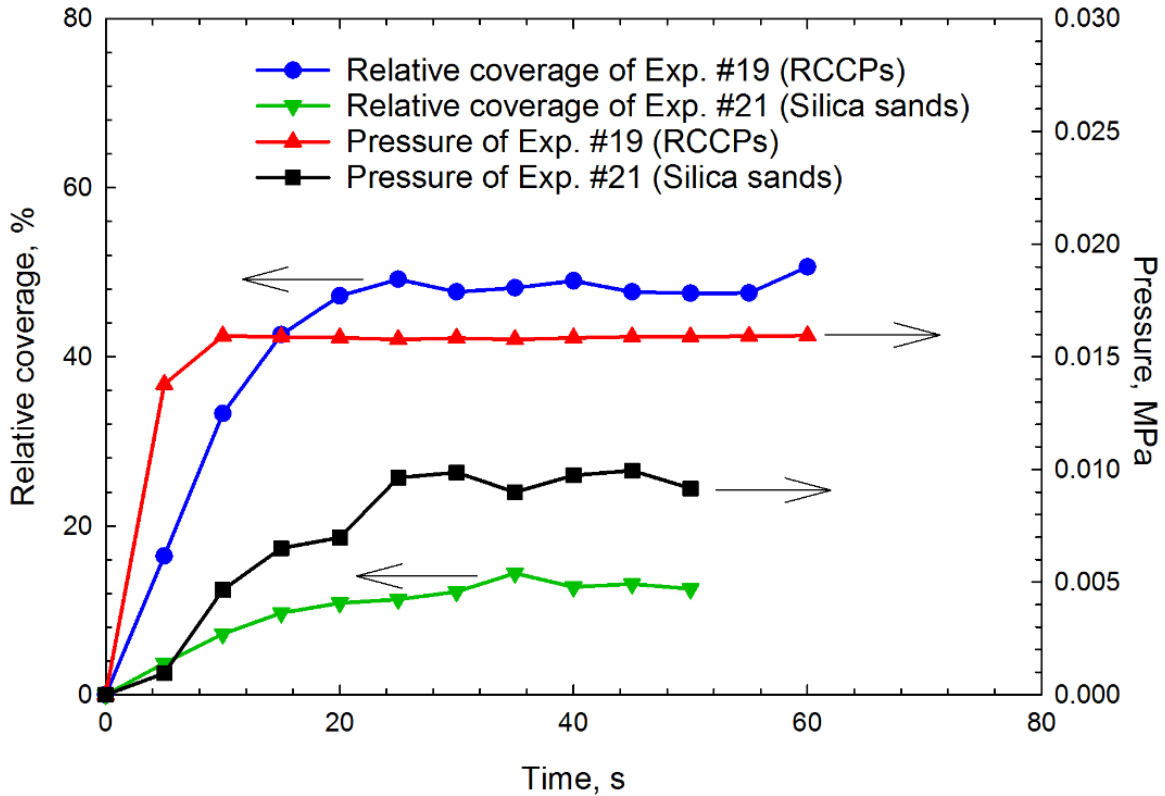
Figure 3.5 shows the change in the relative proppant coverage and injection pressure as time elapses in Experiments #1, #3, #10, #12, #19, and #21. These experiments are conducted to study the effect of proppant type on the proppant settling behavior in rough fracture models. Experiments #1, #10, and #19 are conducted by using resin-coated ceramic proppants, while Experiments #3, #12, and #21 are conducted by using traditional silica sands. As shown in **Figure 3.5**, with other experimental conditions kept the same, the relative coverage of resin-coated ceramic proppants obtained at a given time is always larger than that of silica sands. The density of resin-coated ceramic particles is much higher than that of silica sands due to the high density of the ceramic material used to prepare the resin-coated ceramic particles. As aforementioned in **Chapter 2**, a higher particle density contributes to a higher settling velocity of the proppant particles. Therefore, the proppant bed formed by resin-coated ceramic particles is much larger than that formed by silica sands, resulting in a larger relative coverage of resin-coated ceramic proppants. In addition, the injection pressure increases as more area of the fracture model has been covered by proppants.



(a)



(b)











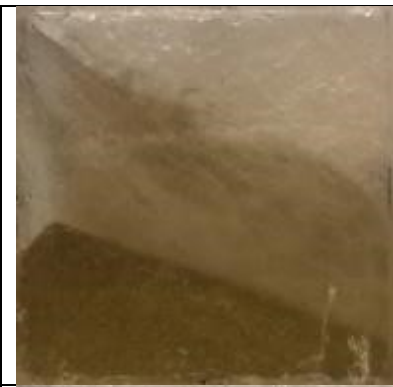







(c)

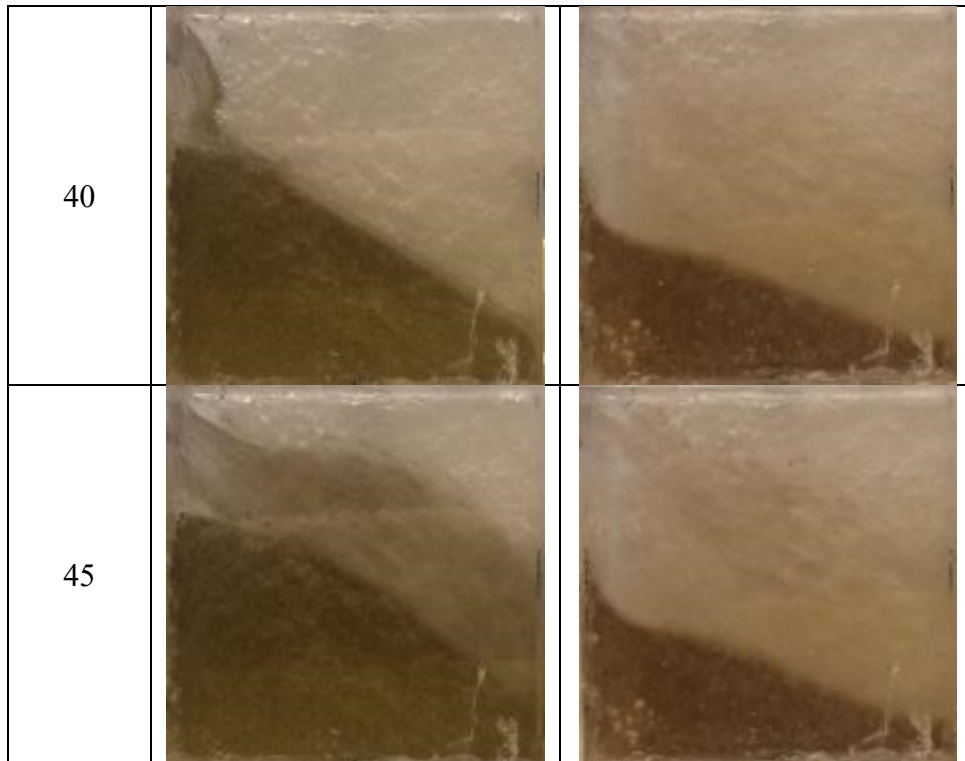
Figure 3.5 Changes in the relative coverage of resin-coated ceramic proppants and pressure as time elapses: (a) evolution of the relative coverage and pressure recorded for Experiments #1 and #3; (b) evolution of the relative coverage and pressure recorded for Experiments #10 and #12; and (c) evolution of the relative coverage and pressure recorded for Experiments #19 and #21. These experiments are conducted to study the effect of proppant type on the proppant settling behavior in rough fracture models.

Table 3.3 shows the images obtained at different times during Experiments #1 and #3. The area occupied by the resin-coated ceramic proppants increases as time elapses. The resin-coated ceramic proppants settle down quicker than the silica sands. Meanwhile, the final relative coverage of resin-coated ceramic proppants is larger than that of silica sands. In general, the present study shows that the resin-coated ceramic proppants can occupy more area of the fracture model and thus can provide a better performance in maintaining the opening of fractures than silica sands.

Table 3.3 Digital images captured at different time during Experiments #1 and #3

Time, s	#1 Resin-coated ceramic	#3 Silica sand
0		
5		
10		
15		

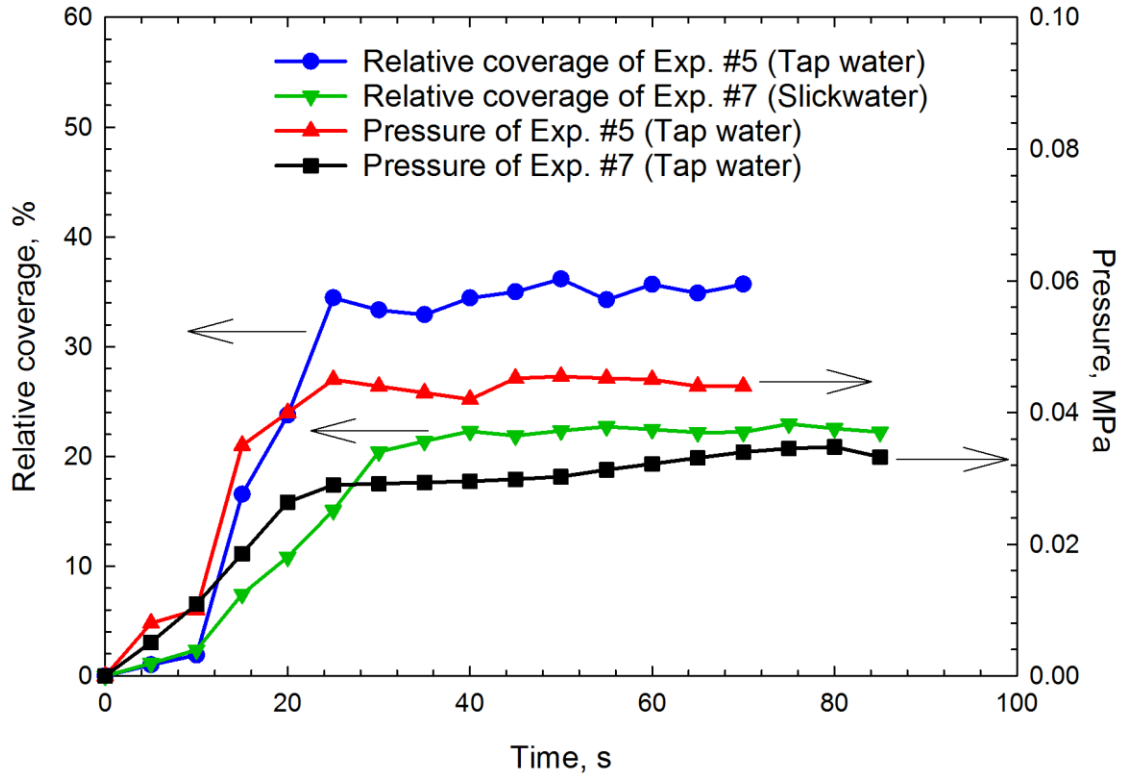
20		
25		
30		
35		



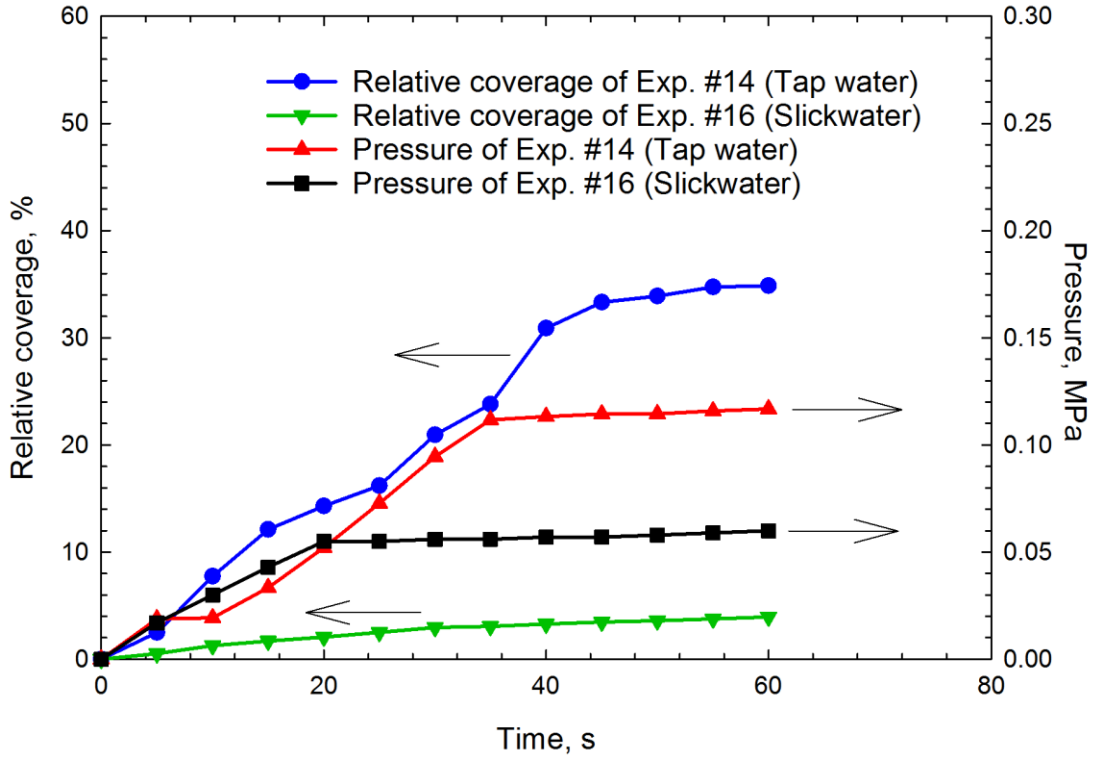
3.3.4. Effect of Fracturing Fluid Type

Two types of fracturing fluid are used to carry the proppants into the fracture models. The fracturing fluid used in Experiments #5, #14, and #23 is tap water, while the fracturing fluid used in #7, #16 and #25 is slickwater. Other experimental conditions are kept the same. **Figure 3.6** shows the changes in relative coverage of resin-coated ceramic proppants and pressure as time elapses in Experiments #5, #7, #14, #16, #23, and #25. As seen from **Figure 3.6**, at a given time, the flow experiments conducted with the tap water yields a larger relative proppant coverage than the slickwater. Accordingly, the injection pressure recorded in the experiments using the tap water is higher than that recorded in the experiments using the slickwater. We postulate that the reason behind this result is that the slickwater with a low-concentration polymer can act as a friction reducer, leading to a lower pressure required to pump the slickwater slurry through the rough fracture model than the tap water counterpart; thus more proppants can be carried into

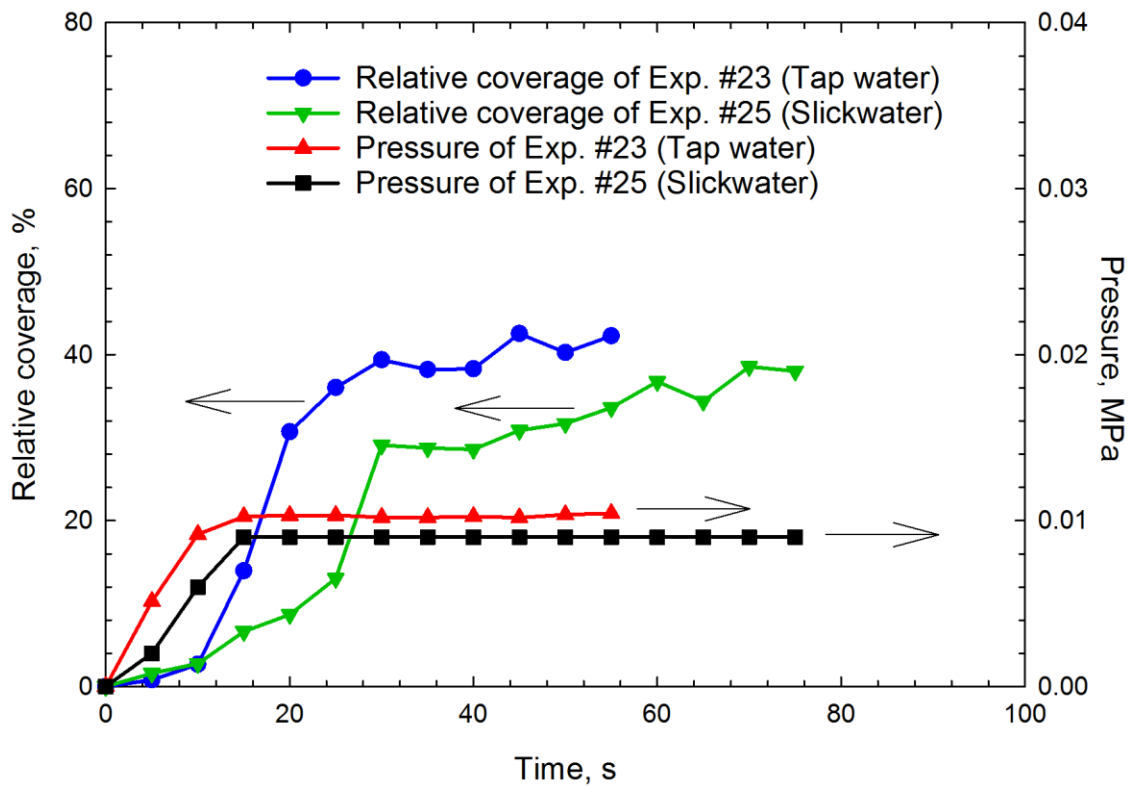
deeper locations of the fracture, eventually resulting in a lower relative coverage of resin-coated ceramic proppants carried by slickwater than that obtained using the tap water.



(a)



(b)

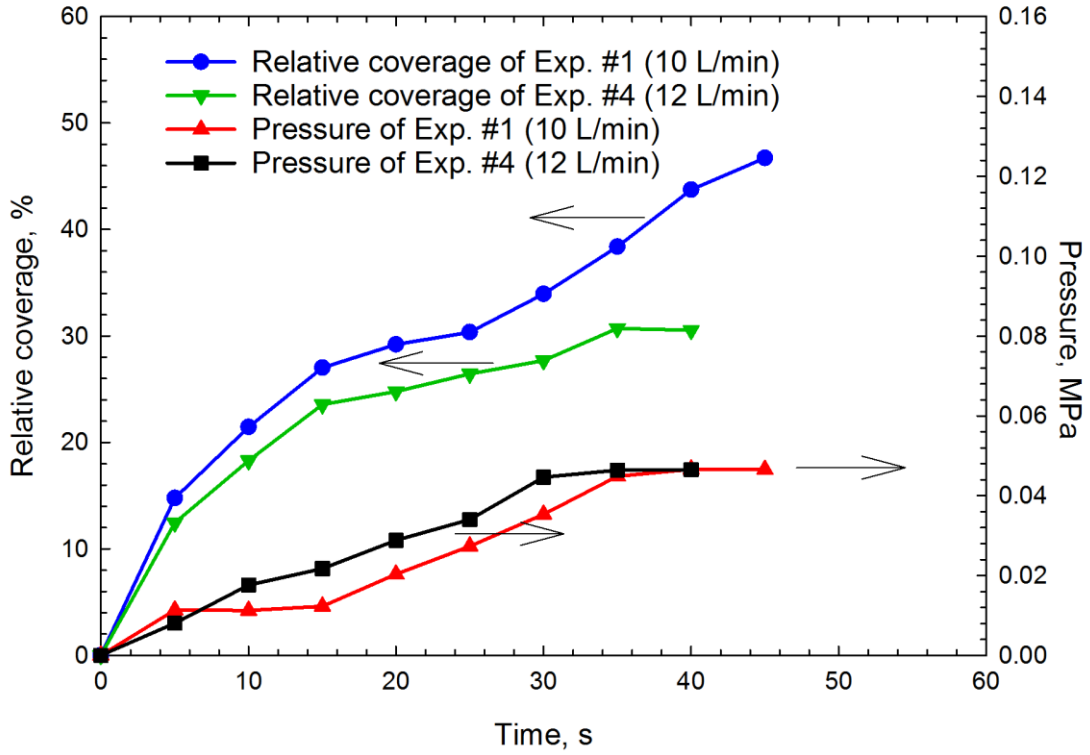


(c)

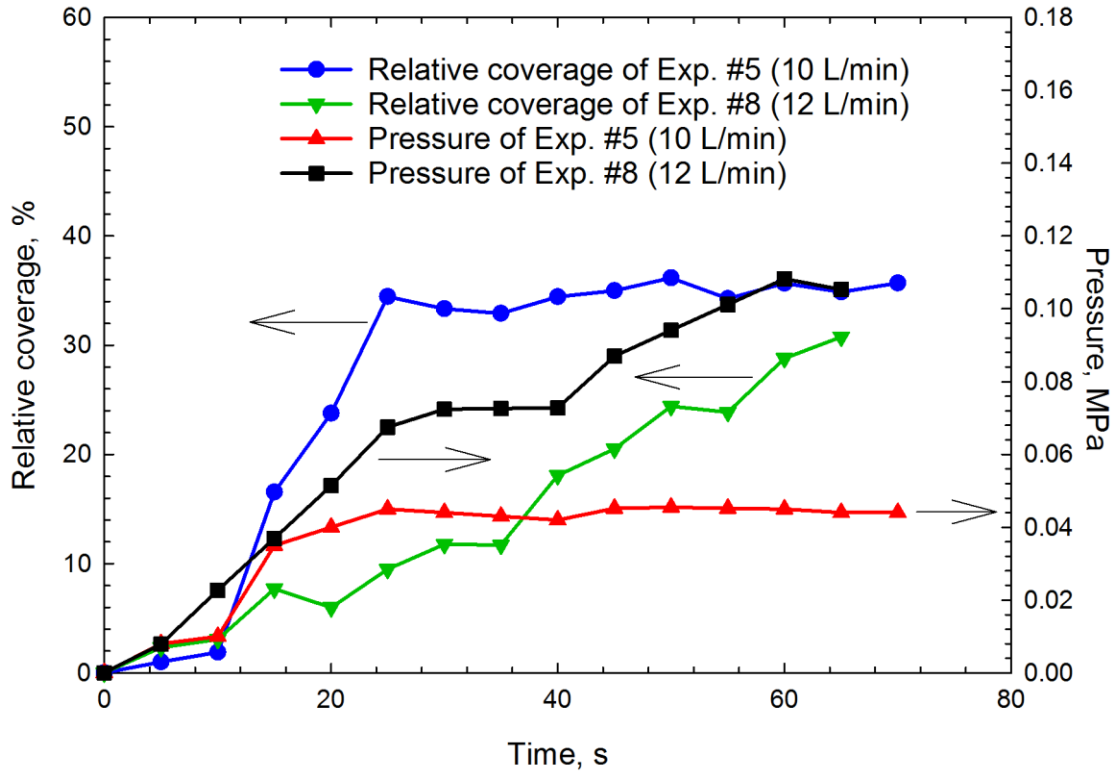
Figure 3.6 Changes in the relative coverage of resin-coated ceramic proppants and pressure as time elapses: (a) evolution of the relative coverage and pressure recorded for Experiments #5 and #7; (b) evolution of the relative coverage and pressure recorded for Experiments #14 and #16; and (c) evolution of the relative coverage and pressure recorded for Experiments #23 and #25. These experiments are conducted to study the effect of fracturing fluid type on the proppant settling behavior in rough fracture models.

3.3.5. Effect of Flow Rate

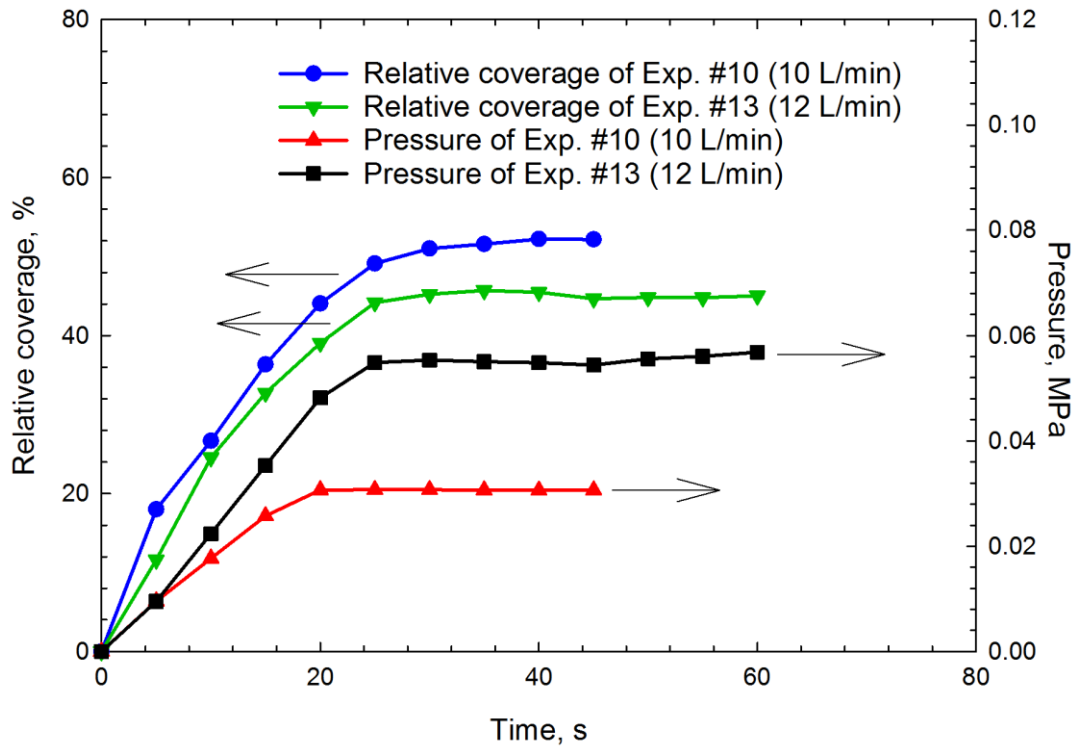
Figure 3.7 shows the changes in the relative coverage of resin-coated ceramic proppants and pressure as time elapses in Experiments #1, #4, #5, #8, #10, #13, #14, #17, #19, #22, #23 and #26. The injection rate used in Experiments #1, #5, #10, #14, #19, and #23 is 10 L/min, while that used in Experiments #4, #8, #13, #17, #22, and #26 is 12 L/min. As seen from **Figure 3.7**, at a given time, the relative coverage of resin-coated ceramic proppant obtained with the injection rate of 10 L/min is higher than obtained with the injection rate of 12 L/min. This can be attributed to the fact that a higher injection rate may carry proppants into deeper locations of fractures, but due to the limited length of the fracture model, fewer proppants will precipitate in the 20 cm fracture model; this is one of the drawbacks of the present experimental work. Besides, the injection pressures recorded in Experiments #4, #8, #13, #17, #22, and #26 are higher than those recorded in Experiments #1, #5, #10, #14, #19, and #23. This is because a higher flow rate requires a high injection pressure to pump the slurry across the fracture model.



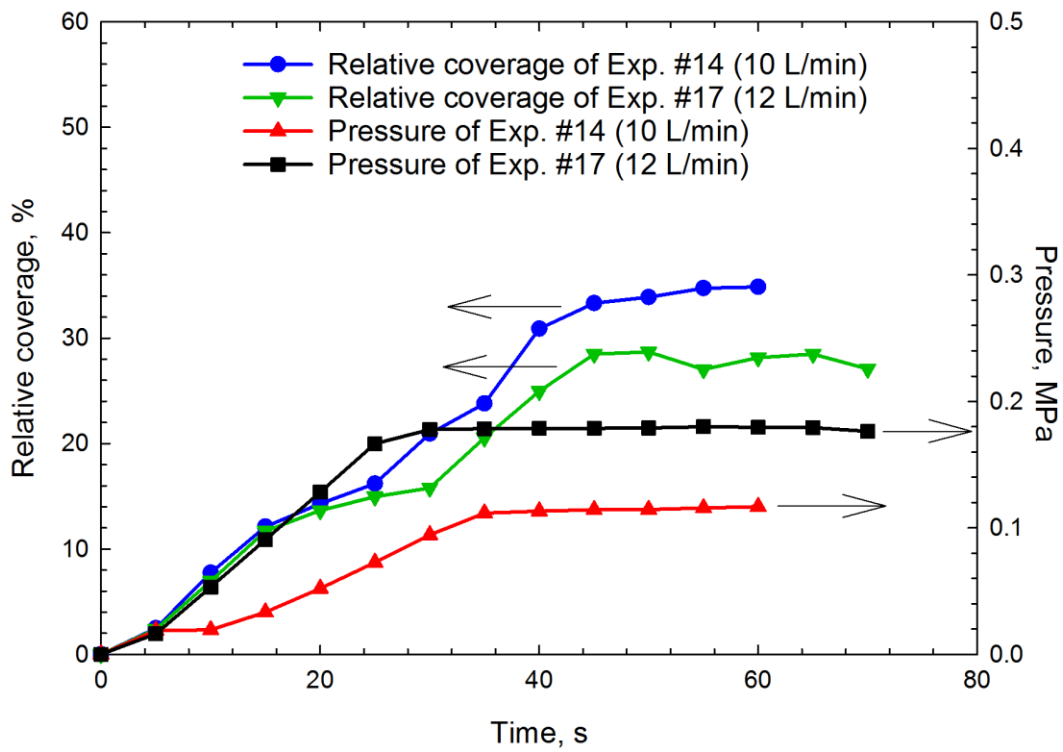
(a)



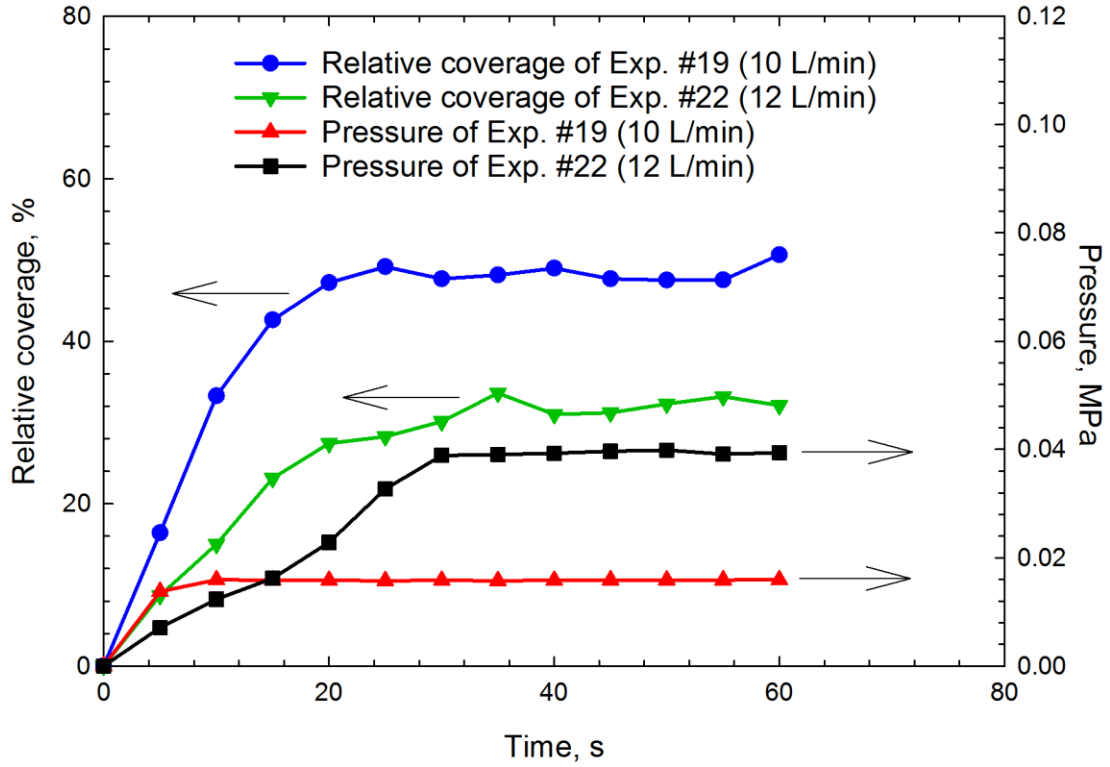
(b)



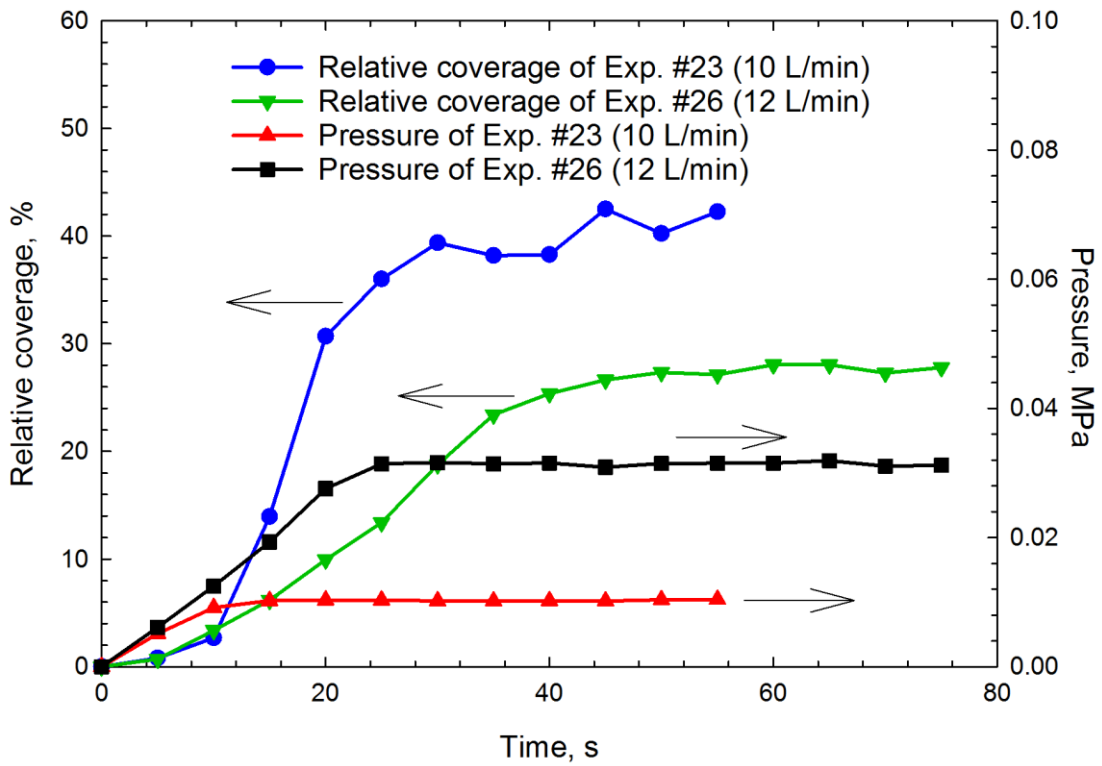
(c)



(d)



(e)

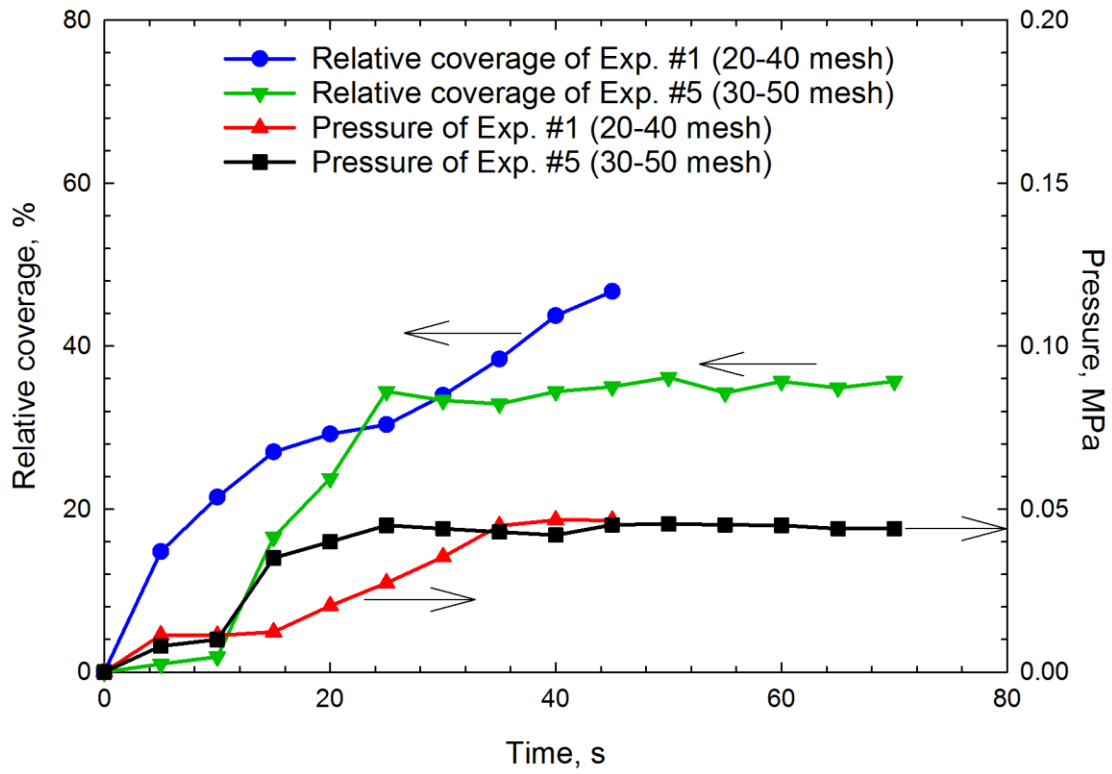


(f)

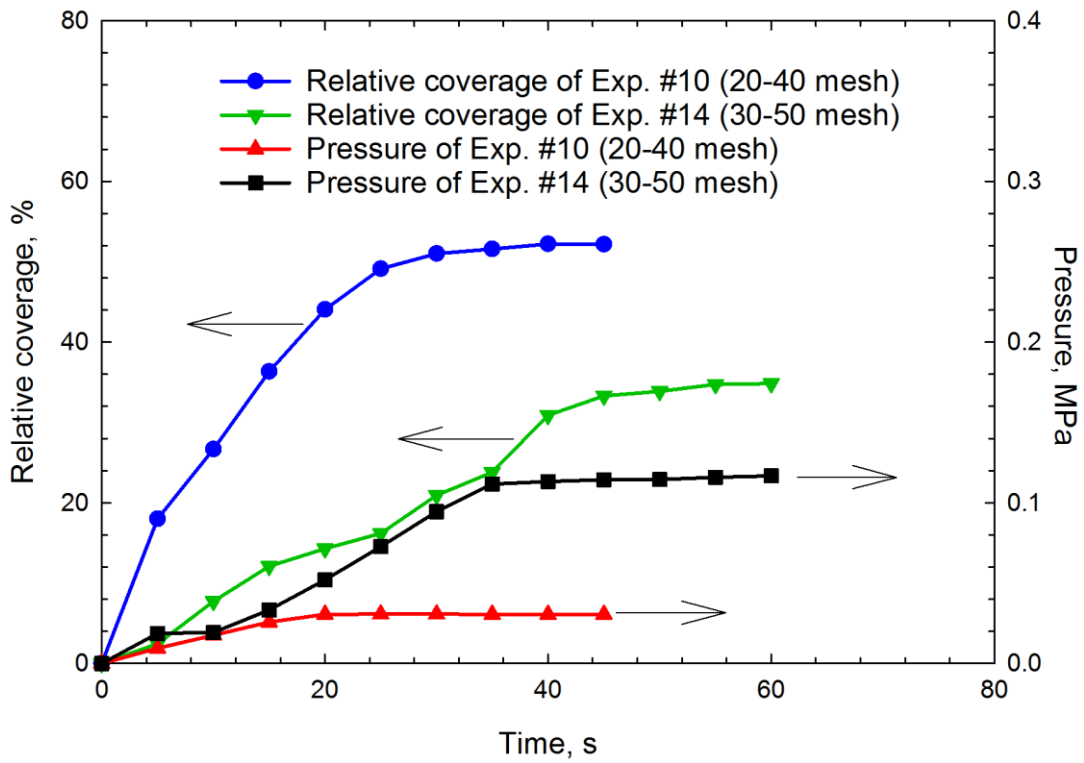
Figure 3.7 Changes in the relative coverage of resin-coated ceramic proppants and pressure as time elapses: (a) evolution of the relative coverage and pressure recorded for Experiments #1 and #4; (b) evolution of the relative coverage and pressure recorded for Experiments #5 and #8; (c) evolution of the relative coverage and pressure recorded for Experiments #10 and #13; (d) evolution of the relative coverage and pressure recorded for Experiments #14 and #17; (e) evolution of the relative coverage and pressure recorded for Experiments #19 and #22; and (f) evolution of the relative coverage and pressure recorded for Experiments #23 and #26. These experiments are conducted to study the effect of flow rate on the proppant settling behavior in rough fracture models.

3.3.6. Effect of Particle Size of Resin-Coated Ceramic Proppant

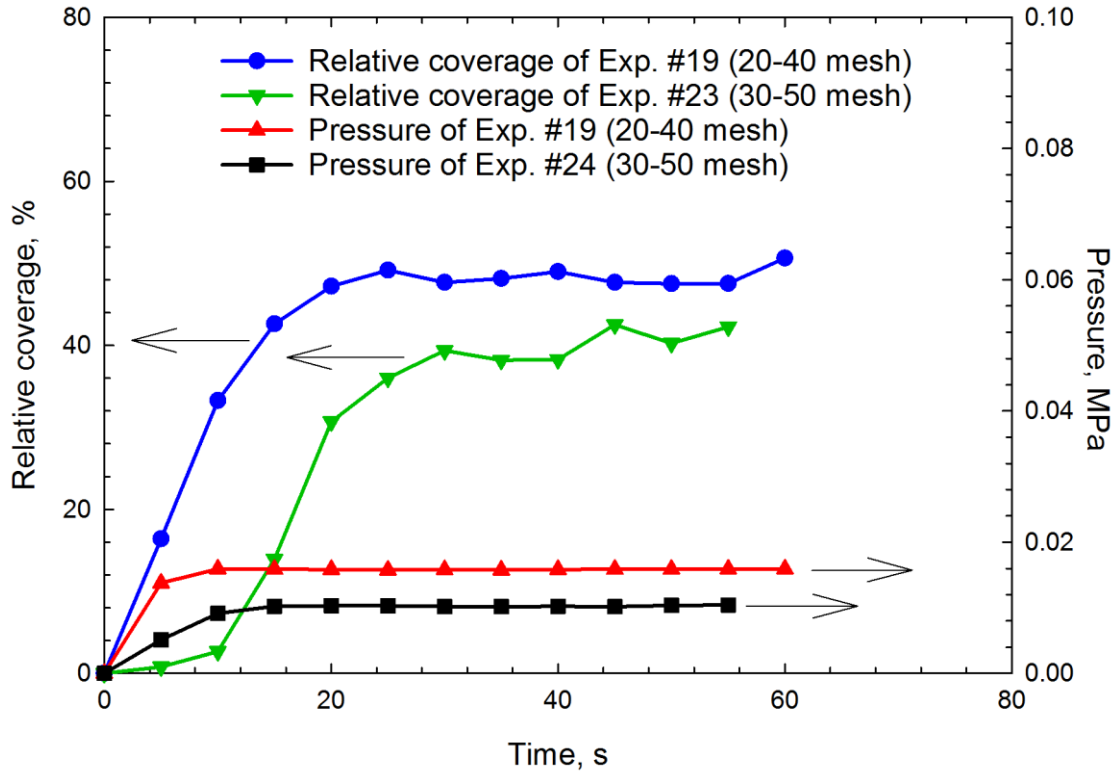
Figure 3.8 shows the changes in the relative coverage of resin-coated ceramic proppants and pressure as time elapses in Experiments #1, #5, #10, #14, #19, and #23. The particle size of resin-coated ceramic proppants used in Experiments #1, #10, and #19 is 20-40 mesh, while that used in Experiments #5, #14, and #23 is 30-50 mesh. At a given time, the relative coverage obtained with 20-40 mesh resin-coated ceramic proppants is larger than that obtained with 30-50 mesh resin-coated ceramic proppants. The 20-40 mesh resin-coated ceramic particles have a relatively larger average size than the 30-50 mesh ones and thus require less amount of particles to fill the fracture aperture. Furthermore, the friction between the larger particles and rough fracture surface retards the movement of resin-coated ceramic particles, leading to the accumulation of proppant particles. This enables 20-40 mesh resin-coated ceramic particles to cover more area in the fracture model than the 30-50 mesh ones.



(a)



(b)



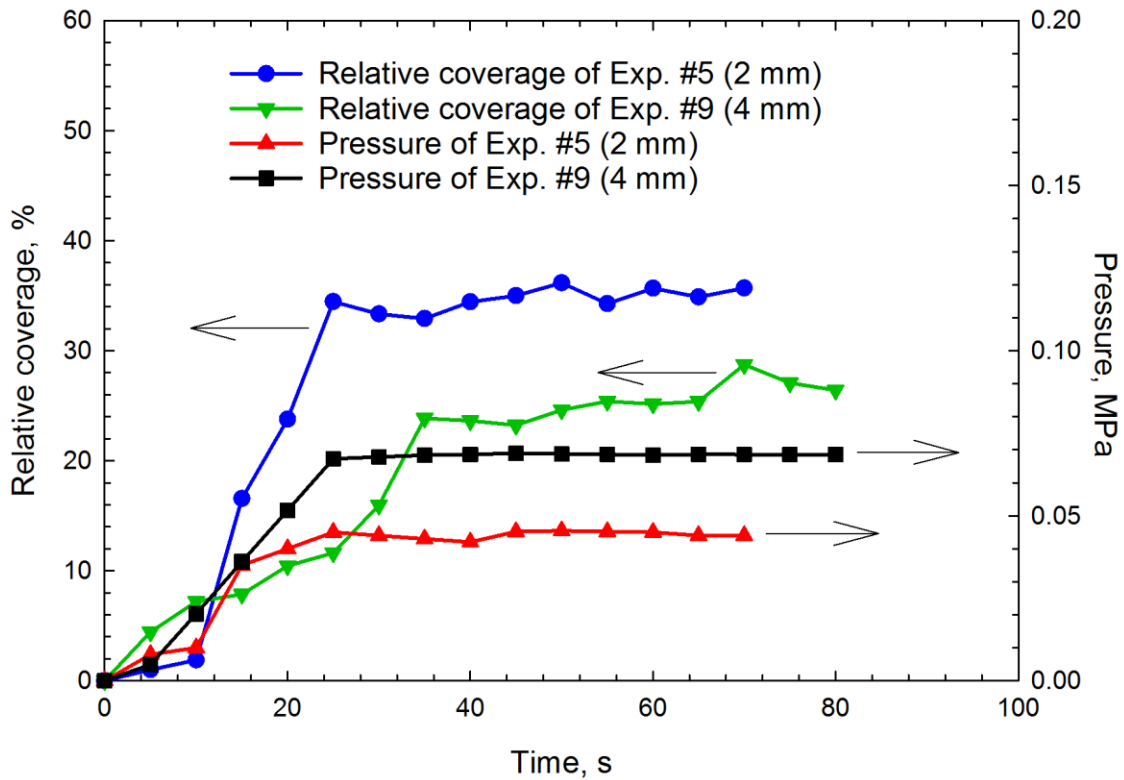
(c)

Figure 3.8 Changes in the relative coverage of resin-coated ceramic proppants and pressure as time elapses: (a) evolution of the relative coverage and pressure recorded for Experiments #1 and #5; (b) evolution of the relative coverage and pressure recorded for Experiments #10 and #14; (c) evolution of the relative coverage and pressure recorded for Experiments #19 and #23. These experiments are conducted to study the effect of particle size of resin-coated ceramic proppant on the proppant settling behavior in rough fracture models.

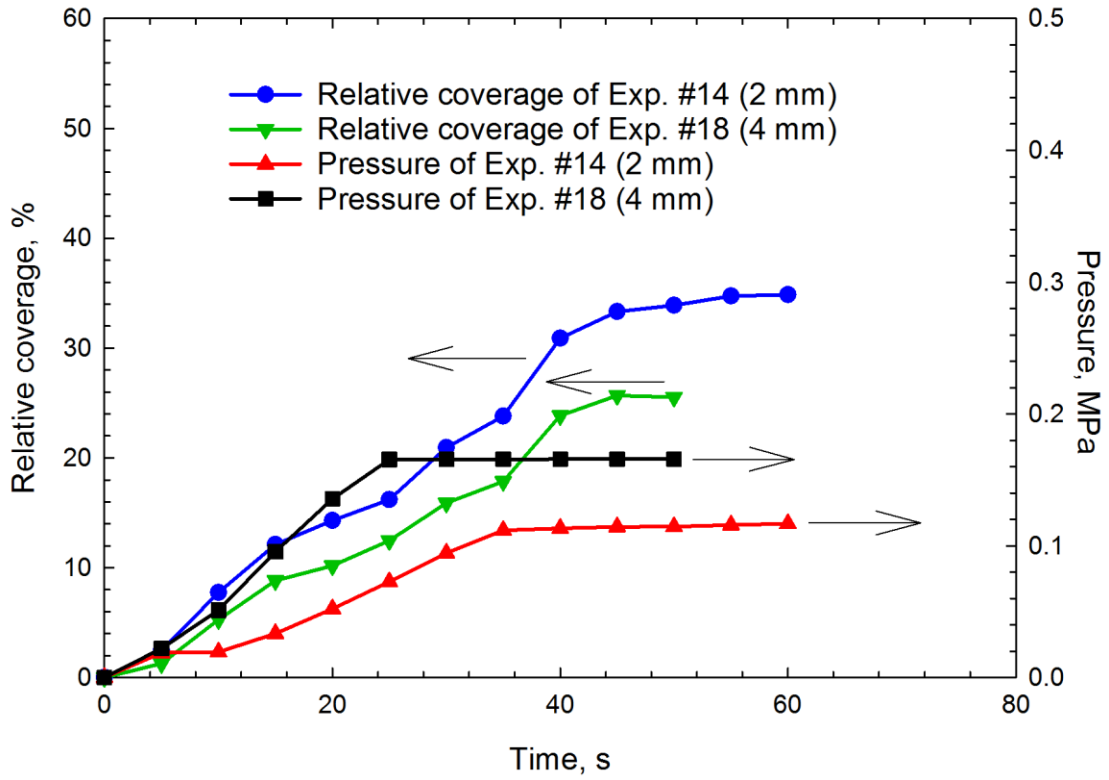
3.3.7. Effect of Fracture Aperture

Figure 3.9 shows the changes in the relative coverage of resin-coated ceramic proppants and pressure as time elapses in Experiments #5, #9, #14, #18, #23, and #27. The fracture aperture used in Experiments #5, #14, and #23 is 2 mm, while that used in Experiments #9, #18, and #27 is 4 mm. As seen from Figure 3.9, at a given time, the relative coverage of resin-coated ceramic proppants recorded in Experiments #5, #14 and #23 is larger than that recorded in Experiments #9, #18 and #27. The injection pressures recorded in Experiments #9, #18 and #27 are higher than those recorded in Experiments #5, #14 and #23. The reasons underlying such observation

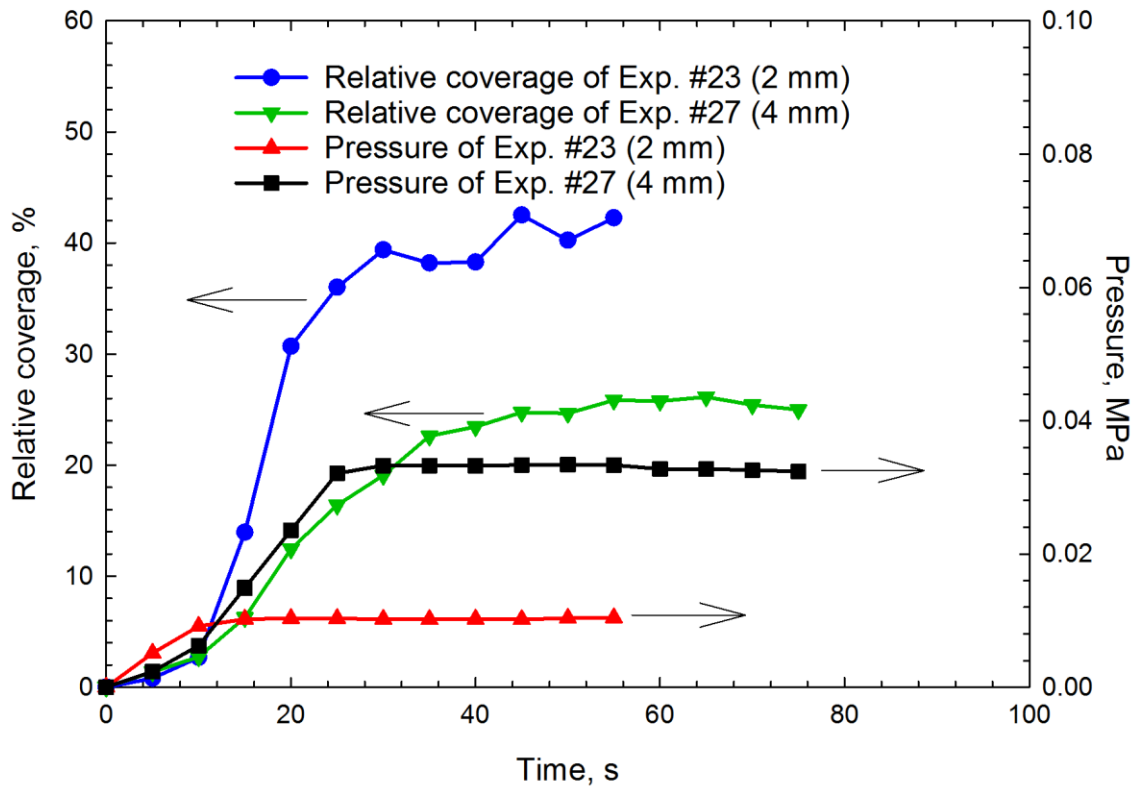
can be physically explained as follows. The collisions between the large particles and rough fracture surface in a 2 mm fracture are more likely to happen than that in a 4 mm fracture; more collisions will tend to more retard the particle movement in the fracture, yielding a higher chance of proppant settling and accumulation. As a result, a higher injection pressure is required to accommodate a larger relative proppant coverage as obtained in the experiments using 2 mm fracture models (See Figure 3.9).



(a)



(b)



(c)

Figure 3.9 Changes in the relative coverage of resin-coated ceramic proppants and pressure as time elapses: (a) evolution of the relative coverage and pressure recorded for Experiments #5 and #9; (b) evolution of the relative coverage and pressure recorded for Experiments #14 and #18; (c) evolution of the relative coverage and pressure recorded for Experiments #23 and #27. These experiments are conducted to study the effect of fracture aperture size on the proppant settling behavior in rough fracture models.

3.3.8. Effect of Fracture Model

In order to reveal the effect of fracture model on the transport behavior of the resin-coated ceramic particles in fractures, we need to compare the relative coverage of resin-coated ceramic proppants and injection pressure obtained in all the experiments conducted with the use of the three fracture models. **Figure 3.10** shows the changes in the relative coverage and injection pressure in Experiments #1, #10 and #19, which are conducted using Fr.1, Fr.4, and Fr.5, respectively. Among these three experiments, the highest final relative coverage of resin-coated ceramic proppants is obtained in Experiment #10 (Fr.4), and the final relative coverage of resin-coated ceramic proppants in Experiment #19 (Fr.5) is slightly lower than that in Experiment #10 (Fr.4). The relative proppant coverage in Experiment #1 (Fr.1) is the lowest among these three experiments. Besides, the highest injection pressure can be found in Experiment #1 (Fr.1), while the injection pressure recorded in Experiment #19 (Fr.5) is the lowest. Unfortunately, due to the limited number of fracture models used in the experiments, we cannot correlate the experimental findings with the fractal properties of the fracture models.

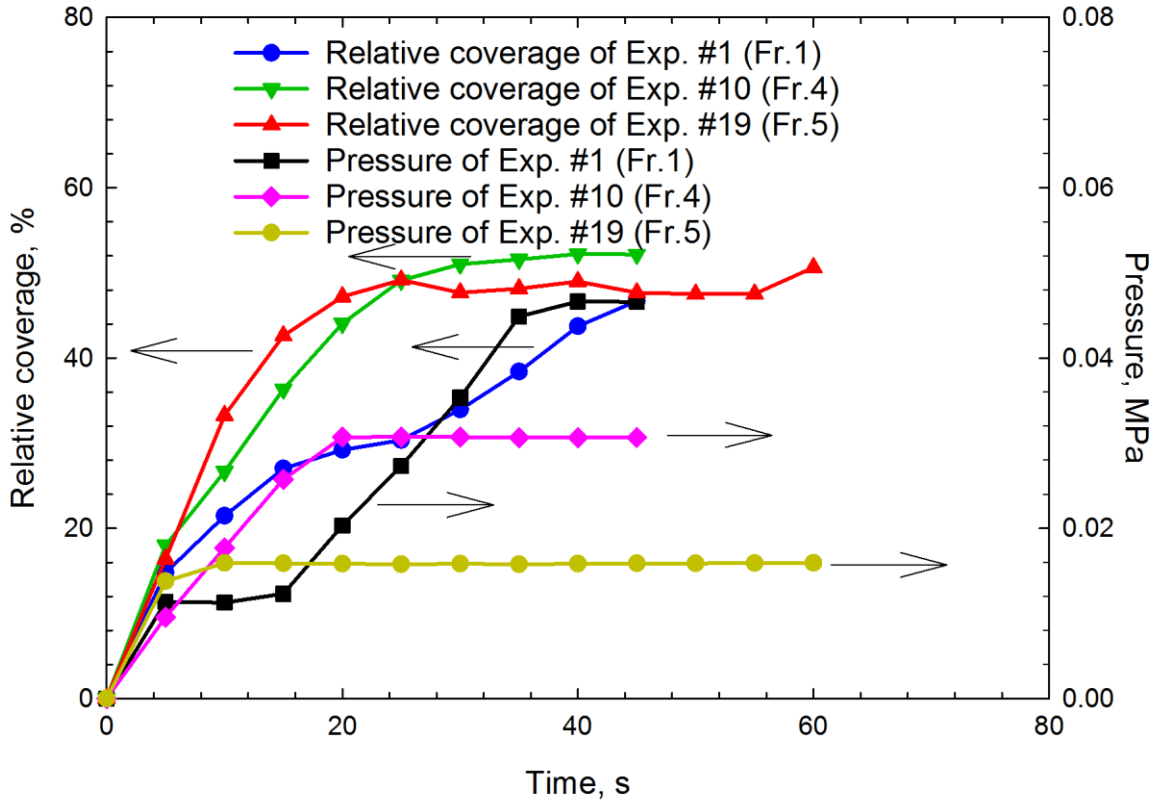


Figure 3.10 Changes in the relative coverage of resin-coated ceramic proppants and injection pressure as time elapses in Experiments #1, #10 and #19. These results are shown together to demonstrate the effect of fracture model on the proppant settling behavior in rough fracture models.

3.4. Conclusions

In order to reveal the transport behavior of resin-coated ceramic proppants in rough fracture models, this study monitors the pressure across the vertical fracture when the slurry flows through the aperture and measures the relative areal coverage of the proppant particles in the fracture versus time. Major influential factors on the proppants transport behavior have been studied, including the location of the injection port (top and bottom), proppant type (silica sands and resin-coated ceramic proppants), fracturing fluid type (tap water and slickwater), flow rate (10 L/min and 12 L/min), particle size of proppant (20-40 mesh and 30-50 mesh), fracture aperture (2 mm and 4 mm) and fracture model type (Fr.1, Fr.4, and Fr.5). The major findings can

be summarized as follows (note that the following conclusions have been made by just changing one condition but keeping other experimental conditions the same):

- 1) At a given time, the area occupied by the proppants injected through the top injection point is much larger than that occupied by the proppants injected through the bottom injection point. The reason behind is the proppant particles settle down gradually when the slurry is injected through top injection point, while the proppant particles can hardly settle down due to the high velocity of the slurry at the bottom when the slurry is injected through bottom injection point.
- 2) The settling velocity of resin-coated ceramic particles is higher than that of silica sands due to the higher density of resin-coated ceramic particles, resulting in a larger relative coverage of resin-coated ceramic proppants than that of silica sands at a given time.
- 3) The relative coverage of proppants carried by slickwater is lower than that of proppants carried by tap water at a given time. Meanwhile, the slickwater can dramatically reduce the pumping pressure of injecting proppants into the fracture models. The slickwater containing a low-concentration polymer can act as a friction reducer, leading to lower pressure required to pump the slickwater slurry through the rough fracture model than the tap water.
- 4) A higher flow rate tends to transport the particles into deeper locations of the fracture model, leading to a lower relative coverage of resin-coated ceramic proppants in the fracture at a given time due to the limited length of the fracture model.
- 5) The particle size of 20-40 mesh resin-coated ceramic proppants are larger than that of 30-50 mesh ones, leading to that less amount of 20-40 mesh resin-coated ceramic proppants particles is needed to fill the fracture aperture. The collisions between the larger particles

and fracture surface retard the movement of resin-coated ceramic particles, leading to the accumulation of proppant particles. This enables 20-40 mesh resin-coated ceramic particles to cover more area in the fracture model than the 30-50 mesh ones at a given time.

- 6) When we are injecting the slurry mixed with proppants into a fracture with a smaller fracture aperture, the collisions between the proppant particles and fracture surface are more likely to happen and retard the movement of resin-coated ceramic particles, yielding a higher chance of proppant settling and accumulation.
- 7) The highest relative coverage of resin-coated ceramic proppants is obtained in Fr.4 (a replication of coarse-grained white marble), while the lowest relative coverage of resin-coated ceramic proppant can be obtained in Fr.1 (a replication of beige limestone with abundant coarse fossil shells). The highest injection pressure can be found in Fr.1 (a replication of beige limestone with abundant coarse fossil shells), while the injection pressure recorded in Fr.5 (a replication of holocrystalline amphibole granite) is the lowest.
- 8) Unfortunately, due to the limited number of fracture models used in the experiments, we cannot correlate the experimental findings with the fractal properties of the fracture models.

References

- [1] G.A. Al-Muntasheri, L. Li, F. Liang, A.M. Gomaa, Concepts in cleanup of fracturing fluids used in conventional reservoirs: a literature review. *SPE Prod. Oper.* 33 (02) (2018) 196-213.
- [2] A. Kamenov, D. Zhu, A.D. Hill, J. Zhang, Laboratory measurement of hydraulic fracture conductivities in the Barnett shale. *SPE Prod. Oper.* 29 (03) (2014) 216-227.
- [3] N.R. Warpinski, M. Mayerhofer, K. Agarwal, and J. Du, Hydraulic-fracture geomechanics and microseismic-source mechanisms. *SPE J.* 18 (04) (2013) 766-780.
- [4] W. Zhou, R. Banerjee, B. Poe, J. Spath, M. Thambynayagam, Semianalytical production simulation of complex hydraulic-fracture networks. *SPE J.* 19 (01) (2013) 6-18.
- [5] P.C. Harris, H.G. Walters, J. Bryant, Prediction of proppant transport from rheological data. *SPE Prod. Oper.* 24 (04) (2009) 550-555.
- [6] E.J. Novotny, Proppant transport, Paper SPE 6813 presented at the 52nd Annual Fall Technical Conference and Exhibition, Denver, Colorado, USA, 9-12, October 1977.
- [7] N.V. Queipo, A.J. Verde, J. Canelón, S. Pintos, Efficient global optimization for hydraulic fracturing treatment design. *J. Petrol. Sci. Eng.* 35(3-4) (2002) 151-166.
- [8] B.T. Dewprashad, J.D. Weaver, P.D. Nguyen, M. Parker, and M. Blauch, Modifying the proppant surface to enhance fracture conductivity. Paper SPE 50733 presented at the SPE International Symposium on Oilfield Chemistry, Houston, Texas, USA, 16-19, February 1999.

- [9] P.D. Nguyen, B.T. Dewprashad, J.D. Weaver, A new approach for enhancing fracture conductivity. Paper SPE 50002 presented at the SPE Asia Pacific Oil and Gas Conference and Exhibition, Perth, Australia, 12-14, October 1998.
- [10] R.A. Cutler, D.O. Enniss, A.H. Jones, and S.R. Swanson, Fracture conductivity comparison of ceramic proppants. *SPE J.* 25 (02) (1985) 157-170.
- [11] S. Liu, P.P. Valkó, Optimization of spacing and penetration ratio for infinite-conductivity fractures in unconventional reservoirs: A section-based approach. *SPE J.* 22 (06) (2017) 1877-1892.
- [12] S.W. Almond, G.S. Penny, M.W. Conway, Factors affecting proppant flow back with resin coated proppants. Paper SPE 30096 presented at the European Formation Damage Conference, The Hague, The Netherlands, 15-16, May 1995.
- [13] W. Lu, B. O'Neil, K. Zhang, C. Wang, H. Quintero, Enhancing proppant flow back control through surface treatment of proppant. Paper IPTC 18796 presented at the International Petroleum Technology Conference, Bangkok, Thailand, 14-16, November 2016.
- [14] M. Parker, J. Weaver, D.V. Batenburg, Understanding proppant flow back. SPE 56726 presented at the SPE Annual Technical Conference and Exhibition, Houston, Texas, USA, 3-6, October 1999.
- [15] S. Songire, C. Prakash, R. Belakshe, Effects of resin-fluid interaction on fracturing fluid stability, proppant flow back, and preventive control methods. Paper SPE 194959 presented at the SPE Middle East Oil and Gas Show and Conference, Manama, Bahrain, 18-21, March 2019.

- [16] F. Liang, M. Sayed, G.A.A. Muntasheri, F.F. Chang, L. Li, A comprehensive review on proppant technologies. *Petroleum*. 2 (2016) 26-39.
- [17] A.R. Sinclair, J.W. Graham, C.P. Sinclair, Improved well stimulation with resin-coated proppants. Paper SPE 11579 presented at the SPE Production Operation Symposium, Oklahoma City, Oklahoma, USA, 27 February-1 March 1983.
- [18] A.R. Rickards, H.D. Brannon, W.D. Wood, High strength, ultralightweight proppant lends new dimensions to hydraulic fracturing applications. *SPE Prod. Oper.* 21 (02) (2006) 212-221.
- [19] X. Hu, K. Wu, X. Song, W. Yu, L. Zuo, G. Li, Z. Shen, Development of a new mathematical model to quantitatively evaluate equilibrium height of proppant bed in hydraulic fractures for slickwater treatment. *SPE J.* 23 (06) (2018) 2158-2174.
- [20] M. Ba Geri, A. Imqam, S. Dunn-Norman, Proppant transport behavior in inclined versus vertical hydraulic fractures: an experimental study. Paper SPE 191813 presented at the SPE Eastern Regional Meeting, Pittsburgh, Pennsylvania, USA, 7-11, October 2018.
- [21] M. Mack, J. Sun, C. Khadilkar, Quantifying proppant transport in thin fluids: theory and experiments. Paper SPE 168637 presented at the SPE Hydraulic Fracturing Technology Conference, The Woodlands, Texas, USA, 2-4, February 2014.
- [22] L.R. Kern, T.K. Perkins, R.E. Wyant, The mechanics of sand movement in fracturing. *J. Pet. Tech.* 11 (07) (1959) 55-57.

- [23] S. Malhotra, M.M. Sharma, A general correlation for proppant settling in VES fluids. Paper SPE 139581 presented at the SPE Hydraulic Fracturing Technology Conference, The Woodlands, Texas, USA, 24-26, January 2011.
- [24] Y. Liu, M.M. Sharma, Effect of fracture width and fluid rheology on proppant settling and retardation: an experimental study. Paper SPE 96208 presented at the SPE Annual Technical Conference and Exhibition, Dallas, Texas, USA, 9-12 October 2005.
- [25] M.A. Alotaibi, J.L. Miskimins, Slickwater proppant transport in hydraulic fractures: new experimental findings and scalable correlation. *SPE Prod. Oper.* 33 (02) (2018) 164-178.
- [26] L. Luo, I. Tomac, Experimental investigation of particle agglomeration effects on slurry settling in viscous Fluid. *Transport Porous Med.* 121 (2) (2018) 333-352.
- [27] S. Briggs, B.W. Karney, B.E. Sleep, Numerical modeling of the effects of roughness on flow and eddy formation in fractures. *J. Rock. Mech. Geotech. Eng.* 9 (1) (2017) 105-115.
- [28] X. Huang, P. Yuan, P. Zhang, J. Han, A. Mezzatesta, and J. Bao, Numerical study of wall roughness effect on proppant transport in complex fracture geometry. Paper SPE 183818 presented at the SPE Middle East Oil & Gas Show and Conference, Manama, Kingdom of Bahrain, 6-9, March 2017.
- [29] T. Babadagli, S. Raza, X. Ren, K. Develi, Effect of surface roughness and lithology on the water–gas and water–oil relative permeability ratios of oil-wet single fractures. *Int. J. Multiphase Flow.* 75 (2015) 68-81.
- [30] H. Huang, T. Babadagli, H. Li, K. Develi, Visual analysis on the effects of fracture-surface characteristics and fracture model on proppant transport in vertical fractures. Paper SPE

189892 presented at the SPE Hydraulic Fracturing Technology Conference & Exhibition, Woodlands, Texas, USA, 23-25, January 2018.

- [31] H. Huang, T. Babadagli, H. Li, A quantitative and visual experimental study: effect of fracture roughness on proppant transport in a vertical fracture. Paper SPE 187520 presented at the SPE Eastern Regional Meeting, Lexington, Kentucky, USA, 4-6, October 2017.
- [32] A. Raimbay, T. Babadagli, E. Kuru, K. Develi, Quantitative and visual analysis of proppant transport in rough fractures. *J. Nat. Gas Sci. Eng.* 33 (2016) 1291-1307.
- [33] A. Raimbay, T. Babadagli, E. Kuru, K. Develi, Effect of fracture surface roughness and shear displacement on permeability and proppant transportation in a single fracture. Paper 171577 presented at the SPE/CSUR Unconventional Resources Conference – Canada, Calgary, Alberta, Canada, 30 September–2 October 2014.
- [34] A. Raimbay, T. Babadagli, E. Kuru, K. Develi, Effect of fracture roughness, shear displacement, fluid type, and proppant on the conductivity of a single fracture: a visual and quantitative analysis. *SPE Reser. Eval. Eng.* 20 (02) (2017) 446-470.
- [35] K. Develi, T. Babadagli, Quantification of natural fracture surfaces using fractal geometry. *Math. Geol.* 30 (8) (1998) 971-998.
- [36] K. Develi, T. Babadagli, Experimental and visual analysis of single-phase flow through rough fracture replicas. *Int. J. Rock Mech. Min. Sci.* 73 (2015) 139-155.

CHAPTER 4 CONCLUSIONS AND RECOMMENDATIONS

4.1. Conclusions

In this study, we determine the drag coefficients of the resin-coated ceramic particles in water and investigate the flow characteristics and transport behavior of resin-coated ceramic proppants in rough vertical fractures.

In chapter 2, we measure the drag coefficients of resin-coated ceramic particles in a Newtonian fluid (water). Volumes, mean diameters, and fractions of three constituents (i.e., resin, ceramic body, and air pockets) in eight resin-coated ceramic particles are obtained by using CT scan. CT scan shows that the resin-coated ceramic particles are nearly spherical particles but inhomogeneous, and the surface of the resin-coated ceramic particles is rough. Based on the CT measurements, the volumetric fractions of the resin contents in the resin-coated ceramic particles are found to be from 1.7% to 6.7%, while the volumetric fractions of the air pockets are found to be from 11.7% to 16.1%. The mass of each particle can be obtained by using a high-precision electronic balance. The settling velocities of resin-coated ceramic particles are calculated by dividing the travel distance of the tested particle in static water by travel durations as obtained by a high-speed camera. Three methods are tried to determine particle volume and particle density. Among these three methods, the smallest average density is estimated by method #1. The average density estimated by method #1 is 2337 kg/m^3 and is much smaller than the average value provided by the supplier (i.e., 2630 kg/m^3). The densities estimated by using methods #2 (2757 kg/m^3) and #3 (2709 kg/m^3) are much higher than the density estimated by method #1. A comparison between the drag coefficient estimated in this work and those estimated by five empirical correlations is conducted, showing that drag coefficient estimated by using Roos and Willmarth's correlation is more accurate than the drag coefficient estimated by other four

correlations in predicting the drag coefficients of resin-coated ceramic particles. In addition, another comparison between the density of resin-coated ceramic particles calculated by three methods and the “ideal particle density” shows that the densities estimated by using method #3 are more accurate than the densities estimated by methods #1 and #2.

In chapter 3, we investigate the transport behavior of proppants based on visual experimental methods, i.e., monitoring the pressure across the vertical fracture and observing the distribution of proppant particles in the fracture model. The experimental results indicate that the resin-coated ceramic proppants exhibit higher relative coverage in the fracture models than silica sands, which helps to enhance the fracture conductivity. Major influential factors on the proppants transport behavior have also been experimentally examined, including the location of the injection port (top and bottom), fracturing fluid type (tap water and slickwater), flow rate (10 L/min and 12 L/min), particle size of proppant (20-40 mesh and 30-50 mesh), fracture aperture (2 mm and 4 mm) and fracture model type (Fr.1, Fr.4, and Fr.5). At a given time, the relative coverage of resin-coated ceramic proppants obtained by injecting resin-coated ceramic proppants through the top injection point is larger than that of resin-coated ceramic proppants obtained by injecting resin-coated ceramic proppants through the bottom injection point. The area occupied by resin-coated ceramic proppants is much larger than that occupied by silica sands at a given time. The relative coverage of resin-coated ceramic proppants carried by slickwater is lower than that of resin-coated ceramic proppants carried by tap water at a given time. Besides, the slickwater containing a low-concentration polymer can act as a friction reducer, leading to that the injection pressure recorded in the experiments using the slickwater is lower than that recorded in the experiments using the tap water. A higher flow rate can transport the proppants into deeper locations in the fractures, resulting in a lower relative coverage of proppants in the

fracture models due to the limited length of the fracture models at a given time. A particle size of 20-40 mesh gives a higher relative proppant coverage in the fracture models at a given time than the 30-50 mesh resin-coated ceramic particles; this can be attributed to the fact that the collisions between the larger particles (i.e., 20-40 mesh particles) and fracture surface are more likely to happen and will retard the movement of resin-coated ceramic particles, leading to a higher relative coverage of 20-40 mesh resin-coated ceramic particles in the fracture models. Besides, when the slurry carries the proppants through the fracture models, there are more collisions between the fractures wall and proppant particles in the 2-mm-aperture fracture than the 4-mm-aperture fracture. Therefore, at a given time, the relative coverage obtained in experiments using a 2-mm-aperture fracture model is larger than that obtained in experiments using a 4-mm-aperture fracture model. Among three fracture models, the highest relative coverage of resin-coated ceramic proppants is obtained in Fr.4 (a replication of coarse-grained white marble), while the lowest relative coverage of resin-coated ceramic proppant can be obtained in Fr.1 (a replication of beige limestone with abundant coarse fossil shells). The highest injection pressure can be found in Fr.1 (a replication of beige limestone with abundant coarse fossil shells), while the injection pressure recorded in Fr.5 (a replication of holocrystalline amphibole granite) is the lowest.

4.2. Recommendations

To better understand the settling behavior of resin-coated ceramic particles in water contained in narrow spaces, more realistic experimental conditions should be considered. For instance, we can conduct additional experiments to quantitatively investigate the effect of roughness and resin coating on the settling behavior of resin-coated ceramic particles in water. To delineate the wall

effect on the settling velocity of resin-coated ceramic proppants in narrow fractures, narrow channels with varied widths should be used in the particle-settling experiments.

Due to the limited length of the fracture model used in our experiments, transport behavior of resin-coated ceramic proppants can only be recorded and observed within a short distance. In reality, the underground hydraulic fractures may have a half length of many meters. To have a more realistic understanding of the transport behavior of the resin-coated ceramic particles in the actual fractures, fracture models with a larger length are needed. Besides, filtration of slurry via the fracture walls is another factor that may affect the transport of the proppants in the fractures, which is, however, not taken into account in this study. In future work, we may manufacture fracture models with porous walls and apply them in the flow experiments in order to better mimic the real underground conditions.

BIBLIOGRAPHY

- Abraham, F.F., Functional dependence of drag coefficient of a sphere on Reynolds number. *Phys. Fluids*. 13 (8) (1970) 2194-2195.
- Almedeij, J., Drag coefficient of flow around a sphere: Matching asymptotically the wide trend. *Powder Technol.* 186 (3) (2008) 218-223.
- Almond, S.W., Penny, G.S., Conway, M.W., Factors affecting proppant flow back with resin coated proppants. Paper SPE 30096 presented at the European Formation Damage Conference, The Hague, The Netherlands, 15-16, May 1995.
- Al-Muntasheri, G.A., Li, L., Liang, F., Gomaa, A.M., Concepts in cleanup of fracturing fluids used in conventional reservoirs: a literature review. *SPE Prod Oper.* 33 (02) (2018) 196-213.
- Alotaibi, M.A., Miskimins, J.L., Slickwater proppant transport in hydraulic fractures: new experimental findings and scalable correlation. *SPE Prod. Oper.* 33 (02) (2018) 164-178.
- Arnipally, S.K., Kuru, E., Settling velocity of particle in viscoelastic fluids: a comparison of the shear-viscosity and elasticity effects. *SPE J.* 23 (05) (2018) 1689-1705.
- Babadagli, T., Raza, S., Ren, X., Develi, K., Effect of surface roughness and lithology on the water-gas and water-oil relative permeability ratios of oil-wet single fractures. *Int. J. Multiphase Flow.* 75 (2015) 68-81.
- Ba Geri, M., Imqam, A., Dunn-Norman, S., Proppant transport behavior in inclined versus vertical hydraulic fractures: an experimental study. Paper SPE 191813 presented at the SPE Eastern Regional Meeting, Pittsburgh, Pennsylvania, USA, 7-11, October 2018.

- Bagheri, G., Bonadonna, C., On the drag of freely falling non-spherical particles. *Powder Technol.* 301 (2016) 526-544.
- Bestaoui-Spurr, N., Materials science improves silica sand strength. Paper SPE 168158 presented at the SPE Symposium and Exhibition on Formation Damage Control, Lafayette, Louisiana, USA, 26-28, February 2014.
- Briggs, S., Karney, B.W., Sleep, B.E., Numerical modeling of the effects of roughness on flow and eddy formation in fractures. *J. Rock Mech. Geotech. Eng.* 9 (1) (2017) 105-115.
- Brown, P.P., Lawler, D. F., Sphere drag and settling velocity revisited. *J. Environ. Eng.* 129 (3) (2003) 222–231.
- Brown, S., Cprihan, A., Hardy, R., Experimental observation of fluid flow channels in a single fracture. *J Geophys. Res.* 103 (1998) 5125-5132.
- Cheng, N.S., Simplified settling velocity formula for sediment particle. *J. Hydraulic. Eng.* 123 (2) (1997) 149-152.
- Cheng, N.S., Comparison of formulas for drag coefficient and settling velocity of spherical particles. *Powder Technol.* 189 (3) (2009) 395-398.
- Chien, S.F., Settling velocity of irregularly shaped particles. *SPE Drill & Compl.* 9 (04) (1994) 281-289.
- Clift, R., Gauvin, W.H., Motion of entrained particles in gas streams. *Can. J. Chem. Eng.* 49 (4) (1971) 439-448.

- Concha, F., Christiansen, A., Settling velocities of particulate systems, 5. Settling velocities of suspensions of particles of arbitrary shape. *Int. J. Miner. Process.* 18 (3-4) (1986) 309-322.
- Cox, E.P., A method of assigning numerical and percentage value to the degree of roundness of sand grains. *J. Paleontol.* 1 (3) (1927) 179-183.
- Cutler, R.A., Enniss, D.O., Jones, A.H., Swanson, S.R., Fracture conductivity comparison of ceramic proppants. *SPE J.* 25 (02) (1985) 157-170.
- Davaadorj, B.E., Kim, Y., Lee, J., Settling velocity of irregularly shaped particles in Newtonian fluids. *Geosyst. Eng.* 16 (3) (2013) 225-230.
- Dejam, M., Hassanzadeh, H., Chen, Z., Shear dispersion in a rough-walled fracture. *SPE J.* 23 (05) (2018) 1669-1688.
- Develi, K., Babadagli, T., Quantification of natural fracture surfaces using fractal geometry. *Math. Geol.* 30 (8) (1998) 971-998.
- Develi, K., Babadagli, T., Experimental and visual analysis of single-phase flow through rough fracture replicas. *Int. J. Rock Mech. Min. Sci.* 73 (2015) 139-155.
- Dewprashad, B.T., Weaver, J.D., Nguyen, P.D., Parker, M., Blauch, M., Modifying the proppant surface to enhance fracture conductivity. Paper SPE 50733 presented at the SPE International Symposium on Oilfield Chemistry, Houston, Texas, USA, 16-19, February 1999.
- Dietrich, W.E., Settling velocity of natural particles. *Water Resour. Res.* 18 (6) (1982) 1615-1626.

- Dioguardi, F., Mele, D., A new shape dependent drag correlation formula for non-spherical rough particles. Experiments and results. *Powder Technol.* 277 (2015) 222-230.
- Drazer, G., Koplik, J., Tracer dispersion in two-dimensional rough fractures. *Phys. Rev. E.* 63 (2001) 056104.
- Dronfield, D.G., Silliman, S.E., Velocity dependence of dispersion for transport through a single fracture of variable roughness. *Water Resour. Res.* 29 (1993) 3477-3483.
- Droppert, D., Fiore, P., Dessureault, Y., Cardarelli, F., High strength, heat- and corrosion-resistant ceramic granules for proppants. Canadian Patent CA 2329834 (2002).
- Elgaddafi, R., Ahmed, R., George, M., Growcock, F., Settling behavior of spherical particles in fiber-containing drilling fluids. *J. Petrol. Sci. Eng.* 84-85 (2012) 20-28.
- Etilib, R.A.E.E., AlKaiem, H.H., Jaafar, A., Investigation on the particle settling velocity in non-Newtonian fluids. *J. Applied Sci.* 11 (9) (2011) 1528-1535.
- Flemmer, R.L.C., Banks, C.L., On the drag coefficient of a sphere. *Powder Technol.* 48 (3) (1986) 217-221.
- Fu, L., Zhang, G., Ge, J., Liao, K., Jiang, P., Pei, H., Li, X., Surface modified proppants used for proppant flow back control in hydraulic fracturing. *Colloids Surf. A Physicochem. Eng. Asp.* 507 (2016) 18-25.
- Ganser, G.H., A rational approach to drag prediction of spherical and nonspherical particles. *Powder Technol.* 77 (2) (1993) 143-152.

- Gelhar, L.W., Stochastic subsurface hydrology from theory to application. *Water Resour. Res.* 22 (1986) 135S-145S.
- Gibbs, R.J., Matthews, M.D., Link, D.A., The relationship between sphere size and settling velocity. *J. Sediment. Res.* 41 (1) (1971) 7-18.
- Haider, A., Levenspiel, O., Drag coefficient and terminal velocity of spherical and nonspherical particles. *Powder Technol.* 58 (1989) 63-70.
- Harris, P.C., Walters, H.G., Bryant, J., Prediction of proppant transport from rheological data. *SPE Prod. Oper.* 24 (04) (2009) 550-555.
- Hartman, M., Trnka, O., Svoboda, K., Free settling of nonspherical particles. *Ind. Eng. Chem. Res.* 33 (1994) 1979-1983.
- Hensley, Z.D., Papavassiliou, D.V., Drag coefficient correction for spherical and nonspherical particles suspended in square microducts. *Ind. Eng. Chem. Res.* 53 (25) (2014) 10465-10474.
- Hu, K., Schmidt, A., Barhaug, J., Wong, J., Tian, J., Hall, B.E., Sand, resin-coated sand or ceramic proppant? The effect of different proppants on the long-term production of Bakken shale wells. Paper SPE 174816 presented at the SPE Annual Technical Conference and Exhibition, Houston, Texas, USA, 28-30, September 2015.
- Hu, X., Wu, K., Song, X., Yu, W., Zuo, L., Li, G., Shen, Z., Development of a new mathematical model to quantitatively evaluate equilibrium height of proppant bed in hydraulic fractures for slickwater treatment. *SPE J.* 23 (06) (2018) 2158-2174.

- Huang, H., Babadagli, T., Li, H., A quantitative and visual experimental study: effect of fracture roughness on proppant transport in a vertical fracture. Paper SPE 187520 presented at the SPE Eastern Regional Meeting, Lexington, Kentucky, USA, 4-6, October 2017.
- Huang, H., Babadagli, T., Li, H., Develi, K., Visual analysis on the effects of fracture-surface characteristics and fracture model on proppant transport in vertical fractures. Paper SPE 189892 presented at the SPE Hydraulic Fracturing Technology Conference & Exhibition, Woodlands, Texas, USA, 23-25, January 2018.
- Huang, X., Yuan, P., Zhang, P., Han, J., Mezzatesta, A., Bao, J., Numerical study of wall roughness effect on proppant transport in complex fracture geometry. Paper SPE 183818 presented at the SPE Middle East Oil & Gas Show and Conference, Manama, Kingdom of Bahrain, 6-9, March 2017.
- Hölzer, A., Sommerfeld, M., New simple correlation formula for the drag coefficient of non-spherical particles. *Powder Technol.* 184 (3) (2008) 361-365.
- Ippolite, I., Daccord, G., Hinch, E.J., Hulin, J.P., Echo tracer dispersion in model fractures with a rectangular geometry. *J. Contam Hydrol.* 16 (1994) 87-108.
- Kamenov, A., Zhu, D., Hill, A.D., Zhang, J., Laboratory measurement of hydraulic fracture conductivities in the Barnett shale. *SPE Prod Oper.* 29 (03) (2014) 216-227.
- Kern, L.R., Perkins, T.K., Wyant, R.E., The mechanics of sand movement in fracturing. *J. Pet. Tech.* 11 (07) (1959) 55-57.
- Khan, A.R., Richardson, J.F., The resistance to motion of a solid sphere in a fluid. *Chem. Eng. Commun.* 62 (1-6) (1987) 135-150.

- Klyachko, L.S., Equations of motion of dust particles in dust collectors. *Otoplenie Ventilyatsiya*, 4 (1934).
- Liang, F., Sayed, M., Al-Muntasheri, G.A., Chang, F.F., Li, L., A comprehensive review on proppant technologies. *Petroleum*. 2 (2016) 26-39.
- Liu, Y., Sharma, M.M., Effect of fracture width and fluid rheology on proppant settling and retardation: An experimental study. Paper SPE 96208 presented at the SPE Annual Technical Conference and Exhibition, Dallas, Texas, USA, 9-12, October 2005.
- Liu, S., Valkó, P.P., Optimization of spacing and penetration ratio for infinite-conductivity fractures in unconventional reservoirs: A section-based approach. *SPE J.* 22 (06) (2017) 1877-1892.
- Lu, W., O'Neil, B., Zhang, K., Wang, C., Quintero, H., Enhancing proppant flow back control through surface treatment of proppant. Paper IPTC 18796 presented at the International Petroleum Technology Conference, Bangkok, Thailand, 14-16, November 2016.
- Luo, L., Tomac, I., Experimental investigation of particle agglomeration effects on slurry settling in viscous fluid. *Transport Porous Med.* 121 (2) (2018) 333-352.
- Mack, M., Sun, J., Khadilkar, C., Quantifying proppant transport in thin fluids: theory and experiments. Paper SPE 168637 presented at the SPE Hydraulic Fracturing Technology Conference, The Woodlands, Texas, USA, 2-4, February 2014.
- Makhuvha, M., Arellano, R.M., Harney, D.M.W., Determination of bulk density, methods and impacts, with a case study from Los Bronces Mine, Chile. *Appl. Earth. Sci.* 123 (3) (2014) 196-205.

- Malhotra, S., Sharma, M.M., A general correlation for proppant settling in VES fluids. Paper SPE 139581 presented at the SPE Hydraulic Fracturing Technology Conference, The Woodlands, Texas, USA, 24-26, January 2011.
- Mandø, M., Yin, C., Sørensen, H., Rosendahl, L., On the modelling of motion of non-spherical particles in two-phase flow. Paper presented at the 6th International Conference on Multiphase Flow, Leipzig, Germany, 9-13, July 2007.
- McNown, J.S., Lee, H.M., McPherson, M.B., Engez, S.M., Influence of the boundary proximity on the drag of spheres. *Proc. Int. Cong. Appl. Mech.* 31 (1) (1950) 74-82.
- Mikhailov, M.D., Freire, A.P.S., The drag coefficient of a sphere: An approximation using Shanks transform. *Powder Technol.* 237 (2013) 432-435.
- Nguyen, P.D., Dewprashad, B.T., Weaver, J.D., A new approach for enhancing fracture conductivity. Paper SPE 50002 presented at the SPE Asian Pacific Oil & Gas Conference and Exhibition, Perth, Australia, 12-14, October 1998.
- Novotny, E.J., Proppant transport, Paper SPE 6813 presented at the 52nd Annual Fall Technical Conference and Exhibition, Denver, Colorado, USA, 9-12, October 1977.
- Ouchene, R., Khalij, M., Acren, B., Taniere, A., A new set of correlations of drag, lift and torque coefficients for non-spherical particles and large Reynolds numbers. *Powder Technol.* 303 (2016) 33-43.
- Parker, M., Weaver, J., Batenburg, D.V., Understanding proppant flow back. SPE 56726 presented at the SPE Annual Technical Conference and Exhibition, Houston, Texas, USA, 3-6, October 1999.

- Patel, S.M., Sondergeld, C.H., Rai, C.S., Laboratory studies of cyclic injection hydraulic fracturing. *Int. J. Rock Mech. Min. Sci.* 95 (2017) 8-15.
- Queipo, N.V., Verde, A.J., Canelón, J., Pintos, S., Efficient global optimization for hydraulic fracturing treatment design. *J. Petrol. Sci. Eng.* 35(3-4) (2002) 151-166.
- Raimbay, A., Babadagli, T., Kuru, E., Develi, K., Quantitative and visual analysis of proppant transport in rough fractures. *J. Nat. Gas Sci. Eng.* 33 (2016) 1291-1307.
- Raimbay, A., Babadagli, T., Kuru, E., Develi, K., Effect of fracture surface roughness and shear displacement on permeability and proppant transportation in a single fracture. Paper 171577 presented at the SPE/CSUR Unconventional Resources Conference – Canada, Calgary, Alberta, Canada, 30 September–2 October 2014.
- Raimbay, A., Babadagli, T., Kuru, E., Develi, K., Effect of fracture roughness, shear displacement, fluid type, and proppant on the conductivity of a single fracture: a visual and quantitative analysis. *SPE Reserv. Eval. Eng.* 20 (02) (2017) 446-470.
- Reynolds, P.A., Jones, T.E.R., An experimental study of the settling velocities of single particles in non-Newtonian fluids. *Int. J. Miner. Process.* 25 (1-2) (1989) 47-77.
- Rickards, A.R., Brannon, H.D., Wood, W.D., High strength, ultralightweight proppant lends new dimensions to hydraulic fracturing applications. *SPE Prod. Oper.*, 21 (02) (2006), pp.212-221.
- Roos, F.W., Willmarth, W.W., Some experimental results on sphere and disk drag. *AIAA J.* 9 (2) (1971) 285-291.

- Sarifzadeh, M., Javadi, M., Shahriar, K., Effect of surface roughness on velocity field through rock fractures. Paper ISRM-EUROCK-2009-054 presented at the ISRM Regional Symposium, Cavtat, Croatia, 29-31, October 2009.
- Sinclair, A.R., Graham, J.W., Sinclair, C.P., Improved well stimulation with resin-coated proppants. Paper SPE 11579 presented at the SPE Production Operation Symposium, Oklahoma City, Oklahoma, USA, 27 February-1 March 1983.
- Smith, R., Longitudinal dispersion coefficients for varying channels. *J. Fluid Mech.* 130 (1983) 299-314.
- Song, X., Xu, Z., Li, G., Pang, Z., Zhu, Z., A new model for predicting drag coefficient and settling velocity of spherical and non-spherical particle in Newtonian fluid. *Powder Technol.* 321 (2017) 242-250.
- Songire, S., Prakash, C., Belakshe, R., Effects of resin-fluid interaction on fracturing fluid stability, proppant flow back, and preventive control methods. Paper SPE 194959 presented at the SPE Middle East Oil and Gas Show and Conference, Manama, Bahrain, 18-21, March 2019.
- Stokes, G.G., On the effect of the internal friction of fluids on the motion of pendulums. *Trans. Camb. Phil. Soc.* 9 (8) (1851).
- Tang, Y., Ranjith, P.G., Perera, M.S.A., Major factors influencing proppant behavior and proppant-associated damage mechanisms during hydraulic fracturing. *Acta Geotechnica.* 13 (4) (2018) 757-780.

- Turton, R., Levenspiel, O., A short note on the drag correlation for spheres. *Powder Technol.* 47 (1) (1986) 83-86.
- Underdown, D.R., Das, K., New proppant for deep hydraulic fracturing, *SPE J.* 37(1) (1985) 98-104.
- Vítěz, T., Trávníček, P., Study of settling velocity of sand particles located in wastewater treatment plant. *Acta Univ. Agric. Silvic. Mendelianae Brun.* 59 (1) (2014) 249-254.
- Warpinski, N.R., Mayerhofer, M., Agarwal, K., Du, J., Hydraulic-fracture geomechanics and microseismic-source mechanisms. *SPE J.* 18 (04) (2013) 766-780.
- Zhou, W., Banerjee, R., Poe, B., Spath, J., Thambynayagam, M., Semianalytical production simulation of complex hydraulic-fracture networks. *SPE J.* 19 (01) (2013) 6-18.
- Zoveidavianpoor, M., Gharibi, A., Application of polymers for coating of proppant in hydraulic fracturing of subterranean formations: A comprehensive review. *J. Nat. Gas. Sci. Eng.* 24 (2015) 197-209.